

NUCLEAR MAGNETIC RESONANCE SATURATION AND  
RAPID PASSAGE EXPERIMENTS IN  
NON-METALLIC SOLIDS

by

WAYNE ROGER JANZEN

B.Sc., University of British Columbia, 1961

M.Sc., University of British Columbia, 1963

A THESIS SUBMITTED IN PARTIAL FULFILMENT OF  
THE REQUIREMENTS FOR THE DEGREE OF  
DOCTOR OF PHILOSOPHY

in the Department

of

Chemistry

We accept this thesis as conforming to the  
required standard

THE UNIVERSITY OF BRITISH COLUMBIA

JULY 1968

In presenting this thesis in partial fulfilment of the requirements for an advanced degree at the University of British Columbia, I agree that the Library shall make it freely available for reference and study. I further agree that permission for extensive copying of this thesis for scholarly purposes may be granted by the Head of my Department or by his representatives. It is understood that copying or publication of this thesis for financial gain shall not be allowed without my written permission.

Department of Chemistry

The University of British Columbia  
Vancouver 8, Canada

Date September 4, 1968

ABSTRACT

for

Dissertation Abstracts

Nuclear Magnetic Resonance Saturation and  
Rapid Passage Experiments in Non-Metallic Solids

by

Wayne Roger Janzen

Supervisor: Professor Basil A. Dunell

abstract

Nuclear magnetic resonance lock-in absorption mode and dispersion mode spectra of polycrystalline samples of  $\text{CaF}_2$ , potassium caproate ( $\text{KC}_6$ ), and lithium stearate ( $\text{LiC}_{18}$ ) have been obtained at various levels of saturation. The line widths narrow and the line shapes change in both the absorption and dispersion mode spectra on saturation. This behaviour is not predicted by previous theories of saturation, but is predicted by the new magnetic resonance saturation theory of Provotorov. The effects of modulation saturation have also been demonstrated. They are in agreement with Goldman's extension of Provotorov theory to include the audio modulation field.

An important prediction of Provotorov-Goldman theory is that saturation narrowing and modulation saturation do not affect the signal at the centre of resonance (within certain limiting conditions) and so the signals at this point are expected to saturate with the normal saturation factor:  $Z(0) = [1 + \gamma^2 H_1^2 T_1 f(0)/2]^{-1}$ , where  $H_1$  is the rf field amplitude,  $f(\Delta)$  is the absorption line shape function normalized to  $2\pi$ , and  $\Delta$  is in rad/sec. Therefore the progressive saturation of the lock-in dispersion signal,  $u_1(0)$ , has been studied in the

CaF<sub>2</sub>, KC<sub>6</sub>, and LiC<sub>18</sub> samples at room temperature. The results verify the above prediction and yield the spin lattice relaxation times ( $T_1$ ) of the samples. The CaF<sub>2</sub> result of  $0.385 \pm 0.03$  sec compares well with  $0.45 \pm 0.05$  sec, the value found by adiabatic rapid passage.

A modified Linder signal decay technique has also been used to measure  $T_1$  values in KC<sub>6</sub> and LiC<sub>18</sub>. The innovation being that the signal  $u_1(0)$  was used instead of the lock-in maximum absorption signal. The results are in good agreement with the progressive saturation results. It is concluded that one is finally in a position to measure correct  $T_1$  values in solids by CW techniques.

A technique for recording the true shapes of rapid passage signals has been developed. Using the shape of the rapid passage signal as a criterion of whether or not the passage was also adiabatic, it was found that the Bloch adiabatic condition,  $dH_0/dt \ll \gamma H_L^2$ , is also applicable to solids. The inequality, however, must be larger for solids than for liquids.

The width at half its peak height of an adiabatic rapid passage (ARP) signal in a solid was shown to be  $[12(H_L^2 + H_V^2)]^{\frac{1}{2}}$ , where  $H_L^2 = \langle \Delta H^2 \rangle / 3$ ,  $H_L$  is called the local magnetic field, and  $\langle \Delta H^2 \rangle$  is the Van Vleck second moment. ARP signals were used to find local field and second moment values in polycrystalline and single crystal forms of CaF<sub>2</sub> and also in polycrystalline LiC<sub>18</sub>, all at room temperature. The results are in excellent agreement with theory and CW measurements.

It is believed that this is the first time this method has been used.

The ARP technique was also used to measure  $T_1$  values. A symmetric sweep method was used for the above samples and a two pass method (equivalent to the  $\pi - \pi/2$  sequence used in pulse spectrometry) was used for a very pure crystal of maleic anhydride. A value of 76 min was found for this sample at room temperature. This is a particularly good example of the usefulness of the ARP technique since it is difficult to measure such a long  $T_1$  by the usual pulse method.

Normal and saturation narrowed lock-in absorption spectra of  $\text{LiC}_{18}$  have been obtained over the temperature range  $25^\circ$  to  $193^\circ\text{C}$ . There are two phase transitions in this region. They were revealed by both the normal and saturation narrowed spectra.

TABLE OF CONTENTS

	page
chapter 1.	
SATURATION I. SATURATION THEORIES	1
I. BLOEMBERGEN, PURCELL and POUND THEORY	1
A. Introduction	1
B. Fundamental Equation of BPP	2
C. RF Power Absorption	3
D. Magnetic Susceptibilities	4
E. Comparison of the Various Theories with Experiment	5
II. REDFIELD THEORY	6
A. Introduction	6
B. Rotating Frame Formulation	7
C. Spin Temperature and Canonical Distribution	10
D. Spin Lattice Relaxation	11
E. Complex Magnetic Susceptibility at High $H_1$	13
III. PROVOTOROV THEORY	15
A. Introduction	15
B. Derivation of the Density Matrix	15
C. Evolution of the Spin Temperatures	16
D. Spin Lattice Relaxation	17
E. Power Absorption	19
F. Complex Magnetic Susceptibility	19
G. Narrowing of the Line on Saturation	23
IV. GOLDMAN ANALYSIS	24
A. Introduction	24
B. General Remarks	26
C. Absorption Signal	26
D. Dispersion Signal	27
E. $T_1$ by Progressive Saturation of Dispersion	28
F. The Chameleonic Local Field	29
REFERENCES	30
chapter 2.	
SATURATION II. PROGRESSIVE SATURATION IN CALCIUM FLUORIDE	32
I. INTRODUCTION	32
II. EXPERIMENTAL	34
A. Spectrometer	34
B. $H_1$ Calibration	35
C. Sample	36

	Page
D. Second Moment	37
E. Line Shape Function at Resonance	37
F. Line Shape Fitting	38
III. RESULTS AND DISCUSSION	39
A. Absorption Saturation	39
1. Absorption spectra at various rf levels	39
2. Ratio of the Zeeman and dipolar relaxation times	41
3. Progressive saturation of the absorption signal	43
B. Dispersion Saturation	44
1. Dispersion spectra at various rf levels	44
2. Progressive saturation of the dispersion signal	45
3. Spin lattice relaxation time	46
4. Check on restrictions	46
C. Comparison with $T_1$ Measured by Adiabatic Rapid Passage	49
IV. CONCLUSIONS	50
REFERENCES	51
chapter 3.    SATURATION III.	
PROGRESSIVE SATURATION IN	
POTASSIUM CAPROATE AND LITHIUM STEARATE	52
I. EXPERIMENTAL	52
II. RESULTS AND DISCUSSION	53
A. Potassium Caproate	53
1. Absorption spectra at various rf levels	53
2. Progressive saturation of absorption	54
3. Progressive saturation of dispersion	56
B. Lithium Stearate	58
1. Absorption saturation	58
2. Progressive saturation of dispersion	59
III. CONCLUSIONS	60
REFERENCES	62
chapter 4.    SATURATION IV.	
SIGNAL DECAY EXPERIMENTS IN	
POTASSIUM CAPROATE AND LITHIUM STEARATE	63
I. INTRODUCTION	63
II. EXPERIMENTAL	64
A. Samples	64
B. Spectrometer	64
C. Method	65
III. RESULTS AND DISCUSSION	66
A. Potassium Caproate	66
B. Lithium Stearate	67
IV. CONCLUSIONS	69
REFERENCES	70

chapter 5.	ADIABATIC RAPID PASSAGE I. THEORY AND REVIEW	71
	I. INTRODUCTION	72
	II. ADIABATIC RAPID PASSAGE SIGNAL	74
A.	Adiabatic Variation of the Magnetization	74
B.	The Rapid Passage Experiment	76
C.	ARP Signal Shape	77
	III. ADIABATIC INVERSION CONDITIONS	78
A.	Bloch Adiabatic Condition	78
B.	Possible Weaker Adiabatic Condition	79
C.	Comments on the $H_1$ to $H_L$ Ratio, Spin Temperature, and $T_2$	79
	IV. MEASUREMENT OF THE RELAXATION TIME $T_1$	81
A.	ARP Two Pass Method	81
B.	ARP Symmetric Sweep Method	85
	REFERENCES	88
chapter 6.	ADIABATIC RAPID PASSAGE II. RAPID PASSAGE EXPERIMENTS	89
	I. EXPERIMENTAL	89
A.	Spectrometer	89
B.	Samples	93
C.	Method	94
	II. RESULTS AND DISCUSSION	96
A.	Signal Shape and the Adiabatic Condition	96
B.	Local Field Measurements	101
C.	$T_1$ Measurements	107
	REFERENCES	112
chapter 7.	VARIATION OF THE NORMAL AND SATURATION NARROWED LINES IN LITHIUM STEARATE WITH TEMPERATURE	113
	I. EXPERIMENTAL	113
	II. RESULTS AND DISCUSSION	114
	REFERENCES	116
APPENDIX A.	Two Pass ARP with Low then High $H_1$	117
APPENDIX B.	Trigger Pulse Delay Unit	120
APPENDIX C.	Comments on "Adiabatic Rapid-Passage Experiments in Some Solids" by Janzen, Cyr, and Dunell	121

LIST OF ILLUSTRATIONS

Figure	Follows Page
chapter 1	
1 - Effective magnetic field in the rotating frame.	8
2 - Plot of $H_1/u_1(0)$ versus $H_1^2$ predicted by equation 40.	28
chapter 2	
1 - Absorption spectra of $\text{CaF}_2$ powder at various rf levels.	39
2 - Fitted normal and saturation narrowed absorption spectra of $\text{CaF}_2$ powder.	40
3 - Saturation narrowed spectra of $\text{CaF}_2$ at 40 and 80 Hz modulation frequencies.	41
4 - The absorption signal, $v_1(\text{max})$ , and $v_1(\text{max})/H_1$ as a function of the rf field intensity in $\text{CaF}_2$ .	43
5 - $H_1/v_1(\text{max})$ as a function of $H_1^2$ in $\text{CaF}_2$ .	43
6 - Dispersion spectra of $\text{CaF}_2$ powder at various rf levels and a modulation frequency of 20 Hz.	44
7 - Dispersion spectra of $\text{CaF}_2$ powder at various rf levels and a modulation frequency of 200 Hz.	44
8 - The dispersion signal, $u_1(0)$ , and $u_1(0)/H_1$ as a function of the rf field intensity in $\text{CaF}_2$ .	45
9 - $H_1/u_1(0)$ as a function of $H_1^2$ in $\text{CaF}_2$ .	45
chapter 3	
1 - Absorption spectra of potassium caproate at three rf field intensities.	53
2 - Maximum absorption signal in potassium caproate as a function of rf field intensity.	54
3 - Normalized dispersion signal, $u_1(0)/H_1$ , in potassium caproate as a function of rf field intensity.	56
4 - $H_1/u_1(0)$ in potassium caproate as a function of $H_1^2$ .	57
5 - Absorption spectra of lithium stearate at three rf field intensities.	58

	Follows Page
6 - Normalized dispersion signal, $u_1(0)/H_1$ , in lithium stearate as a function of rf field intensity.	59
7 - $H_1/u_1(0)$ in lithium stearate as a function of $H_1^2$ .	59

chapter 4

1 - Typical dispersion signal decay curves for potassium caproate and lithium stearate.	66
2 - Semilog plot of $a-a_s$ versus time for a potassium caproate dispersion signal decay curve.	66
3 - Semilog plot of $a-a_s$ versus time for a lithium stearate dispersion signal decay curve,	66

chapter 5

1 - Magnetization and effective field in the rotating reference frame.	74
--	----

chapter 6

1 - Diagram of Adiabatic Rapid Passage Spectrometer.	91
2 - Rapid passage signal shape in lithium stearate as a function of the adiabatic parameter A.	97
3 - Rapid passage signal shape in $\text{CaF}_2$ , $H_0$ along [100], as a function of the adiabatic parameter A.	97
4 - Rapid passage signal shape in $\text{CaF}_2$ , $H_0$ along [111], as a function of the adiabatic parameter A.	99
5 - ARP signals in polycrystalline $\text{CaF}_2$ and liquid trifluoroacetic acid at 16 MHz. $A = 6.7$ .	101
6 - ARP signals in the $\text{CaF}_2$ single crystal for $H_0$ along the [111], [011], and [100] directions. $A = 6.7$ .	102
7 - ARP signals in polycrystalline $\text{CaF}_2$ and liquid trifluoroacetic acid at 8 MHz. $A = 27$ .	104
8 - $T_1$ measurement in $\text{CaF}_2$ crystal by ARP symmetric sweep method. Intervals between sweeps and scope ranges are given in figure.	107
9 - $T_1$ measurement in $\text{CaF}_2$ powder by ARP symmetric sweep method.	110

- 10 -  $T_1$  measurement in maleic anhydride single crystal by ARP two-pass method. The period between the sweeps was 20 min 35 sec. 110

chapter 7

- 1 - Line width in fused and not-fused lithium stearate as a function of temperature. 114
- 2 - Saturation narrowed and normal line widths in not-fused lithium stearate as a function of temperature. 114
- 3 - Second moment in fused and not-fused lithium stearate as a function of temperature. 115

### ACKNOWLEDGEMENTS

I would like to thank Professor B.A. Dunell for introducing me to the field of nuclear magnetic resonance and for encouraging and supporting me in this work.

I am indebted to Dr. R.F. Snider who tried to teach me density matrices and was considerable help in understanding Provotorov theory.

The financial assistance of the National Research Council, the Standard Oil Company of British Columbia, and the University of British Columbia are gratefully acknowledged.

Finally, I would like to express my sincere appreciation to my wife, Marilyn, for her moral support and patience during the long time it took to do the research and write this thesis.

## chapter 1.

## SATURATION I.

## SATURATION THEORIES

## I. BLOEMBERGEN, PURCELL, and POUND THEORY

A. Introduction

The BPP /1/ theory of nuclear magnetic resonance saturation in solids is based on the following three assumptions which are nicely set out in Redfield /2/.

(1) The first is that the effect of the spin lattice interaction is to relax the spins to their equilibrium state with a time constant  $T_1$ .

(2) The second is that the spins interact strongly with one another. Then any energy absorbed at one frequency of the dipolar broadened resonance line is quickly transferred to all the spins whether or not they are in a local field exactly corresponding to the resonance value for the applied radio-frequency field. This appears to be justified because of the possibility of mutual spin flips between neighbouring nuclei brought about by the dipolar interaction.

(3) The third assumption is that the complex rf magnetic

susceptibility  $\chi = \chi' - i\chi''$  is proportional to the difference in population of the nuclear spin levels and is not affected by the presence of the rf field except via the spin level populations, which are. When the spin system becomes saturated, the populations of the nuclear spin levels become more nearly equal. It follows then from this third assumption that both the real  $\chi'$  and the imaginary  $\chi''$  parts of the rf susceptibility saturate in the same way.

### B. Fundamental Equation of BPP

Consider a system of spins  $I$  placed in a magnetic field  $H_0$  (taken to be along the z-axis) and subjected to a radio frequency field of amplitude  $H_1$  perpendicular to  $H_0$  and rotating with an angular frequency  $\omega$  close to the Larmor frequency  $\omega_0 = \gamma H_0$  of the spins. The fundamental equation of BPP theory for this system is the following spin transition rate equation which includes both thermal processes (the spin-lattice relaxation) and transitions induced by the applied rf field:

$$\frac{dn(t)}{dt} = \frac{n(0) - n(t)}{T_1} - 2W n(t). \quad (1)$$

Here  $n(t)$  is the difference in the populations of the two levels between which the rf field induces transitions;  $n(0)$  is the equilibrium population difference before application of the rf field;  $T_1$  is the spin-lattice relaxation time;  $W = \gamma^2 H_1^2 \pi g(\Delta)/2$  and is the probability per unit time of a transition by a spin between the two levels induced by the rf field;  $\Delta = \omega_0 - \omega$ ; and  $g(\Delta)$ , normalized to  $\int_{-\infty}^{+\infty} g(\Delta) d\Delta = 1$ , is the shape function of the unsaturated resonance line.

Since the nuclear magnetism  $M_Z$  of a system of spins in a magnetic field  $H_0$ , which is taken to be in the  $Z$  direction, will be proportional to the spin population difference  $n(t)$ , we can, following Abragam /3, chap 3 and 12/, use equation (1) to obtain a rate equation for the Zeeman energy of the spins:

$$\frac{d}{dt} (-M_Z H_0) = -\frac{(M_0 - M_Z)}{T_1} H_0 + 2W M_Z H_0, \quad (2)$$

where the equilibrium magnetization  $M_0 = \chi_0 H_0$  and  $\chi_0$  is the static magnetic susceptibility. In the steady state, equation (2) gives us the energy transferred per unit time to the lattice:

$$\frac{(M_0 - M_Z)}{T_1} H_0 = \frac{2W M_0 H_0}{1 + 2W T_1}, \quad (3)$$

which is equal to the rate of rf energy absorption by the spins.

### C. RF Power Absorption

The rotating field  $H_1$  is actually produced by a linearly polarised field  $H_x = 2 H_1 \cos \omega t$ , the counter-rotating component having a negligible effect. If this excitation is sufficiently small, the response  $M_x(t)$  of the spin system may be assumed proportional to it and can be written:

$$M_x(t) = 2 H_1 \left\{ \chi'(\omega) \cos \omega t + \chi''(\omega) \sin \omega t \right\}, \quad (4)$$

where the rf susceptibility  $\chi = \chi' - i \chi''$ .

The rate of rf energy absorbed by the spin system is:

$$P = - \frac{\overline{M \cdot \frac{dH}{dt}}}{dt} = - \overline{M_x \frac{dH_x}{dt}}. \quad (5)$$

Using  $H_x = 2 H_1 \cos \omega t$  and equation (4), and evaluating equation (5) by integrating, we find  $P = 2 H_1^2 \chi'' \omega$ . (6)

Equation (6) also indicates why  $\chi''$  is usually called the absorption component of  $\chi$ .

#### D. Magnetic Susceptibilities

We can now find the imaginary or absorption part  $\chi''$  of the rf susceptibility. Equating expressions (3) and (6) and substituting for  $W$  we have:

$$\chi'' = \frac{\chi_0 \omega_0 \pi g(\Delta)/2}{1 + \gamma^2 H_1^2 T_1 \pi g(\Delta)} \quad (7)$$

Finally the dispersion part  $\chi'$  of  $\chi$  can be deduced from  $\chi''$  by the Kramers-Kronig relations. Although the K-K relations are not valid in the presence of saturation it was generally believed that the saturation behaviour obtained from them would at least be qualitatively correct.

At the centre of resonance when  $\Delta = 0$ , equation (7) becomes:

$$\chi''(0) = \frac{\chi_0 \omega_0 \pi g(0)/2}{1 + \gamma^2 H_1^2 T_1 \pi g(0)} \quad (8)$$

and for very strong rf fields when  $\gamma^2 H_1^2 T_1 \pi g(0) \gg 1$

$$\chi''(0) = \frac{\chi_0 \omega_0}{2 \gamma^2 H_1^2 T_1} = \frac{M_0}{2 \gamma H_1^2 T_1} \quad (9)$$

### E. Comparison of the Various Theories with Experiment

While in principle equation (1) provides a correct description of absorption observed in the region of weak saturation, that is, up to values of  $H_1$  such that  $\gamma^2 H_1^2 T_1 \pi g(\Delta) \approx 1$ , it strongly disagrees with experiment in the region of strong saturation /2,4/. For example, both  $\chi''$  and  $\chi'$  become narrower and nearly Lorentzian in shape on saturation and the dispersion signal does not decrease nearly as rapidly as that of absorption with increasing  $H_1$ . Equation (7), on the other hand, indicates that the absorption line should widen with increasing  $H_1$  for all values of  $H_1$ .

Although the above effects were observed in metals by Redfield /2/ in 1955 and by Abell and Knight in 1954 /4/, they did not seem to become widely known until recently. Abragam /3/ in "Nuclear Magnetism" (1961) chap 12, mentions Redfield's observation of the anomolous behaviour of the  $\chi'$  signal amplitude but not a word about narrowing of the lines.

It was the observation of suspiciously narrow absorption lines in some fatty acid salts in 1962 while the author was working on his Masters Thesis that led to the work presented here. The narrowing was observed in dispersion also and was found to be caused by the inadvertent use of high rf levels. Fortunately, at about this time Provotorov's theory, "Magnetic Resonance Saturation in Crystals" /5/ was published in English and did predict saturation narrowing in solids. Unfortunately it did not come immediately to our attention. When it did, however, it happily

made our task somewhat easier although it made much of the work already done of diminished importance. These experiments did at least give us a feeling for the practical aspects of saturation.

Before going on it is useful here to anticipate another of the results of Provotorov. If  $\Delta = 0$  the BPP equations agree with Provotorov theory even for strong saturation. Equation (9) also agrees with a theory developed by Redfield /2/ which is applicable to solids only at very high rf levels. Unfortunately the field modulation and lock-in amplifier technique usually used to record wide lines in solids yields the first derivative of  $\chi''(\Delta)$  which is zero at  $\Delta = 0$ . One might consider taking complete  $\frac{d}{d\Delta} \chi''(\Delta)$  curves and integrating them to get  $\chi''(0)$  and study saturation but we shall see that other complications arise.

## II. REDFIELD THEORY

### A. Introduction

The results of BPP can also be obtained using the concept of a spin temperature distinct from the lattice temperature. The assumption that the complex susceptibility is proportional to the difference in population of the adjacent nuclear spin levels is equivalent to the assumption that the spin system behaves as if it were at equilibrium at a spin temperature (referred to the laboratory frame of reference) higher than the lattice temperature, the equilibrium corresponding to the actual

distribution of nuclear spins among the  $2I + 1$  levels /2/.

In order to explain the NMR signals he observed in the solids  $Al^{27}$  and  $Cu^{63}$  — the important feature being that the dispersion does not saturate at the same level as the absorption, although both  $\chi'$  and  $\chi''$  become narrower in width on saturation — Redfield /2/ proposed that, when a strong rf magnetic field is applied, the spin system can be described by the existence of a spin temperature in a frame of reference rotating about  $H_0$  with a frequency  $\omega$ . In addition the spin temperature can be different from the lattice. A theory was then developed which is applicable only to solids at high rf field intensities when  $\gamma^2 H_1^2 \pi g(\Delta) \gg 1$  and which was in reasonable agreement with his experimental observations. Redfield transforms the spin system Hamiltonian which includes dipole-dipole interactions and also interactions of the spins with  $H_0$  and with  $H_1(\omega)$  into the rotating frame described above. The resulting time-dependent parts of the spin-spin interaction are weak perturbations on the time-independent part, and can be ignored. Statistical mechanics is applied to the remaining stationary spin Hamiltonian; specifically it is assumed that the spin system is in a canonical distribution of quantum states with respect to the transformed spin Hamiltonian. It is also assumed that the spin-lattice interaction is small compared to that of the rf field.

### B. Rotating Frame Formulation

The Schrodinger equation describing the behaviour of a spin wave function  $\Psi$  in a fixed coordinate system is:

$$i\hbar \dot{\Psi} = \widehat{H} \Psi .$$

Transformation to the coordinate frame rotating about the z-axis, direction of  $H_0$ , with angular frequency  $\omega$  is performed with the unitary operator /3, p 23/,

$$\widehat{U}_r = e^{-i\omega t \widehat{I}_z} = e^{-i\omega t \sum_j I_j z}$$

so that

$$\Psi = \widehat{U}_r \Psi_r ,$$

where the subscript  $r$  designates quantities relative to this rotating frame. If this transformation is applied to the Schrodinger equation we obtain:

$$\begin{aligned} i\hbar \dot{\Psi}_r &= [-\hbar \omega \widehat{I}_z + \widehat{U}_r^{-1} \widehat{H} \widehat{U}_r] \Psi_r , \\ &= [-\hbar \omega \widehat{I}_z + \widehat{H}_r] \Psi_r , \\ &= \widehat{H}_{er} \Psi_r \end{aligned} \quad (10)$$

where  $\widehat{H}_{er}$  is called the effective Hamiltonian in this rotating frame.

If the lattice is neglected, i.e., no relaxation, the Hamiltonian for our spin system is:

$$\begin{aligned} \widehat{H}_{er} &= \widehat{Z}_r + \widehat{H}_D^r \\ &= \widehat{Z}_r + \widehat{H}_D' + \text{time dependent terms.} \end{aligned} \quad (11)$$

The first term is the Zeeman energy of the system

$$\widehat{Z}_r = -\gamma \hbar H_{er} \cdot \sum_1 \widehat{I}_1 \quad (12a)$$

in which  $\tilde{H}_{er}$  is the effective external magnetic field in the rotating frame and is:

$$\tilde{H}_{er} = H_1 \tilde{i} + (H_0 - \omega/\gamma) \tilde{k} \quad (12b)$$

The diagram illustrates the vector addition of the external magnetic field  $H_0$  (vertical) and the effective field  $H_{er}$ . The effective field  $H_{er}$  is the resultant of  $H_1$  (horizontal) and  $(H_0 - \omega/\gamma)$  (vertical). The angle  $\theta$  is shown between  $H_{er}$  and  $H_1$ . A dashed line indicates the vertical component of  $H_{er}$  is  $H_0 - \omega/\gamma$ .

Fig. 1 - Effective magnetic field in the rotating frame.

The axes of the rotating frame have been chosen so that

$$\tilde{H}_0 = H_0 \tilde{k}, \quad \tilde{H}_1 = H_1 \tilde{i}, \quad \text{and} \quad \tilde{\omega} = -\omega \tilde{k}.$$

$\tilde{H}_{er}$  then is constant in time and we see that the transformation has made the solution to the motion of the system much simpler.

The time independent portion of the dipolar energy of the spins  $\hat{H}_D'$ , sometimes called the truncated spin-spin Hamiltonian, is given by:

$$\hat{H}_D' = \sum_{i>j} \frac{1}{2} \frac{\gamma^2 \hbar^2}{r_{ij}^3} (3 \cos^2 \phi_{ij} - 1) \left[ \tilde{I}_i \cdot \tilde{I}_j - 3 \tilde{I}_{iz} \tilde{I}_{jz} \right] \quad (12c)$$

Here,  $\phi_{ij}$  is the angle between the vector  $\tilde{r}_{ij}$  joining two spins  $\tilde{I}_i$  and  $\tilde{I}_j$  and the z-axis. We have supposed that indirect spin-spin interactions are absent.

The time-dependent terms of  $\hat{H}_{er}$  have a frequency of the order of  $\omega$  and  $2\omega$  and can connect states which differ in effective energy by  $\pm \hbar\omega$  or  $\pm 2\hbar\omega$ , whereas the eigenstates

of  $\hat{\mathcal{H}}_{er}$  (time independent part) differ by about  $\gamma \hbar (H_{er} \pm H_L)$  which is of the order of tens of kHz rather than the MHz radio frequencies of  $\omega$ . Therefore the time dependent terms will be ineffective in perturbing the eigenstates of  $\hat{\mathcal{H}}_{er}$  and will be ignored. The "local field"  $H_L$  will be defined later.

### C. Spin Temperature and Canonical Distribution

The hypothesis of a spin temperature and a canonical distribution in the rotating frame means that the occupational probability  $P_i$  of the energy levels of the system is given by the Boltzmann distribution:

$$P_i \propto \exp (E_i/kT_s)$$

where  $E_i$  is an energy level of the spin system as viewed by an observer in the rotating frame, and  $T_s$  is the temperature of the spin system in the rotating frame. The spin system can then be described by a density matrix of the form:

$$\hat{\rho}_r = \frac{\exp (-\hat{\mathcal{H}}_{er}/kT_s)}{\text{tr} [\exp (-\hat{\mathcal{H}}_{er}/kT_s)]} . \quad (13)$$

With  $\hat{\rho}_r$  one is able to calculate the canonical average expectation value  $\langle\langle Q \rangle\rangle$  of an observable  $Q$  whose operator is  $\hat{Q}$ , by a trace calculation  $\langle\langle Q \rangle\rangle = \text{tr} (\hat{Q} \hat{\rho}_r)$ .  $\langle\langle Q \rangle\rangle$ , sometimes denoted  $\overline{\langle Q \rangle}$ , is also called the ensemble average of  $\langle Q \rangle$  and occasionally just thermal average. The second bra-ket or the bar are frequently omitted in the literature to simplify the notation. We shall do the same. The situation is clarified if we remember that whenever the density matrix is used, the canonical average is intended.

On applying the above relation to the energy operators  $\hat{Z}_r$  and  $\hat{H}_D'$  one obtains /6/,

$$\frac{\langle Z_r \rangle}{H_{er}^2} = \frac{\langle H_D' \rangle}{H_L^2} = \frac{\langle H_{er} \rangle}{H_{er}^2 + H_L^2} = -N \frac{I(I+1) \gamma^2 \hbar^2}{3 kT_s} \quad (14a)$$

where  $N$  is the number of spins and

$$H_L^2 = \frac{\text{tr} (\hat{H}_D')^2}{\text{tr} (\gamma^2 \hbar^2 \sum_1 I_{1z}^2)} = \frac{1}{3} \langle \Delta H^2 \rangle \quad (14b)$$

$H_L$  is called the local field and  $\langle \Delta H^2 \rangle$  is the Van Vleck second moment of the unsaturated absorption line. Using the total magnetization operator  $\hat{M} = \gamma \hbar \sum_1 I_1$  it is found that the observable magnetization  $\langle \underline{M} \rangle$ , which will also be called  $\underline{M}_r$ , is along  $\underline{H}_{er}$  and equals /6/,

$$\langle \underline{M} \rangle = - \frac{\langle Z_r \rangle}{\underline{H}_{er}} \quad (14c)$$

#### D. Spin Lattice Relaxation

We now wish to determine the expectation value of  $\hat{H}_{er}$  when the spin-lattice interaction is taken into account. Redfield assumes that the effect of the interaction is to relax each nucleus independently into its equilibrium state with a time constant  $T_1$ :

$$\frac{\partial}{\partial t} \Big|_{SL} \langle \underline{I}_j \rangle = - \frac{(\langle \underline{I}_j \rangle - \langle \underline{I} \rangle_0)}{T_1} \quad (15)$$

where the left-hand side is the spin-lattice contribution to the time derivative of the expectation value of  $I_{\tilde{j}}$ , and  $\langle I_{\tilde{j}} \rangle_0$  is the static thermal equilibrium value of  $I_{\tilde{j}}$ , given by:

$$\langle I_{\tilde{j}} \rangle_0 = \frac{g \beta I(I+1) H}{3 kT}$$

Here  $g$  is the nuclear  $g$ -factor,  $\beta$  is the Bohr magneton and  $H$  is the applied field which can be closely approximated by  $H_0 k$  since  $H_1 \ll H_0$ . The field  $H$  is used above rather than  $H_{er}$  because it is assumed that electrons are responsible for the relaxation and they are little affected by the rf field and see only the large field  $H_0$ .

It is also assumed that the spin-lattice interaction does not perturb the spin system canonical distribution appreciably except to bring about a slow change in  $\langle \mathcal{H}_{er} \rangle$ . The contribution of the first term in equation (15) to the variation of  $\langle \mathcal{H}_{er} \rangle$  is

$$\frac{\partial}{\partial t} \Big|_1 \langle \mathcal{H}_{er} \rangle = - \frac{\langle Z_r \rangle}{T_1} - \frac{2 \langle \mathcal{H}_D' \rangle}{T_1} . \quad (16a)$$

The effective Zeeman energy  $\langle Z_r \rangle$  is linear in the spin operators  $I_{\tilde{j}}$ , and thus expected to decay to zero with characteristic time  $T_1$ . The spin-spin energy  $\langle \mathcal{H}_D' \rangle$ , on the other hand, is quadratic in the spin operators and is therefore expected to decay at twice the rate of the Zeeman energy; thus the factor of two in the second term of equation (16a). The contribution of the second term of equation (15) is:

$$\frac{\partial}{\partial t} \Big|_2 \langle \mathcal{H}_{er} \rangle = - \frac{M_0 H_{er} \cos \theta}{T_1} , \quad (16b)$$

where we recall that  $\underline{M}_0 = \chi_0 \underline{H} \approx \chi_0 H_0 \underline{k}$  and is the total nuclear magnetization in the fixed frame.

We can now obtain the steady-state value of  $\underline{M}_r$  by using equations (14) and setting the sum of equation (16a) and (16b) to zero. The result is Redfield's equation 38 (Red. 38),

$$M_{Or} = \frac{M_0 \cos \theta}{1 + 2 H_L^2 / H_{er}^2} .$$

### E. Complex Magnetic Susceptibility at High $H_1$

The dispersion is given by  $\chi' = M_{Or} \sin \theta / 2H_1$  thus (Red. 40)

$$\chi' = \frac{M_0 \gamma \Delta}{2 \{ \Delta^2 + \gamma^2 [H_1^2 + 2H_L^2] \}} , \quad (17)$$

and we see that the dispersion is Lorentzian for strong saturation. The dispersion derivative at resonance is (Red. 41)

$$\left. \frac{\partial \chi'}{\partial \Delta} \right|_{\Delta=0} = \frac{M_0}{2 \gamma [H_1^2 + 2 H_L^2]} . \quad (18)$$

If  $\underline{M}_r$  is along  $\underline{H}_{er}$ , as equation (14c) indicates it is immediately concluded that there is no component in the x direction and therefore no absorption. Actually  $\underline{M}_r$  is not precisely in the  $\underline{H}_{er}$  direction and at any rf level there is a finite absorption which can be predicted by invoking conservation of energy in the system, as was done in the previous section. The rate of energy transfer from the spin system to the lattice  $-H_0 (M_z - M_0) / T_1$  is calculated and equated to that absorbed by

the spin system from the rf field,  $2\omega H_1^2 \chi''$ , and one gets (Red. 43)

$$\chi'' = \frac{M_0}{2 \gamma H_1^2 T_1} \left\{ 1 + \frac{\Delta^2}{\gamma^2 [H_1^2 + 2H_L^2]} \right\}^{-1}, \quad (19)$$

which is again a Lorentzian line. At resonance, equation (19) agrees with the BPP asymptotic value of  $\chi''$  at high  $H_1$ , equation (9). This agreement corresponds to the fact that, for both theories, at the limit of very large  $H_1$ ,  $M_z \rightarrow 0$  and  $\chi''$  is uniquely determined by this simple conservation of energy argument. This agreement indicates that a progressive saturation method of obtaining  $T_1$  using equation (8) may be correct. This is not necessarily true of the absorption derivative observed by lock-in detection, however, because Redfield /2/ found that energy can also be absorbed from the audio modulation field (rotary saturation), and this effect perturbs the true absorption curve.

Redfield's rotating frame spin temperature hypothesis has been tested and exploited by a number of experimenters, Solomon & Ezzratty /6/, Goldberg /7,8/, and Slichter & Holton /9/. These references are also quite useful in understanding Redfield's theory. In addition Redfield has refined his methods in a "Statistical Theory of Spin Resonance Saturation" /10/ and reaffirmed his earlier hypothesis.

### III. PROVOTOROV THEORY

#### A. Introduction

We now have a theory for saturation of a spin system in a solid under a very weak rf irradiation and a very strong one, but do not know how to find the behaviour in between. Provotorov /5,11/, using powerful statistical mechanical methods, has found the solution to this problem.

Provotorov considers a spin system in a large magnetic field in which a single spin species gives rise to a single ordinary NMR absorption line, the width of which is mainly due to dipole-dipole couplings. He then assumes that such a system can be described as a superposition of a number of subsystems. A "Zeeman" subsystem and a "dipole-dipole" subsystem. A weak applied rf field can be considered as an additional subsystem. The coupling inside each subsystem is strong, whereas the couplings between subsystems are weak. As a consequence, the subsystems reach internal thermal equilibrium independently of each other and one can ascribe a temperature an energy and an entropy to each of them. A theoretical discussion and justification of these ideas has been given by Philippot /12/.

#### B. Derivation of the Density Matrix

Following Redfield, Provotorov transforms into the rotating frame, however, he splits up the Zeeman energy term into its main field and rf field components so that the total effective Hamiltonian in the rotating frame is written:

$$\begin{aligned}\widehat{\mathcal{H}}_{er} &= \hbar \Delta \widehat{I}_z + \widehat{\mathcal{H}}_D' + \hbar \gamma H_1 \widehat{I}_x \\ &= \widehat{\mathcal{H}}_0 + \hbar \gamma H_1 \widehat{I}_x\end{aligned}\quad (20)$$

where  $\widehat{I}_x$ ,  $\widehat{I}_y$  and  $\widehat{I}_z$  are the projection operators of the total spin on the coordinate axes. If  $H_1$  is small so that  $H_1 \ll H_L$ ,  $\hbar \gamma H_1 \widehat{I}_x$  can be considered as a small perturbation which will couple the operators  $\hbar \Delta \widehat{I}_z$  and  $\widehat{\mathcal{H}}_D'$ . He goes over into the interaction representation so that:

$$\widehat{\rho}'' = e^{\frac{1}{\hbar} \widehat{\mathcal{H}}_0 t} \widehat{\rho}' e^{-\frac{1}{\hbar} \widehat{\mathcal{H}}_0 t} \quad (21)$$

where  $\widehat{\rho}''$  is the density matrix in the interaction representation and  $\widehat{\rho}'$  the density matrix in the rotating frame.

Assuming the usual high temperature approximation ( $\widehat{\mathcal{H}}_{er} \ll k T_s$ ) and allowing for different Zeeman and dipolar term temperatures in  $\widehat{\mathcal{H}}_0$ , a density matrix for the spin system in this representation is proposed to be of the form:

$$\widehat{\rho}''(t) \propto \alpha(t) \widehat{I}_z + \beta(t) \widehat{\mathcal{H}}_D' \quad (22)$$

A kinetic equation for  $\widehat{\rho}''(t)$  (the master equation) is obtained using Zwanzig's method /13/ in which the density matrix is required to obey the Liouville equation:

$$\frac{\partial \widehat{\rho}''(t)}{\partial t} = -\frac{1}{\hbar} [\widehat{X}(t), \widehat{\rho}''(t)] \quad (23)$$

where

$$\widehat{X}(t) = \hbar \gamma H_1 e^{\frac{1}{\hbar} \widehat{\mathcal{H}}_0 t} \widehat{I}_x e^{-\frac{1}{\hbar} \widehat{\mathcal{H}}_0 t}$$

A projection operator is then applied to extract from  $\hat{\rho}''$  the diagonal part  $\hat{\rho}_1$  and the nondiagonal part  $\hat{\rho}_2$ . The Liouville equation becomes a pair of equations and solutions are found for  $\hat{\rho}_1(t)$  and  $\hat{\rho}_2(t)$ . From these solutions Provotorov then derives the nuclear magnetic resonance equations. In doing so he assumes

$$1/T_1 \ll \delta H_L ,$$

however, this condition is usually fulfilled in solids and presents no problem.

### C. Evolution of the Spin Temperatures

The result of the  $H_1$  perturbation is to cause a slow evolution of  $\hat{\rho}''$  with time, and this is manifested as a variation of  $\alpha(t)$  and  $\beta(t)$ . The diagonal part of the density matrix yields the power absorption equation and the conservation of energy law:

$$\frac{d}{dt} \text{tr} (\hat{\rho}_1(t) \hat{\mathcal{H}}_0) = 0 \quad (24)$$

In the course of his derivation, Provotorov obtains the following equations for the ensemble average values of  $\hat{I}_z(t)$  and  $\hat{\mathcal{H}}_D(t)$  (Prov. 34),

$$\begin{aligned} \langle I_z \rangle &= \frac{\alpha(t) \text{tr} \hat{I}_z^2}{(2I + 1)^N} , \\ \langle \mathcal{H}_D' \rangle &= \frac{\beta(t) \text{tr} (\hat{\mathcal{H}}_D')^2}{(2I + 1)^N} , \end{aligned} \quad (25)$$

where  $N$  is the number of spins in the sample, and the variation

of  $\langle I_z \rangle$  with time (Prov. 33<sup>r</sup>)

$$\frac{d}{dt} \langle I_z \rangle = -\gamma^2 H_1^2 \pi g(\Delta) [\alpha(t) - \hbar \Delta \beta(t)] . \quad (26)$$

Substitution of  $\alpha(t)$  and  $\beta(t)$  from expressions (25) into equation (26) yields (Prov. 35)

$$\frac{d}{dt} \langle I_z \rangle = -\gamma^2 H_1^2 \pi g(\Delta) [\langle I_z \rangle - \hbar(t)] \quad (27)$$

in which

$$\hbar(t) = \hbar \Delta \frac{\langle \chi_D' \rangle}{H_D^2}, \quad \text{and} \quad H_D^2 = \frac{\text{tr} (\hat{\chi}_D')^2}{\text{tr} \hat{I}_z^2} \quad (28)$$

$H_D = \gamma \hbar H_L$  where  $H_L$  is the local field of Redfield theory. An expression for  $d\hbar(t)/dt$  is obtained using the conservation law equation (24)

$$\frac{d}{dt} \langle \chi_D' \rangle + \hbar \Delta \frac{d}{dt} \langle I_z \rangle = 0$$

so

$$\frac{d}{dt} \hbar(t) = \frac{\hbar^2 \Delta^2}{H_D^2} \pi g(\Delta) [\langle I_z \rangle - \hbar(t)] \quad (29)$$

#### D. Spin Lattice Relaxation

Taking into account the spin-lattice interaction in the manner of BPP /1/ the following system of equations are obtained (Prov. 36,37):

$$\frac{d}{dt} \langle I_z \rangle = -\gamma^2 H_1^2 \pi g(\Delta) [\langle I_z \rangle - \hbar(t)] + \frac{[\langle I_z \rangle_0 - \langle I_z \rangle]}{T_1}$$

(30)

$$\frac{d}{dt} h(t) = \frac{\hbar^2 \Delta^2}{H_D^2} \gamma^2 H_1^2 \pi g(\Delta) [\langle I_z \rangle - h(t)] + \frac{[h(0) - h(t)]}{T_D} \quad (31)$$

Here  $\langle I_z \rangle_0$  and  $h(0)$  are the initial values of  $\widehat{I}_z(t)$  and  $h(t)$ , while  $T_1$  and  $T_D$  are the spin lattice relaxation times of  $\langle I_z \rangle$  and  $\langle \chi_D' \rangle$ . We note that for the centre of resonance when  $\Delta = 0$ ,  $h(t) = 0$ , equation (30) reduces to the Bloembergen, Purcell and Pound equation (1). This means that the average value of the energy of the dipole-dipole interaction in the case  $\Delta = 0$  is not changed after the rf field is turned on, and the ensemble average value of the projection of the total spin  $\widehat{I}_z(t)$  tends to zero at high  $H_1$  in accordance with equation (1).

A completely different situation arises in the case  $\Delta \neq 0$ . In this case the absorption of each quantum of rf energy is accompanied by a change of  $\hbar\Delta$  in the dipole-dipole energy. As a consequence Provotorov finds that  $\langle I_z(t) \rangle$  no longer approaches zero as in BPP theory but reaches an equilibrium value of (Prov. 27)

$$\langle I_z \rangle_\infty = \frac{\langle I_z \rangle_0 \Delta^2}{\Delta^2 + H_D^2} \quad (32)$$

The spin process involved can be described in the following way: one photon of energy  $\hbar\omega$  is absorbed ( $\omega$  is close to  $\omega_0$ ), one spin flips, but the difference in Zeeman levels is  $\hbar\omega_0 = \hbar\gamma H_0$ , so the balance of energy goes into the dipole-dipole system

$$-\hbar\omega + \hbar\omega_0 - \hbar\Delta = 0 .$$

This system will then tend to relax back to its equilibrium value exchanging energy with the lattice with a time constant  $T_D$ .

### E. Power Absorption

The energy absorbed per unit time in steady state is found using equations (30) and (31) and the property that  $\dot{h}(0) \ll \langle I_z \rangle_0$ . (Prov. 38)

$$\begin{aligned} P(\Delta, H_1) &= \hbar \omega 2W(\Delta) [\langle I_z \rangle_{st} - h_{st}] \\ &= \frac{\hbar \omega 2W(\Delta) \langle I_z \rangle_0}{1 + 2W(\Delta) T_1 \left[ \frac{1 + \hbar^2 \Delta^2 T_D}{H_D^2 T_1} \right]} \end{aligned} \quad (33)$$

where we recall that  $2W(\Delta) = \gamma^2 H_1^2 \pi g(\Delta)$ .

The solution to the non-diagonal part of the density matrix  $\hat{\rho}_2(t)$  is necessary to determine the dispersion signal. The solution yields the equations (Prov. 45, 46)

$$\langle I_x \rangle = \gamma H_1 \pi g'(\Delta) \left[ \langle I_z \rangle - h(t) + \frac{\dot{h}(t)}{\Delta} \right] \quad (34)$$

$$\langle I_y \rangle = \gamma H_1 \pi g(\Delta) [\langle I_z \rangle - h(t)] \quad (35)$$

Here  $g'(\Delta)$  is the dispersion line shape function ( $-J_1(\Delta)/\pi$  in Provotorov) obtained from  $g(\Delta)$ , the absorption line shape function, by the Kramers-Krönig relation.

### F. Complex Magnetic Susceptibility

Using the steady state solutions  $\langle I_z \rangle_{st}$  and  $h_{st}$  from

equation (30) and (31) Provotorov obtains expression for  $\chi'$  and  $\chi''$  (Prov. 47, 48)

$$\begin{aligned}\chi' &= \frac{\gamma \hbar}{2H_1} \langle I_x \rangle_{st} \\ &= \frac{\hbar \gamma^2}{2} \langle I_z \rangle_0 \left\{ \frac{\pi g'(\Delta) + \gamma^2 H_1^2 (\Delta/H_D^2) \pi g(\Delta) T_D}{1 + \gamma^2 H_1^2 \pi g(\Delta) T_1 \left[ 1 + \frac{T_D \hbar^2 \Delta^2}{T_1 H_D^2} \right]} \right\} \quad (36)\end{aligned}$$

Our equation (36) is obtained from Provotorov's equation (47) by substituting  $\pi g'(\Delta) = -J_1(\Delta)$ .

$$\begin{aligned}\chi'' &= \frac{\hbar \gamma}{2H_1} \langle I_y \rangle_{st} \\ &= \frac{\hbar \gamma}{2} \langle I_z \rangle_0 \left\{ \frac{\pi g(\Delta)}{1 + \gamma^2 H_1^2 \pi g(\Delta) T_1 \left[ 1 + \frac{T_D \hbar^2 \Delta^2}{T_1 H_D^2} \right]} \right\} \quad (37)\end{aligned}$$

### 1. Dispersion component

At a low rf level  $2W(\Delta) T_1 \ll 1$  and  $\chi'$  becomes

$$\chi' = \frac{\hbar \gamma^2}{2} \langle I_z \rangle_0 g'(\Delta) = \gamma M_0 \pi g'(\Delta) / 2 \quad (38a)$$

At a high level  $2W(\Delta) T_1 \gg 1$  and  $\gg g'(\Delta)$  so

$$\chi' = \frac{\gamma M_0 \Delta}{2 \left[ \frac{T_1 H_D^2}{T_D \hbar^2} + \Delta^2 \right]} \quad (38b)$$

which is Lorentzian and agrees with Redfield's result, equation (17)

for  $H_1 \ll H_L$  and  $T_1/T_D = 2$ .

At the centre of resonance where  $\Delta = 0$ , equation (36) becomes a form which we shall see is quite important to us experimentally:

$$\chi'(0) = \frac{\hbar \gamma^2 \langle I_z \rangle_0 \pi g'(0)/2}{1 + \gamma^2 H_1^2 \pi g(0) T_1} \quad (39)$$

The denominator in this equation is identical to that in our BPP equation (8) for  $\chi''(0)$  and so equation (39) is said to describe a normal saturation. Since the derivative is not zero at the centre of resonance, it appears that we can do a progressive saturation experiment using the usual broad-line techniques to determine  $T_1$ . In section IV we shall see what limiting conditions are necessary to get its true value.

The dispersion derivative at high  $H_1$  is:

$$\frac{d\chi'}{d\Delta} = \frac{\gamma M_0}{2} \left\{ \frac{1}{\frac{T_1 H_D^2}{T_D h^2} + \Delta^2} - \frac{2\Delta^2}{\left[ \frac{T_1 H_D^2}{T_D h^2} + \Delta^2 \right]^2} \right\}, \quad (40)$$

and at  $\Delta = 0$

$$\left. \frac{d\chi'}{d\Delta} \right|_{\Delta=0} = \frac{M_0 \gamma^2 \hbar^2}{2 \gamma (T_1/T_D) H_D^2} \quad (41)$$

On setting  $d\chi'/d\Delta = 0$  in equation (40) we find the dispersion line width at high  $H_1$  to be:

$$\Delta\omega_{ds} = 2 \sqrt{\frac{T_1}{T_D}} \cdot \frac{H_D}{\hbar}.$$

If the line width is measured in gauss we have:

$$\Delta H_{ds} = 2 \sqrt{\frac{T_1}{T_D}} \cdot H_L .$$

## 2. Absorption Component

At a low rf level we have the same result as we would get from BPP equation (7):

$$\chi'' = \frac{\kappa \gamma^2}{2} \langle I_z \rangle_0 \pi g(\Delta) = \gamma M_0 \pi g(\Delta) / 2 , \quad (43)$$

and at a high level the Loretzian curve

$$\chi'' = \frac{M_0}{2 \gamma H_1^2 T_1} \left\{ 1 + \frac{\Delta^2 T_1 \kappa^2}{T_D H_D^2} \right\}^{-1} \quad (44)$$

which again agrees with Redfield. We see that  $\chi''$ , which was a replica of  $g(\Delta)$  before saturation, now contains no information about the line shape function. It is particularly interesting to note that at  $\Delta = 0$  equation (37) Provotorov, and equation (7) BPP, are identical for all rf levels.

The absorption line width (from maximum to minimum slope) at a high rf level is:

$$\Delta \omega_{as} = \frac{2}{\sqrt{3}} \sqrt{\frac{T_1}{T_D}} \frac{H_D}{H} ,$$

and in Gauss:

$$\Delta H_{as} = \frac{2}{\sqrt{3}} \sqrt{\frac{T_1}{T_D}} H_L = \frac{2}{3} \sqrt{\frac{T_1}{T_D}} \langle \Delta H^2 \rangle^{\frac{1}{2}} . \quad (45)$$

Thus we have a means of measuring the  $T_1/T_D$  ratio since equation (45) yields:

$$\frac{T_1}{T_D} = \frac{9}{4} \frac{(\Delta H_{as})^2}{\langle \Delta H^2 \rangle}$$

We could also use the dispersion curve.

### G. Narrowing of the line on Saturation

Provotorov's theory predicts line narrowing on saturation.

Let us consider an absorption curve of gaussian shape:

$$g(x) = g(0) \exp \left( - \frac{x^2}{2 \sigma^2} \right)$$

where  $x = H_0 - H$  and  $\sigma^2$  is the second moment  $\langle \Delta H^2 \rangle$ .

The unsaturated line width will be  $\Delta H_a = 2 \langle \Delta H^2 \rangle^{\frac{1}{2}}$  so the saturated to unsaturated width ratio is:

$$\frac{\Delta H_{as}}{\Delta H_a} = \frac{1}{3} \sqrt{\frac{T_1}{T_D}}$$

and the absorption curve will narrow in the course of saturation

if  $\frac{T_1}{T_D} < 9$ .

Anderson and Redfield /14/ have obtained an expression for the ratio  $T_1/T_D = \delta$  in the case of relaxation by fluctuating fields due to the conduction electrons in metals. The fluctuating field on spin  $i$  is denoted by  $\tilde{h}_i(t)$ . They find

$$\delta = 2 + \frac{\sum_{j>k} K_{jk} r_{jk}^{-6}}{\sum_{j>k} r_{jk}^{-6}} ;$$

$r_{jk}$  is the distance between spins  $j$  and  $k$ , and  $K_{jk}$  expresses the degree of correlation between the fluctuating fields at  $r_j$  and  $r_k$  due to the conduction electrons:

$$K_{jk} = \frac{\langle \tilde{h}_j(t) \cdot \tilde{h}_k(t) \rangle_{av}}{\langle |\tilde{h}_j(t)|^2 \rangle_{av}} .$$

Here  $\langle \rangle_{av}$  denotes the time average.  $K_{jk} = 1$  for complete correlation, and zero if the fields at  $r_j$  and  $r_k$  are statistically independent.

Thus we can have a value of  $\delta$  between 3 and 2, the latter being the value proposed by Redfield /2/ previously for independent relaxation of spins, and we expect saturation narrowing. The above relaxation-correlation theory will not necessarily be true for other solids and other relaxation mechanisms, but does appear to be applicable to relaxation by paramagnetic impurities as is the case in  $\text{CaF}_2$  /6/.

Papers that have been useful in understanding Provotorov have been published by Goldburg /7/, Jeener et. al. /15/ and Goldman /16/.

#### IV. GOLDMAN ANALYSIS

##### A. Introduction

We now have an adequate theory for saturation in solids which covers the entire saturation region assuming only that  $H_1 \ll H_L$  and  $1/T_1 \ll \gamma H_L$ . Provotorov did not, however, calculate the

effects of the audio modulation of the external magnetic field one usually uses in conjunction with a lock-in amplifier and detector in order to record the weak signals from solids. Fortunately this has been done recently by M. Goldman /16/ using Provotorov's methods.

For a very low level of rf irradiation, one records the derivative of the absorption or dispersion curve using field modulation and lock-in detection. For a very high level, one records more complicated signals which have been analysed by Solomon and Ezzratty /6/. Goldman extends this analysis by means of Provotorov theory to the intermediate region. He finds that the recorded signals will not be the derivatives of the true absorption and dispersion curves because they are perturbed by field modulation saturation (rotary saturation of Redfield /2/) when the spin-lattice relaxation times are long. His analysis is developed under restrictive conditions which simplify the calculations, but they correspond, nevertheless, to practical experimental conditions.

The field modulation is parallel to the applied field  $H_0$  of amplitude  $\Delta_m$  and angular frequency  $\Omega$ . The following conditions are imposed:

- (1)  $\Delta_m$  is much less than the line width so that the derivation can be limited to first order,
- (2)  $\Omega \ll D$  where  $D = \gamma H_L$  so that  $\Delta$  varies very little during the time  $1/D$  and that the spin system can be characterised at every instant of time by the density matrix used by Provotorov /5/,
- (3)  $1/\Omega \ll T_1, T_D$ ,

(4)  $2W \ll \Omega^2 T_1, \Omega^2 T_D$  where  $2W(\Delta) = \gamma^2 H_1^2 f(\Delta)/2$ ,  
 $W$  is the transition probability, and Goldman normalizes the  
 line shape function  $f(\Delta)$  to  $2\pi$ .

### B. General Remarks

Modulation saturation (absorption of energy from the modulation) occurs if there exists a component of magnetization in quadrature with the modulated field. For a high rf level the magnetization follows  $\underline{H}_{er}$  as we have seen in Redfield theory. Therefore we have a component perpendicular to  $\underline{H}_0$  and can have absorption of the audio energy. At a low rf level, when  $2W \ll \Omega$ , this magnetism is much less and the modulation saturation will be small. Goldman states that the modulation saturation will be a maximum for values of  $H_1$  such that  $2W \approx \Omega$ . The study is divided into two areas: the region of low rf level defined by the condition  $2W \ll \Omega$  and the region of high rf level. Since we already have the condition of  $1/\Omega \ll T_1, T_D$ ; the situation for medium saturation  $2WT_1, 2WT_D \sim 1$  corresponds to  $2W \ll \Omega$ . We shall report here only the results for the lower rf level region. This means we must confine our studies to the region where  $\Omega \gg 2W$  and  $\gg 1/T_1, 1/T_D$ .

### C. Absorption Signal

The expression Goldman obtains for the lock-in detection absorption signal is: (Gold. 14)

$$v_1 = \frac{\Delta_m \gamma H_1 M_0/2}{1 + \gamma^2 H_1^2 \frac{f(\Delta)}{2} T_1 \left[ 1 + \frac{T_D \Delta^2}{T_1 D^2} \right]} \left\{ \frac{df(\Delta)}{d\Delta} - \gamma^2 H_1^2 \frac{f(\Delta)^2}{2} T_D \frac{\Delta}{D^2} \right\} \quad (46)$$

The first term is proportional to the absorption curve derivative and its saturation is normal. It goes through a maximum when  $2\omega T_1 \sim 1$  and decreases afterward. The second term, on the other hand, does not saturate but tends toward a constant.

The study of a lock-in absorption signal is unsuitable therefore for the measurement of  $T_1$ .

#### D. Dispersion Signal

The lock-in dispersion signal is (Gold.15)

$$u_1 = \frac{\Delta_m \gamma H_1 M_0/2}{1 + \gamma^2 H_1^2 \frac{f(\Delta)}{2} T_1 \left[ 1 + \frac{T_D \Delta^2}{T_1 D^2} \right]} \left\{ \frac{df'(\Delta)}{d\Delta} - f'(\Delta) \gamma^2 H_1^2 \frac{f(\Delta)}{2} T_D \frac{\Delta}{D^2} \right\}, \quad (47)$$

where  $f'(\Delta)$  is the dispersion line shape function. Again the first term saturates and the second does not. However, the derivative of the dispersion line shape function is not zero at  $\Delta = 0$  as it is for absorption, and we can study the saturation of the dispersion signal at the centre of the line. The second terms becomes zero and we have:

$$u_1(0) = \frac{1}{2} \Delta_m \gamma H_1 M_0 \frac{\frac{df'(0)}{d\Delta}}{1 + \gamma^2 H_1^2 T_1 f(0)/2} \quad (48)$$

which saturates normally.

### E. $T_1$ By Progressive Saturation of Dispersion

We are finally in a position to do progressive saturation experiments in solids and be sure we are measuring the true  $T_1$ 's. At a low  $H_1$  level when there is no saturation we have:

$$\frac{u_1(0)}{H_1} = \frac{1}{2} \Delta_m \gamma M_0 \frac{df'(0)}{d\Delta} ; \quad \text{let this} \equiv C$$

$T_1$  can then be determined by the following procedures:

- (1) We can increase  $H_1$  until  $u_1(0)/H_1 = C/2$ , at this point  $\gamma^2 H_1^2 T_1 f(0)/2 = 1$ .
- (2) A better method is to plot  $H_1/u_1(0)$  versus  $H_1^2$  since from equation (48)

$$\frac{H_1}{u_1(0)} = \frac{1}{C} (1 + \gamma^2 H_1^2 T_1 f(0)/2) \quad (49)$$

An extrapolation of the straight line of slope  $\frac{1}{C} \gamma^2 \frac{f(0)}{2} T_1$  to the abscissa yields the intercept value of  $-(H_1^*)^2$  so that

$$\gamma^2 H_1^{*2} T_1 f(0)/2 = 1 .$$

One can determine  $f(0)$  by integrating unsaturated lock-in absorption curves, then

$$f(0) = \frac{2\pi v(0)}{\int_{-\infty}^{+\infty} v(\Delta) d\Delta} \quad (50)$$

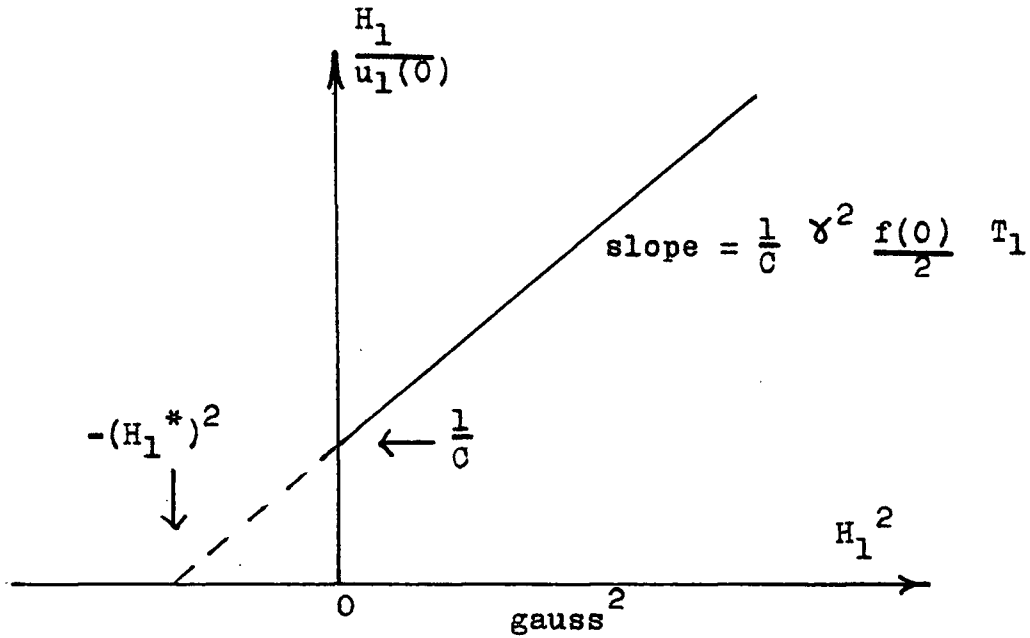


Fig. 2 - Plot of  $H_1/u_1(0)$  versus  $H_1^2$  predicted by equation (48).

F. The Chameleonic Local Field

The reader has probably noticed that the local field has apparently been defined three different ways in this chapter. Summarized they are:

Redfield

$$H_L^2 = \frac{\text{tr} (\widehat{H}_D')^2}{\text{tr} (\gamma^2 \hbar^2 \sum_1 I_{1z}^2)} \text{ gauss}^2 \quad (14b)$$

Provotorov

$$H_D^2 = \frac{\text{tr} (\widehat{H}_D')^2}{\text{tr} \widehat{I}_z^2} = \gamma^2 \hbar^2 H_L^2 \quad (28)$$

Goldman

$$D^2 = \gamma^2 H_L \quad (\text{rad/sec})^2$$



- (10) A.G. Redfield, Phys. Rev. 128, 2251 (1962)
- (11) B.N. Provotorov, Fiz. Tverdogo Tela, 4, 2940 (1962)  
[Transl.: Soviet Phys. Solid State, 4, 2155 (1963)]  
Phys. Rev. 128, 75 (1962)
- (12) J. Philippot, Phys. Rev. 133, A471 (1964)
- (13) Robert Zwanzig, J. Chem. Phys. 33, 1338 (1960)
- (14) A.G. Anderson and A.G. Redfield, Phys. Rev. 116, 583 (1959)
- (15) J. Jeener, H. Eisendrath, and R. Van Steenwinkel, Phys.  
Rev. 133, A478 (1964)
- (16) M. Goldman, Le Journal de Physique, 25, 843 (1964)

## chapter 2.

## SATURATION II.

## PROGRESSIVE SATURATION IN CALCIUM FLUORIDE

## I. INTRODUCTION

In this chapter we present the results of some steady state nuclear magnetic resonance saturation experiments on a powder sample of that perennial favourite  $\text{CaF}_2$ .

$\text{CaF}_2$  was one of the first solids to be studied by progressive saturation. Bloembergen /1/ measured  $T_1$  in several samples: natural and commercial sources, crystal and powder forms. The measured relaxation times  $T_1$  disagreed violently — smaller by more than a factor of  $10^{10}$  — with values calculated using previous theories of relaxation, Waller /2/ BPP /3/. These theories proposed that the dipole-dipole interaction between magnetic nuclei in conjunction with the thermal variation of their space coordinates provided the heat contact between the spins and the lattice. Bloembergen showed that the relaxation time  $T_1$  was determined by paramagnetic impurities in the lattice. An order of magnitude theory was developed taking these impurities into account.

Bloembergen observed the progressive saturation of the maximum value of the lock-in absorption signal. Since the  $H_1$  values were not known, only relative  $T_1$ 's were obtained this way. Another restriction was that the two samples compared had to have similar line shapes. The receiver gain was turned down each time the generator was turned up so that the signal was proportional only to  $\left. \frac{d\chi''}{dH} \right|_{\max}$ . Absolute  $T_1$ 's were obtained by comparison with a sample for which  $T_1$  could also be measured by a direct method: recovery from strong saturation observed with a very weak rf field.

We now know that  $T_1$ 's obtained by this progressive saturation method could be in error because of saturation narrowing. The method implicitly assumed that the line shape be constant. Redfield /4/, in order to measure  $T_1$  in aluminum and copper, avoided this problem by integrating the recorded lock-in absorption curves to get the relative absorption at resonance. The rf field was calibrated so absolute  $T_1$ 's were obtained. He later decided that his first measurements were in error /5/. Modulation saturation also affects the line shape and may have caused the errors.

We shall show that a true  $T_1$  can be found by progressive saturation of the lock-in dispersion signal at the centre of resonance. This method avoids the effects of saturation narrowing and modulation saturation. With improved techniques the measurement could be done in less than an hour. The expression obtained by Goldman /6/, using Provotorov's theory /7/, that describes the behaviour of this signal is verified.

## II. EXPERIMENTAL

### A. Spectrometer

The NMR spectrometer used was essentially a Varian Associates model VF-16 wide line spectrometer with a V-4007 six inch electro-magnet and V-2200B power supply. The magnet gap was  $1\frac{1}{2}$  in. initially, later changed to  $1\frac{5}{8}$  in. The signals were recorded on a Varian model G-10 strip-chart recorder running at 16 in/hr.

The magnet was cooled with a low-cost closed-loop cooling unit designed by the author. The reservoir water, contained in a 16 gal plastic garbage can, was cooled with city water running through a 25 ft coil of  $\frac{1}{2}$  in. copper tubing in the reservoir. The reservoir temperature was kept constant to within  $\pm 0.2$  deg C by controlling the city water with an ASCO solenoid valve operated by a Sun-Vic thermal delay relay in conjunction with a Jumo mercury contact thermometer. The reservoir water was circulated through the magnet with an Eastern  $1/8$  hp centrifugal pump. Magnet protection was provided by a Fanwal thermo switch in the reservoir and a flow switch in the magnet water outlet line.

The magnetic field sweep was calibrated using side bands from a liquid sample that were generated by frequency modulation of the rf unit carrier frequency with a known audio frequency. The audio signal was obtained from a Hewlett Packard model 2000D oscillator whose frequency was measured with a Hewlett Packard

(England) 3734A counter. The standard V-4210 rf unit provides no means for audio modulation so a varicap circuit was added to the oscillator stage. The author is indebted to Mr. Ken Abramson for the initial version of this modification. The modulation width was measured from overmodulated liquid signals. The observed line width then is  $2H_m$ .

### B. $H_1$ Calibration

A jack was installed in the rf unit so that the standard panel meter,  $2\frac{1}{2}$  in. Simpson  $100 \mu\text{a}$  dc panel meter, which indicated rf field level, could be replaced by an external meter. A  $4\frac{1}{2}$  in. Simpson  $100 \mu\text{a}$  dc panel meter with an accuracy of 2% was used. Its 2000 ohm internal resistance was the same as the built-in one. It was found that the meter readings for rf field switch ranges x10 and x100 were in error by a factor of two compared with the x1 position, so new values were determined for the series resistors. R133 was changed to  $100 \text{ k}\Omega$  and R132 to  $7.0 \text{ M}\Omega$ . The error between adjacent ranges was then about  $\pm 5\%$ .

$H_1$  was calibrated using the method of Weston Anderson /8/ which is suitable for a strong rf field. One performs a nuclear resonance experiment in the rotating frame. The resonance frequency  $\omega'$  in this frame is:

$$\omega' = \gamma H_{\text{er}} = \left[ (\gamma H_0 - \omega)^2 + \gamma^2 H_1^2 \right]^{\frac{1}{2}} . \quad (1)$$

A weak rf field is needed to stimulate this resonance and it can be obtained by a small modulation of the magnetic field. A resonance is then achieved when the audio modulation frequency  $\omega_m$  satisfies the condition

$$\omega_m^2 = (\gamma H_0 - \omega)^2 + \gamma^2 H_1^2 \quad (2)$$

As long as  $\omega_m > H_1$ , this equation will be satisfied at two values of  $H_0$ . To measure  $H_1$  one measures the distance  $d$  between these signals as a function of  $\omega_m$  and plots  $d^2$  vs  $\omega_m^2$ . The intercept of this straight line plot is  $(\gamma H_1)^2$ . In order to detect these small sideband signals in the presence of the large main resonance the Varian V-4270 lock-in amplifier was used. See Anderson /8a/ for more details.

For this method to yield precise  $H_1$  values the stability of the radio frequency had to be improved. This was accomplished with a crystal oscillator — built by the chemistry department electronics shop — connected to the sync input of the rf unit. It was a one tube (6CL6) oscillator operating on the fundamental or first harmonic of a 4.000 MHz crystal.

The experiments in this chapter were done with a radio frequency of 16 MHz. The  $H_1$  was measured at seven points on the meter x1 range and four on the x10, using a water sample and the Varian 12 in. magnet with super stabilizer and slow sweep of the DP60 spectrometer system.

### C. Sample

The  $\text{CaF}_2$  powder sample was British Drug Houses precipitated  $\text{CaF}_2$  laboratory reagent grade. The sample was placed in a 15 mm dia test tube, evacuated at 150 to 200 °C for three days then sealed off with a torch. The spectra were run at room temperature.

D. Second Moment

The second moments of the NMR absorption derivative curves were computer calculated on an IBM 7040. The FORTRAN program used the expression\*

$$SM = \frac{\text{scale}^2}{3} \frac{\sum_{1}^N n^3 y_n}{\sum_{1}^N n y_n} - \frac{H_m^2}{4} \quad (3)$$

where SM is the second moment corrected for modulation broadening;  $y_n$  is the curve intensity in arbitrary units,  $n$  increments along from the centre of the line; scale is the number of gauss per increment;  $N$  is the maximum value of  $n$ ;  $H_m$  is the peak modulation amplitude. The moments were calculated for each half of the curve then averaged.

E. Line Shape Function at Resonance

If the line shape function in equation (1-48) is measured in units of gauss<sup>-1</sup> and denoted  $G(0)$  then

$$\gamma^2 H_1^2 T_1 f(0)/2 \quad \text{becomes} \quad \gamma H_1^2 T_1 G(0)/2, \quad (4)$$

and equation (1-50) becomes:

$$G(0) = \frac{2 \pi v(0)}{\int_{-\infty}^{+\infty} v(x) dx} \quad (5)$$

---

\* A numerical integration form of equation (5) in Andrew /9/.

where  $x = H_0 - H$ .  $G(0)$  was calculated from absorption derivative curves using the numerical integration

$$G(0) = \frac{\pi}{\text{scale}} \frac{\sum_{-N}^{+N} |y_n|}{\sum_{-N}^{+N} n y_n} \quad (6)$$

The variables have already been defined (section D).

### F. Line Shape Fitting

The derivative of the Gaussian function  $z = a \exp(-x^2/2\sigma^2)$  is

$$z' = -\frac{a}{\sigma^2} x e^{-\frac{x^2}{2\sigma^2}} \quad (7)$$

The maximum and minimum values of  $z'$  occur for  $x^2 = \sigma^2$  (call it  $x_L^2$ ) so the constant  $a = e^{\frac{1}{2}} x_L z'_{\max}$ .

The derivative of the Lorentzian function  $z = c/(1 + bx^2)$  is

$$z' = \frac{-2bcx}{(1 + bx^2)^2} \quad (8)$$

In this case we get  $z'_{\max}$  for  $x^2 = 1/3b$  and the constants are  $b = 1/3x_L^2$  and  $c = \frac{8}{3} x_L z'_{\max}$ . The Gaussian and Lorentzian curves calculated were fitted to experimental curves accordingly at  $z'_{\min}$  and  $z'_{\max}$ .

### III. RESULTS AND DISCUSSION

#### A. Absorption Saturation

##### 1. Absorption spectra at various rf levels

Lock-in absorption-mode  $F^{19}$  NMR spectra of  $CaF_2$  powder at various rf levels are shown in Fig 1\*. We see here the line narrowing and shape change caused by saturation. The spectrum for  $H_1 = 2.82$  mG is only slightly saturated. Its second moment is  $6.25 \text{ gauss}^2$ . The average from three such spectra is  $6.19 \text{ gauss}^2$ . The theoretical second moment is  $6.47 \text{ gauss}^2$  /10/. In Table I are listed the line widths of the spectra in Fig 1. The unsaturated line width is 6.7 to 6.8 gauss (based on four spectra). It broadens a little at  $H_1 = 12.1$  to 21.4 mG and then narrows down to 3.2 gauss at 78 mG.

---

\* In Fig 1 the modulation frequency  $\nu_m = 20$  Hz, the peak-to-peak amplitude  $2 H_m = 1.32$  G for the two lowest rf level spectra and 0.66 G for the others. The arrow indicates 0.66 G. The value of  $H_1$  for each spectrum is given in mG. The time is given for a sweep of 10 G and this distance is indicated by the calibration line. The sweep directions alternate. The rf frequency  $\nu_0$  is 16 MHz.

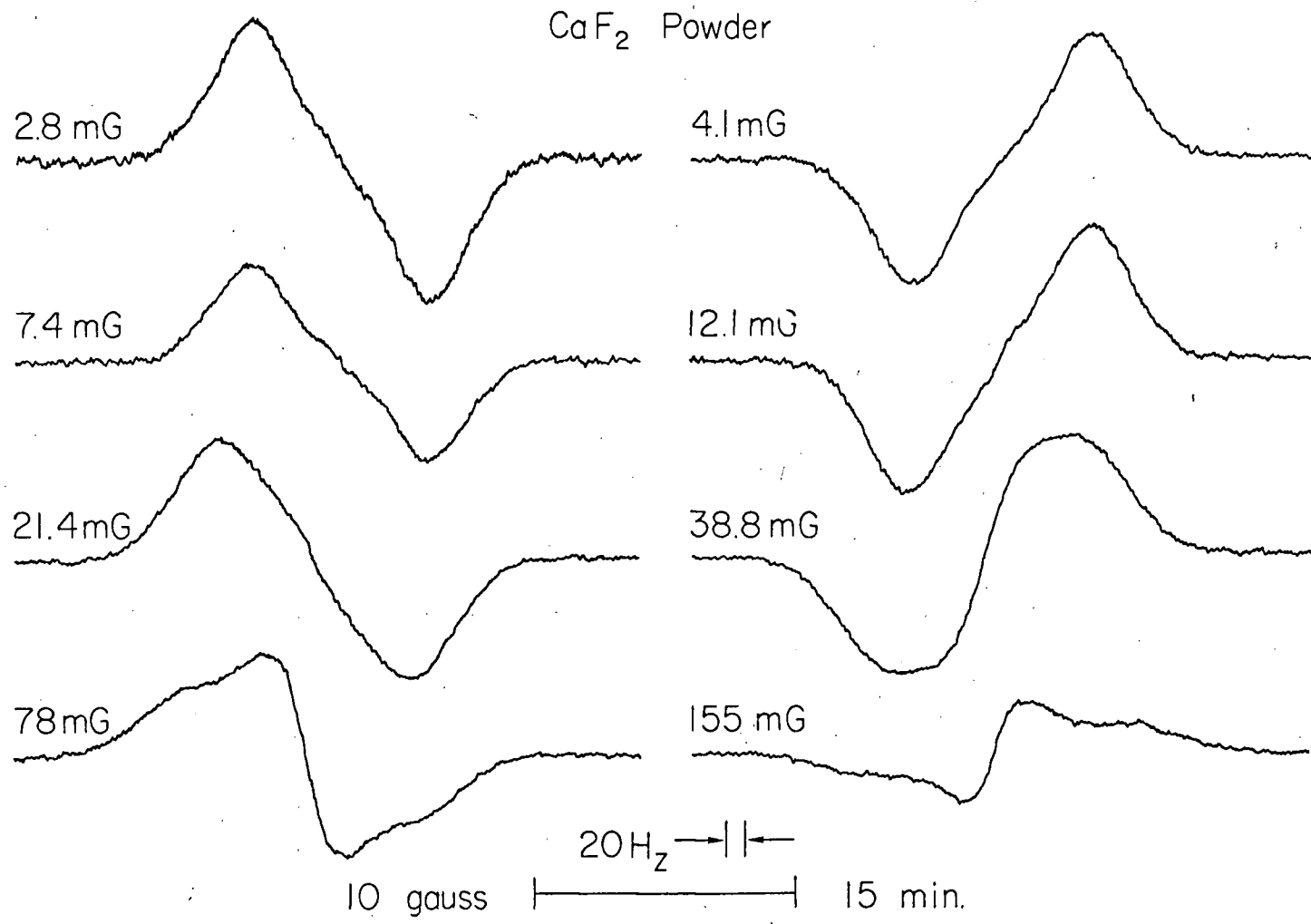


Fig 1 - Absorption spectra of CaF<sub>2</sub> powder at various rf levels.

Table I - Line widths of spectra in Fig 1.

Trace	$H_1$ milligauss	Line Width gauss	Trace	$H_1$ milligauss	Line Width gauss
142	2.82	6.7	145	21.4	7.4
143	4.1	6.8	146	38.8	6.8
149	7.35	6.8	147	78	3.2
144	12.1	7.3	148	155	2.55

In Fig 2\* Lorentzian and Gaussian derivative curves are fitted to a pair of  $\text{CaF}_2$  absorption spectra: normal and saturation narrowed. The line widths are 6.8 and 2.65 gauss obtained at  $H_1 = 4.7$  and 260 mG respectively. The 2.65 gauss line is broadened about 7% by modulation, the 6.8 gauss line less than 1% /1/. We see that the normal line is a squared off Gaussian; viz, the wings go to base line faster and the centre is a little flatter than the computed Gaussian curve. The saturation narrowed line shape is quite different from the normal one. One might call it super Lorentzian, since the wings do not go to base line as quickly as the computed Lorentzian curve.

\*

In Fig 2  $\nu_m = 20$  Hz,  $2 H_m = 1.32$  G. The arrow indicates 1.32 G, the calibration line 5 G.

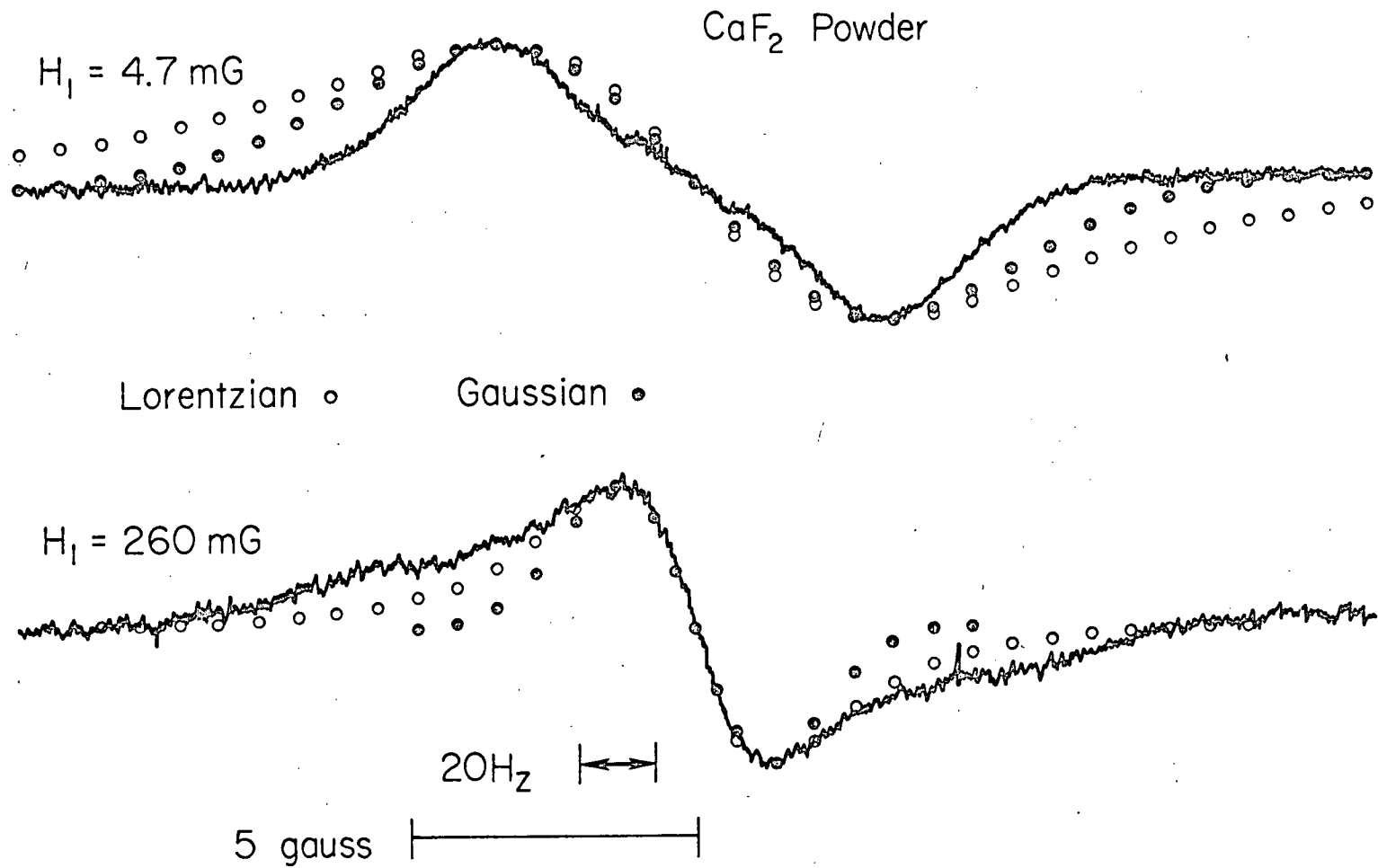


Fig 2 - Fitted normal and saturation narrowed absorption spectra of CaF<sub>2</sub> powder.

The cause of the extra peaks in the saturation narrowed spectra (especially noticeable in Fig 1) and the reason the curves are not truly Lorentzian as predicted, is probably modulation saturation. Additional evidence for this explanation is found in Fig 3\* in which saturation narrowed spectra run at different modulation frequencies, 40 and 80 Hz, are shown. In the 80 Hz spectrum the peaks to high and low field are quite obvious, but in the 40 Hz spectrum they cannot be seen.

## 2. Ratio of the Zeeman and Dipolar relaxation times

From equation (1-45) it was found that:

$$\frac{T_1}{T_D} = \frac{9}{4} \frac{(\Delta H_{as})^2}{\langle \Delta H^2 \rangle} \quad (9)$$

where  $\Delta H_{as}$  is the saturation narrowed line width in gauss,  $\langle \Delta H^2 \rangle$  is the second moment in gauss<sup>2</sup>, and  $T_1/T_D$  is the ratio of the Zeeman and dipolar spin-lattice-relaxation times. Table II lists the  $T_1/T_D$  ratio calculated from several saturation narrowed spectra (20 Hz modulation frequency) using the theoretical second moment of 6.47 gauss<sup>2</sup>/10/. The ratio appears to decrease with rising  $H_1$  and varies from 3.55 to 2.25. It is expected to be constant, however, so we again invoke

---

\*

In Fig 3 the arrows indicate p-p modulation 0.59 G at 40 Hz and 0.70 G at 80 Hz. The calibration line indicates 10 G.  $H_1$  is 207 mG.

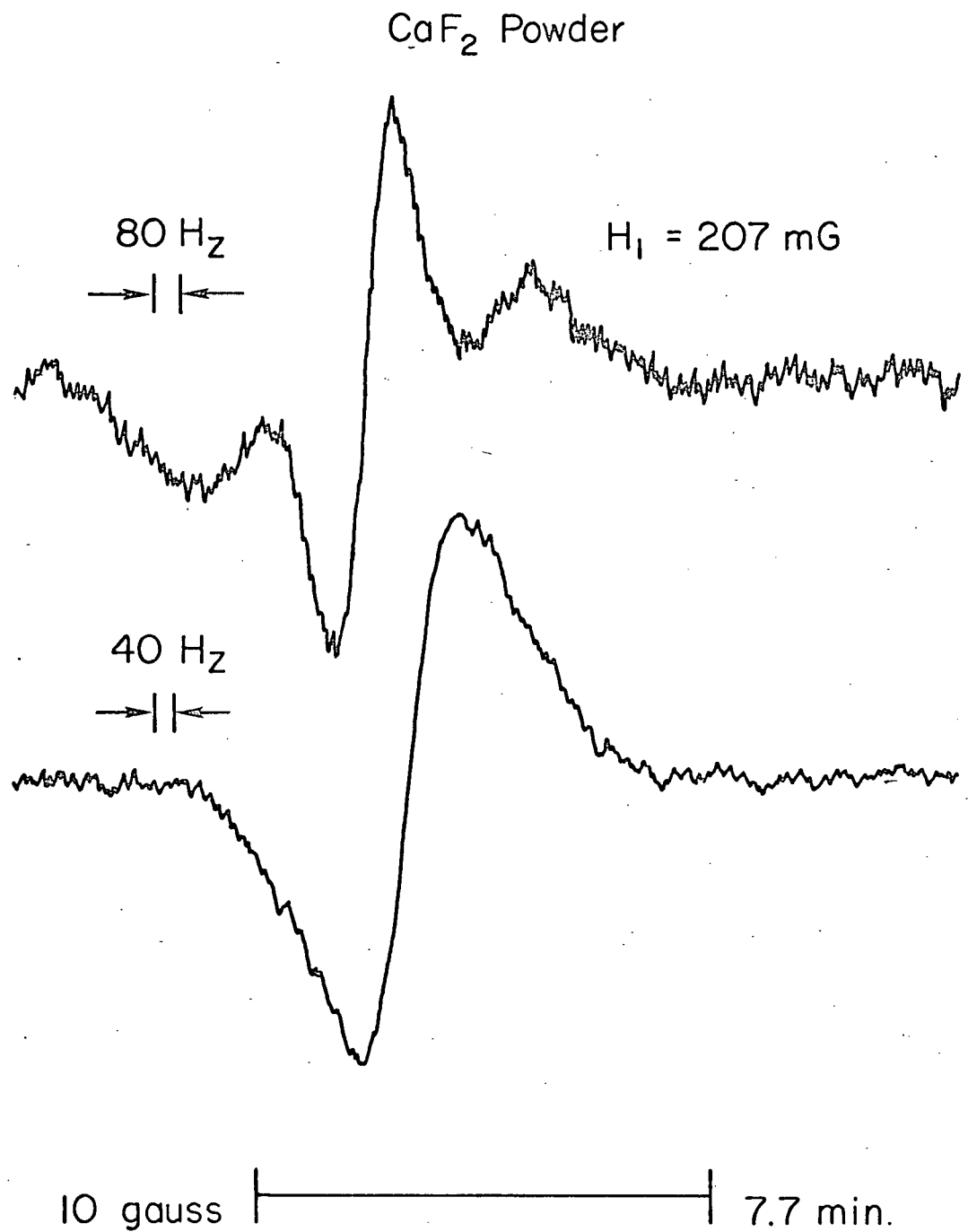


Fig 3 - Saturation narrowed spectra of CaF<sub>2</sub> at 40 and 80 Hz modulation frequencies.

modulation saturation as the culprit and conclude that we are not measuring the true saturation narrowed line width. Jeener /12/, using pulse techniques (NMR frequency 28.7 MHz), has measured  $T_1$  and  $T_D$  in a single crystal of  $\text{CaF}_2$ . The ratio is  $T_1/T_D = 1.14 \text{ sec}/0.38 \text{ sec} = 3.00$ . A ratio of 3.00 means that there is complete correlation between the fluctuating fields (responsible for relaxation) at different spins according to Anderson-Redfield /13/ and Solomon-Ezratty /14/ relaxation theories.

Table II -  $T_1/T_D$  ratio from saturation narrowed curves.

Trace	$H_1$ milligauss	Line Width gauss	$\frac{T_1}{T_D}$
147	78	3.2	3.55
4	120	3.05	3.3
16	120	2.95	3.0
148	155	2.55	2.25
6	230	2.7	2.5
9	230	2.65	2.45
8	260	2.65	2.45

### 3. Progressive saturation of the absorption signal

In Fig 4\* the absorption signal  $v_1(\max)$  and  $v_1(\max)/H_1$  from the spectra in Fig 1 are plotted against the rf field  $H_1$ . If there were no complications (no line narrowing or modulation saturation)  $v_1(\max)/H_1$  would be proportional to the maximum slope of the absorption susceptibility  $\left. \frac{d\chi''}{dH} \right|_{\max}$  and to  $\chi''(0)$ . The plots separate at high  $H_1$ . The lower branches were obtained by measuring  $v_1$  at a constant distance from the centre of the spectrum — the point for  $v_1(\max)$  in the unsaturated curve. This simulates the Bloembergen method /1/. The upper branches follow  $v_1(\max)$  as the line narrows.

In Fig. 5  $H_1/v_1(\max)$  versus  $H_1^2$  is plotted. If  $v_1(\max)/H_1$  were proportional to  $\chi''(0)$ , the plot should be a straight line since we recall that both Provotorov and BPP theory predict:

$$\chi''(0) = \frac{\chi_0 \omega_0 g(0)/2}{1 + \gamma^2 H_1^2 T_1 \pi g(0)} \quad (1-8)$$

The plot is not linear and we shall see that it does not yield the correct  $T_1$ .

---

\* In Fig 4 the absorption signal is actually plotted in  $10^{-2}$  mm units. This is because the peak-to-peak absorption signal was measured in mm on the recorder trace and then adjusted for different modulation levels and amplifier gains;  $v_1(\max)/H_1$  is plotted in cm/G. If we had an absolute calibration,  $v_1(\max)$  would of course be in gauss.

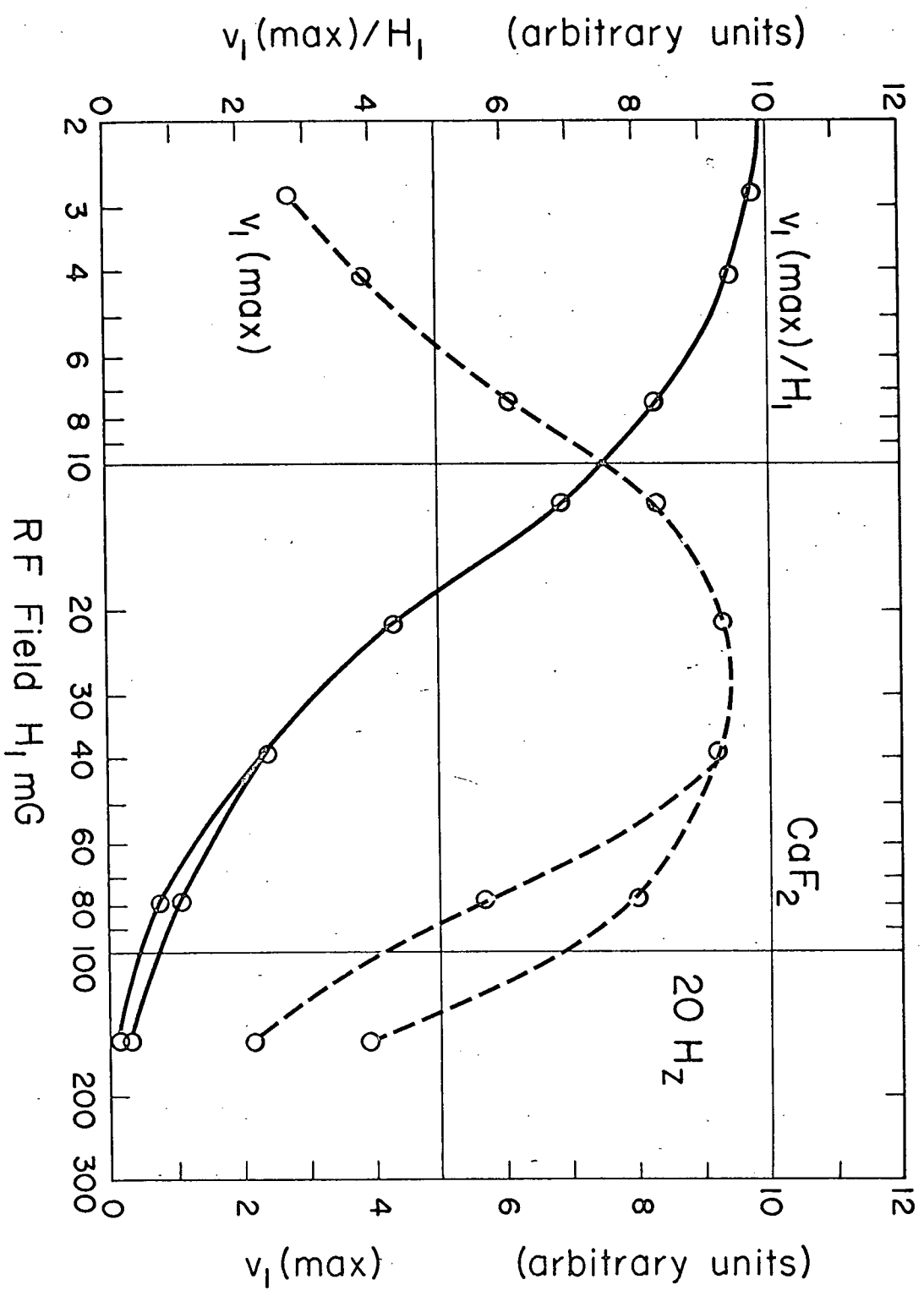


Fig 4 - The absorption signal,  $v_1(\text{max})$ , and  $v_1(\text{max})/H_1$  as a function of the rf field intensity in  $\text{CaF}_2$ .

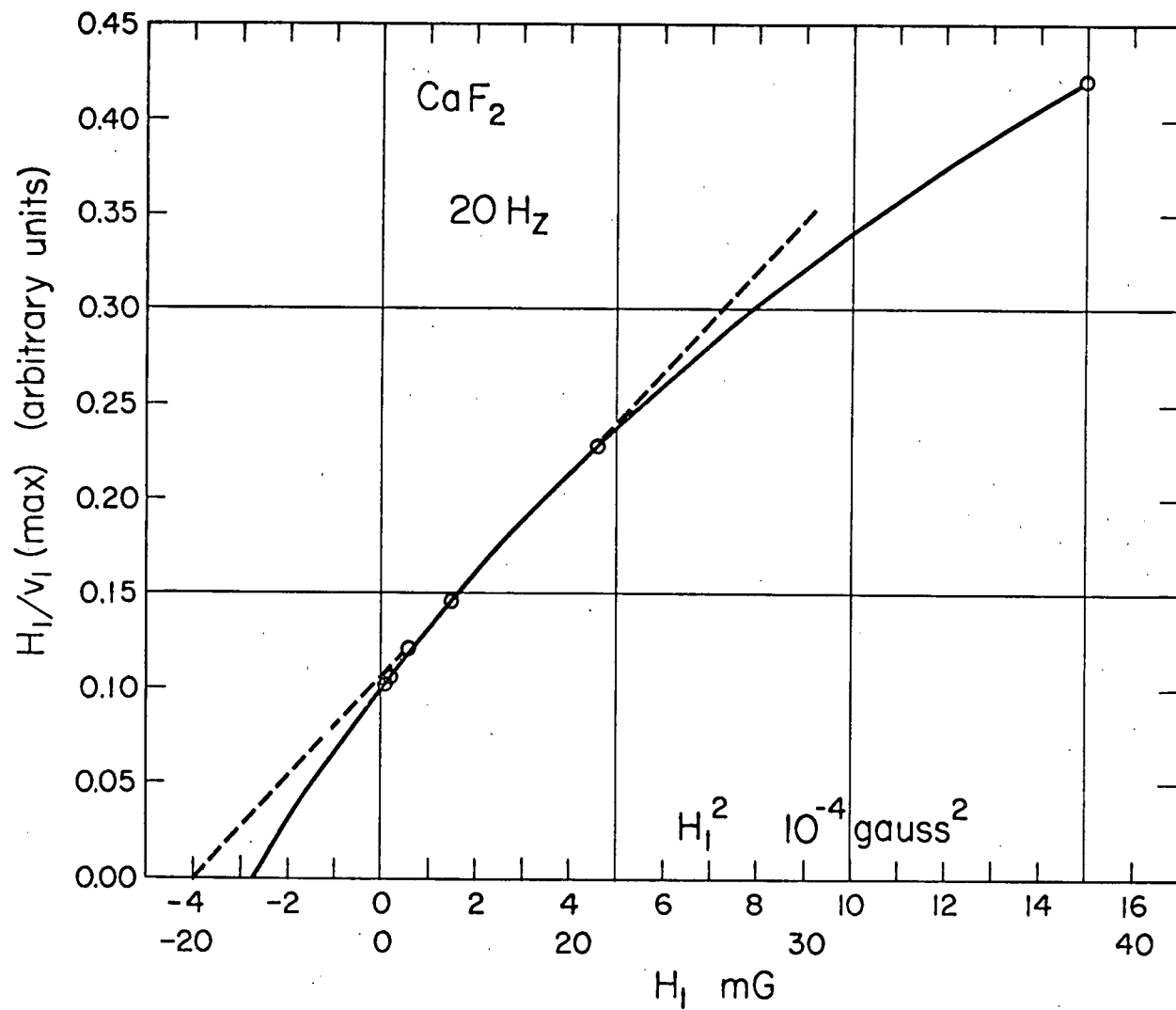


Fig 5 -  $H_1/v_1(\text{max})$  as a function of  $H_1^2$  in CaF<sub>2</sub>.

## B. Dispersion Saturation

### 1. Dispersion spectra at various rf levels

Lock-in dispersion mode  $F^{19}$  spectra of  $CaF_2$  powder at various rf levels and a modulation frequency of 20 Hz are shown in Fig 6\*. We see that the shape changes; the ratio of the signal above the base line to that below increases, the middle of the curve narrows, and finally fine structure appears on the shoulders of the  shaped curve. The spectra in Fig 7# were obtained with a modulation frequency of 200 Hz. The overall behaviour is similar to that at 20 Hz but it is remarkable that there is no hint of fine structure on the shoulders of the curve at high  $H_1$ .

These spectra demonstrate that the signal at the exact centre of resonance  $u_1(0)$  saturates and decreases with  $H_1$  whereas the shoulders continue to grow. Lock-in dispersion spectra of  $CaF_2$  at very high rf fields have been studied by Solomon and Ezzatty /14/.

\* In Fig 6 the modulation  $2 H_m = 0.72$  G and is indicated by the arrow. The  $H_1$  values are in mG. The rf frequency is 16 MHz.

# In Fig 7 the modulation  $2 H_m = 0.90$  G. Complete curves were not always taken because the wings extend a very long way out. To find base-line then the modulation was turned off at a suitable distance from the centre.

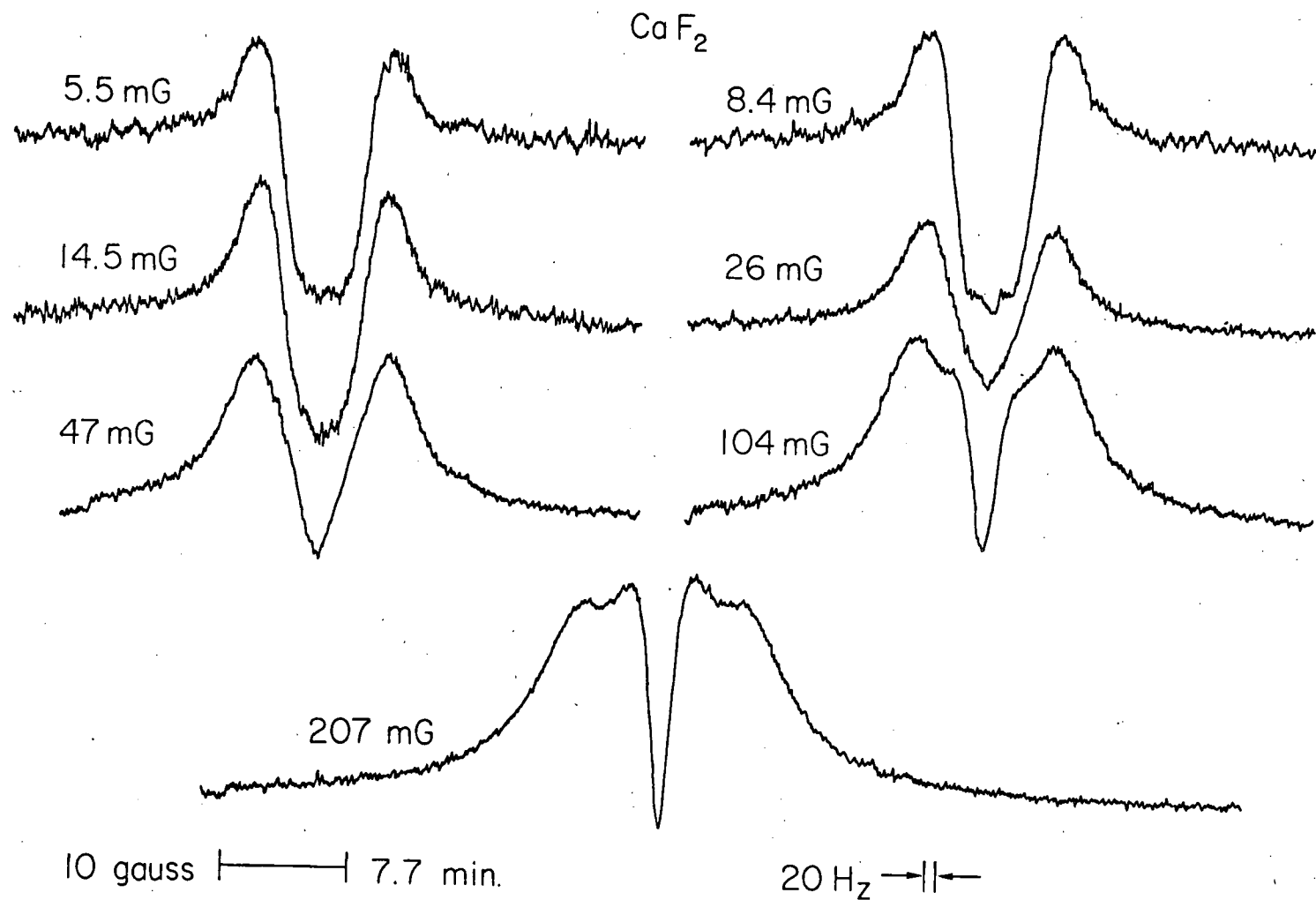


Fig 6 - Dispersion spectra of  $\text{CaF}_2$  powder at various rf levels and a modulation frequency of 20 Hz.

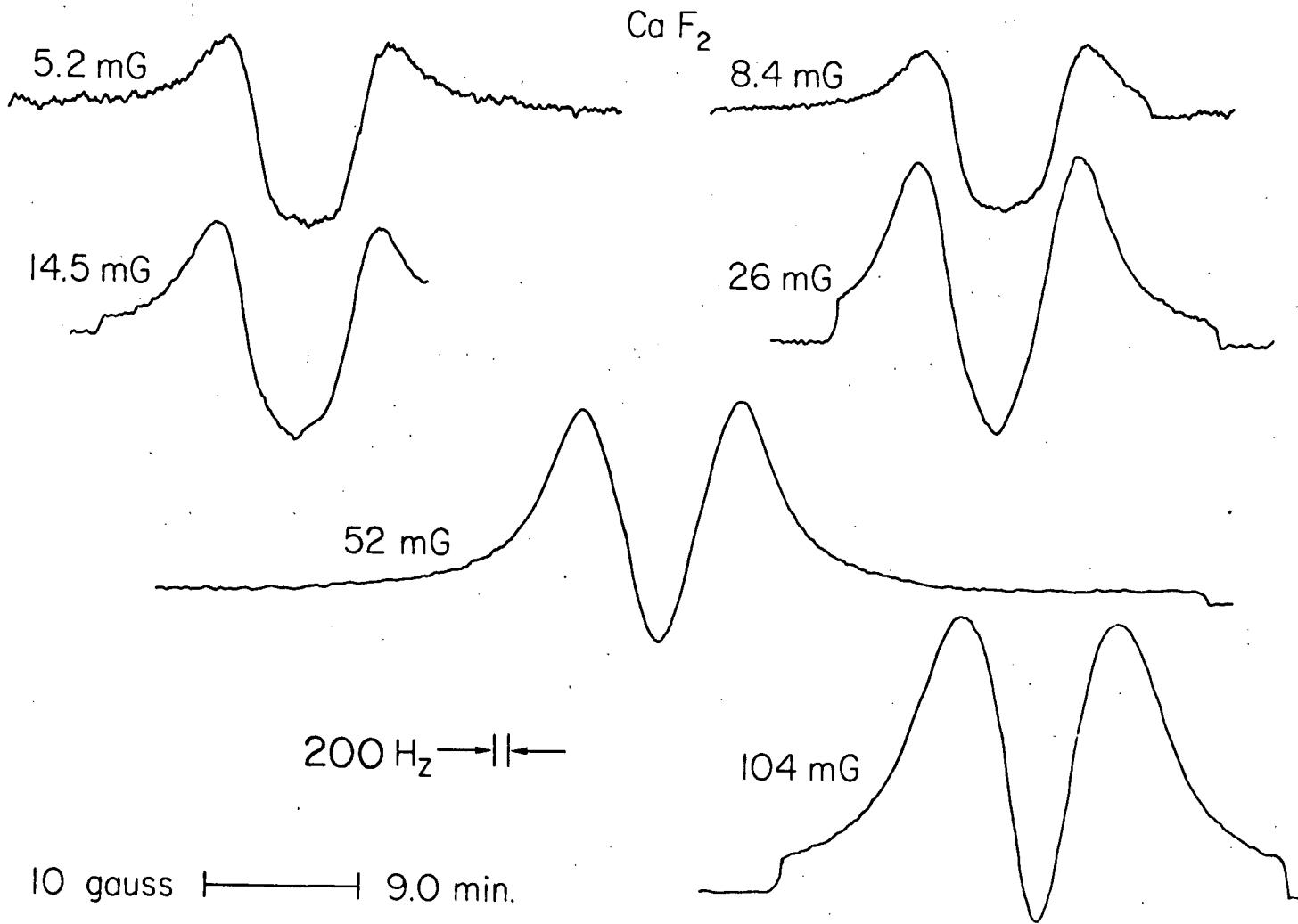


Fig 7 - Dispersion spectra of  $\text{CaF}_2$  powder at various rf levels and a modulation frequency of 200 Hz.

## 2. Progressive saturation of the dispersion signal

The dispersion signal  $u_1(0)$  was measured on the recorder for a series of rf levels by scanning back and forth through the centre of the line. This was done because the magnetic field and/or the rf frequency were not stable enough to sit on the point of the signal — especially where the point sharpens at high  $H_1$ . The modulation was switched off periodically to find the base line. It took three hours to run the series. The dispersion signal  $u_1(0)$ , and  $u_1(0)/H_1$  which is proportional to  $\frac{d\chi'(0)}{dH}$  are plotted against  $H_1$  in Fig 8. The modulation frequency is 200 Hz, the peak-to-peak amplitude  $2 H_m = 0.90$  G. We were fortunate that the  $\text{CaF}_2$  sample did not have a  $T_1$  time any longer than it did — there are just two points that shown negligible saturation. The minimum useful reading on our rf level meter was  $1 \times 1 \mu\text{a}$  and it corresponded to 2.1 mG.

When the distance from resonance (and the modulation  $H_m$ ) is measured in gauss, the expression for  $u_1(0)$ , equation (1-48), becomes:

$$u_1(0) = \frac{\frac{1}{2} H_m H_1 M_0 \frac{dG'(0)}{dH}}{1 + \gamma H_1^2 T_1 G(0)/2}, \quad (10)$$

and if this expression is obeyed, a plot of  $H_1/u_1(0)$  versus  $H_1^2$  should be a straight line. This is done in Fig 9. We see that the plot does yield a straight line and so it appears that equation (1-48) is correct.

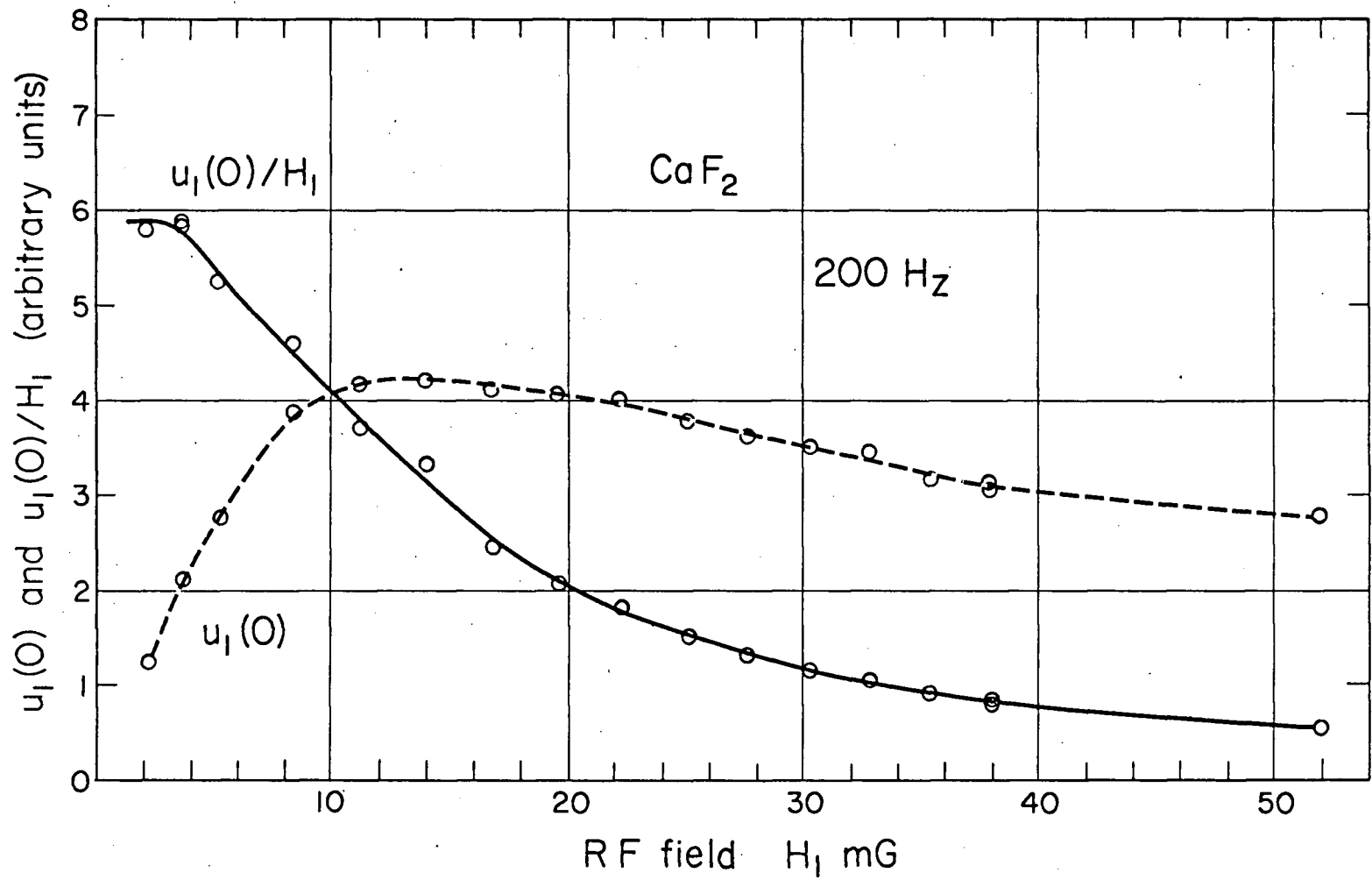


Fig 8 - The dispersion signal,  $u_1(0)$ , and  $u_1(0)/H_1$  as a function of the rf field intensity in  $\text{CaF}_2$ .

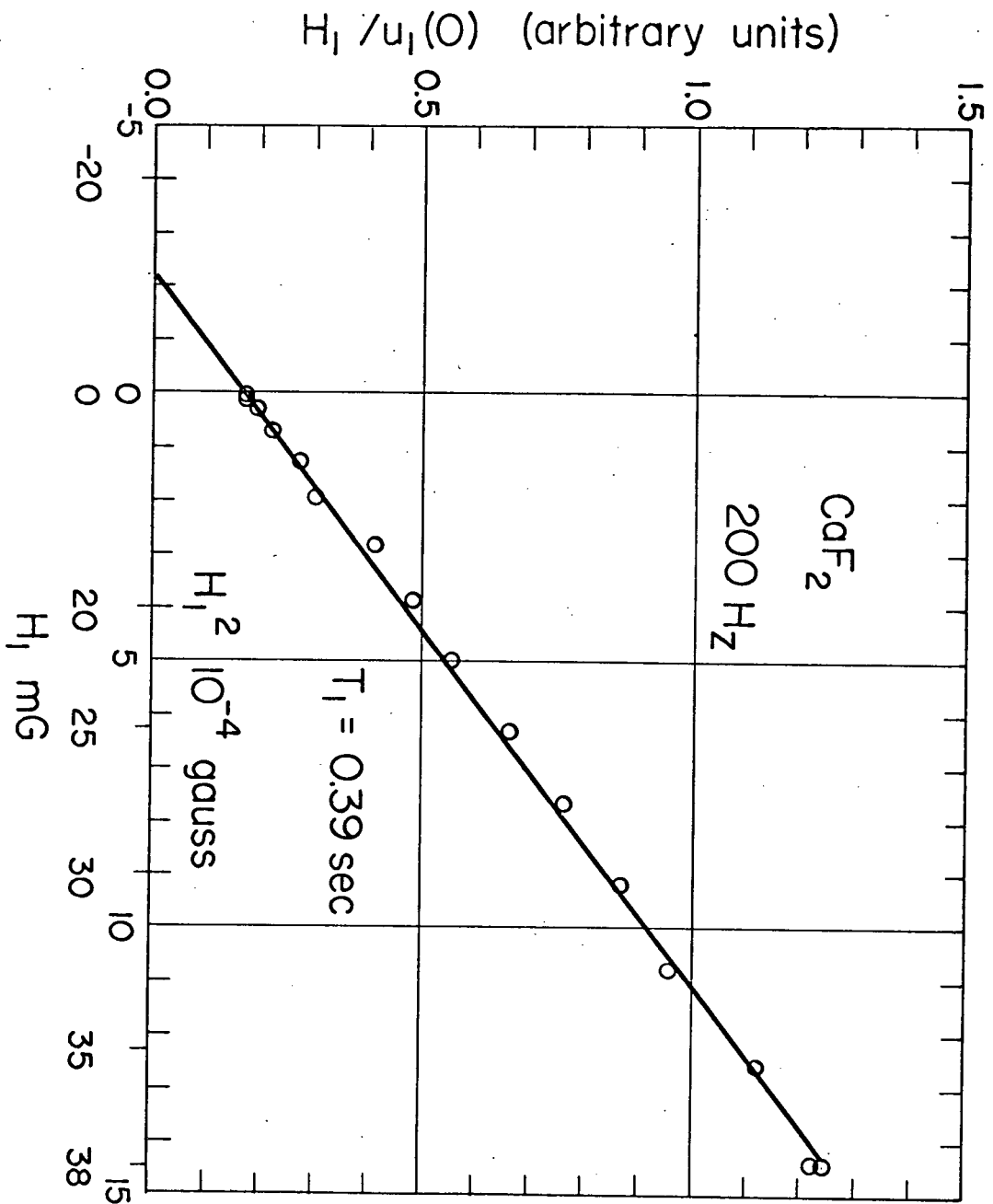


Fig 9 -  $H_1/u_1(0)$  as a function of  $H_1^2$  in  $\text{CaF}_2$ .

### 3. Spin lattice relaxation time

The value of the line shape function at  $x=0$ ,  $G(0)$ , found by integrating the  $H_1 = 2.8$  mG absorption spectrum in Fig 1, is  $0.89 \text{ gauss}^{-1}$ . The average from four such spectra is  $0.896 \text{ gauss}^{-1}$  with a maximum deviation of  $0.018 \text{ gauss}^{-1}$ . The abscissa intercept in Fig 9 is  $2.3 \pm 0.1 \times 10^{-4} \text{ gauss}^2$ . We call it  $(H_1^*)^2$  and this is the value for which the saturation parameter

$$S(0) \equiv \gamma H_1^2 T_1 G(0)/2 = 1 \quad (11)$$

These results yield a spin lattice relaxation time  $T_1$  of  $0.385 \text{ sec}$  with an estimated error of  $\pm 0.030 \text{ sec}$  when errors in  $H_1$  calibration are also included. Fig 8 also gives us the value of  $H_1^*$ . When  $S(0) = 1$ ,  $u_1(0)/H_1$  is down to  $1/2$  its unsaturated value and this occurs for  $H_1 = 15.0 \pm 0.2 \text{ mG}$ . This value agrees quite well with  $15.2 \text{ mG}$ , the square root of the Fig 9 intercept.

On the other hand if we attempt to get  $T_1$  from our absorption signal graphs we find from Fig 4 that  $H_1^* = 18.5 \text{ mG}$  so  $T_1 = 0.26 \text{ sec}$ ; and from Fig 5 we find that  $(H_1^*)^2$  varies from  $2.8$  to  $4.0 \times 10^{-4} \text{ G}^2$  ( $H_1^*$  from  $16.7$  to  $20 \text{ mG}$ ) so  $T_1$  could be from  $0.32$  to  $0.22 \text{ sec}$ .

### 4. Check on restrictions

Now let us see if we have complied with the restrictions assumed by Goldman when he derived his equations. The conditions

were:

$$\frac{1}{T_1}, \frac{1}{T_D} \ll \Omega \ll D, \quad \text{and} \quad 2W \ll \Omega. \quad (12)$$

The modulation frequency  $\nu_m$  in Fig 8 and 9 is 200 Hz so  $\Omega = 2\pi \nu_m = 1256 \text{ sec}^{-1}$ . Assuming  $T_1/T_D = 3.0$  we have  $1/T_1 = 2.6 \text{ sec}^{-1}$  and  $1/T_D = 7.8 \text{ sec}^{-1}$ . The local field  $D$  in rad/sec =  $3.70 \times 10^4 \text{ sec}^{-1}$  calculated from the theoretical second moment ( $D = \gamma H_L = \gamma (\langle \Delta H^2 \rangle / 3)^{1/2} = (2.517) 10^4 (6.47/3)^{1/2}$ ). The line is straight in Fig 9 to about  $H_1 = 38 \text{ mG}$  and at this point the transition probability term  $2W(0) = 16.3 \text{ sec}^{-1}$  ( $2W(0) = \gamma H_1^2 G(0)/2 = (2.517) 10^4 (3.8)^2 10^{-4} (0.896)/2$ ). Summing up we have (in units of  $\text{sec}^{-1}$ ):  $1/T_D = 7.8$ ,  $\Omega = 1256$ ,  $D = 3.7 \times 10^4$ , and  $2W = 16.3$ . We see that the experiments reported in Fig 8 and 9 conform to the restrictions /12/. But if  $H_1/u_1(0)$  for the  $H_1 = 52 \text{ mG}$  point in Fig 8 is plotted on an extended version of Fig 9 we find that it falls below the straight line yet at this point  $2W$  is only  $30.6 \text{ sec}^{-1}$ , which is still  $\ll 1256 \text{ sec}^{-1}$ . There is one other condition we have not discussed yet — namely, that the field modulation amplitude be much less than the line width — and this condition is probably no longer satisfied at this point.

If we look back at Fig 1 we see that at  $H_1 = 38.8 \text{ mG}$  the saturation narrowed component of the spectrum has nearly reached the intensity of the normal line, and at  $H_1 = 52 \text{ mG}$  it will probably be the more intense one. In Fig 9 the p-p modulation  $2 H_m = 0.90 \text{ gauss}$  and so the line width to modulation ratio  $\Delta H_a / 2H_m$

for a normal line such as the  $H_1 = 4.1$  mG one in Fig 1 (line widths in table I) is 7.6. The narrow component is about 3.2 gauss wide (taken from the saturation narrowed curve at  $H_1 = 78$  mG) which means the ratio is down to 3.5 and the modulation amplitude probably can no longer be considered much less than the line width.

In Provotorov theory the magnitude of the saturation parameter  $S(\Delta) = 2W(\Delta) T_1$  determines the region at which the line shape changes and is therefore a more useful measure of saturation. Also  $S(0)$  can easily be found experimentally using a plot like that in Fig 8 since there is a simple relationship between  $S$  and the traditional saturation factor  $Z$  — viz,

$$Z(\Delta) = [1 + S(\Delta)]^{-1} \equiv [1 + \gamma^2 H_1^2 T_1 f(\Delta)/2]^{-1} \quad (13)$$

which is the ratio of the saturated to unsaturated magnetic susceptibility for a given rf level. Or,  $S(0)$  can be calculated once  $G(0)$  and  $T_1$  are known.  $S(0) = 11.8$  at  $H_1 = 52$  mG, and 6.3 at  $H_1 = 38$  mG. So we conclude that when our modulation amplitude is taken into account, the practical saturation limit is reached in this case for  $6.3 \leq S(0) < 11.8$ . The observed signal after this is too large. What probably happens is that the width of the modulation allows some contribution from the second term in equation (1-47), and this term does not saturate. When the modulation amplitude is very small, so is the contribution. But, when the modulation amplitude is not so small and the first term in equation (1-47) has been reduced due to saturation, the contribution from the second term becomes significant.

Just when this happens depends not just on line width and modulation amplitude, but on several factors as we can see from equation (1-47).

As stated in the Goldman section of chapter 1, the modulation saturation is strongest for  $2W \approx \Omega$ . Now look back at Fig 3 in which we showed strongly saturated absorption spectra run at different modulation frequencies; viz, 40 and 80 Hz, or in rad/sec, 251 and 502  $\text{sec}^{-1}$  respectively.  $H_1$  was 207 mG and this gives us  $2W(0) = 483 \text{ sec}^{-1}$  which is very close to  $\Omega$  for the 80 Hz spectra. This confirms our previous assignment of the extra peaks in the 80 Hz spectrum to modulation saturation effects and explains the remarkable difference between it and the 40 Hz one.

### C. Comparison with $T_1$ Measured by Adiabatic Rapid Passage

During the course of these studies it became apparent that an independent measurement of  $T_1$  was highly desirable. The adiabatic rapid passage (ARP) method was selected because, being a transient method, saturation is not involved and  $T_1$  is obtained directly. The equipment available was the other factor in its choice. The ARP experiments are discussed in detail in a later chapter.

The ARP result is  $T_1 = 0.45 \text{ sec}$  with an estimated uncertainty of  $\pm 0.05 \text{ sec}$ . The progressive saturation of dispersion (PSD) result of  $0.385 \text{ sec} \pm 0.030 \text{ sec}$  is about 14% smaller. If

the uncertainties are considered and we remember that these are values obtained by entirely different methods, we can say that the results are in good agreement.

#### IV. CONCLUSIONS

Equation (1-48), the equation for the lock-in dispersion signal  $u_1(0)$ , derived by Goldman /6/ using Provotorov theory /7/, correctly describes the saturation behaviour of  $u_1(0)$  in  $\text{CaF}_2$ . It saturates with the normal saturation factor:

$$Z(0) = [1 + \gamma^2 H_1^2 T_1 f(0)/2]^{-1},$$

where  $f(\Delta)$  is the line shape function normalized to  $2\pi$  and  $\Delta = \omega_0 - \omega$ . The lock-in absorption signal  $v_1(\text{max})$  saturates in a more complicated manner.

The progressive saturation of dispersion signal experiment yields the true  $T_1$  relaxation time. The experiment can be done with an ordinary wide-line NMR spectrometer.

The limiting conditions imposed by Goldman appear to be correct except that for practical modulation amplitudes, the degree of saturation that can be investigated is further restricted. The saturation parameter  $S(\Delta)$  is a more useful measure of saturation than just the transition probability  $2W(\Delta)$ .

The effects of saturation narrowing and modulation saturation have been demonstrated.

## REFERENCES

- (1) N. Bloembergen, *Physica*, 15, 386 (1949)
- (2) I. Waller, *Z. Phys.* 79, 370 (1932)
- (3) N. Bloembergen, E.M. Purcell and R.V. Pound, *Phys. Rev.* 73, 679 (1948)
- (4) A.G. Redfield, *Phys. Rev.* 98, 1787 (1955)
- (5) A.G. Redfield, *Phys. Rev.* 101, 67, (1956)
- (6) M. Goldman, *Le Journal de Physique*, 25, 843 (1964)
- (7) B.N. Provotorov, *Soviet Phys. - JEPT* 14, 1126 (1962)
- (8) (a) W.A. Anderson, "NMR and EPR Spectroscopy", Pergamon Press, New York, (1960) p.164; (b) *Phys. Rev.* 102, 151, (1956)
- (9) E.R. Andrew, *Phys. Rev.* 91, 425 (1953)
- (10) H.S. Gutowsky, R.E. McClure, and C.J. Hoffman, *Phys. Rev.* 81, 635 (1951)
- (11) G.W. Smith, *J. Appl. Phys.* 35, 1217 (1964)
- (12) J. Jeener, R. Du Bois, and P. Broekaert, *Phys. Rev.* 139, A.1959 (1965)
- (13) A.G. Anderson and A.G. Redfield, *Phys. Rev.* 116, 583, (1959)
- (14) I. Solomon and J. Ezzratty, *Phys. Rev.* 127, 78 (1962)

## chapter 3.

## SATURATION III.

PROGRESSIVE SATURATION IN  
POTASSIUM CAPROATE AND LITHIUM STEARATE

## I. EXPERIMENTAL

The spectrometer used was a Varian Associates model DP 60 dual purpose NMR spectrometer. The calibrations were performed in the manner described in chap 2.  $H_1$  was measured for a -20 db attenuation setting on the rf unit. The precision attenuators in the rf unit are accurate to  $\pm 2\%$  according to Varian, so the other  $H_1$  values were determined from the attenuator settings. The signals were recorded on a Varian model G-10 strip-chart recorder running at 16 in/hr.

The potassium caproate sample (abbreviated  $KC_6$ ) was dried but not fused in the course of preparation. The details have been presented previously /1/. The anhydrous lithium stearate sample ( $LiC_{18}$ ) was not fused on preparation either, and also has been described before /2/. The samples were in 5 mm dia sealed pyrex tubes with thinned down walls. A 5 mm dia insert was used in the NMR probe. The spectra were run at room temperature.

## II. RESULTS AND DISCUSSION

### A. Potassium Caproate

#### 1. Absorption spectra at various rf levels

Lock-in absorption-mode proton magnetic resonance spectra of potassium caproate at three different rf power levels are shown in Fig 1\*. The spectrum at  $H_1 = 1.26$  mG is only a little saturated. The one at  $H_1 = 4.0$  mG is interesting because it shows the point at which the saturation narrow component intensity is roughly equal to that of the normal curve. The one at  $H_1 = 22.4$  mG is the saturation narrowed spectrum. The line width is 8.5 gauss at  $H_1 = 1.26$  mG and 3.9 gauss at  $H_1 = 22.4$  mG. Lorentzian and Gaussian derivative curves have been fitted to the normal and saturation narrowed spectra. The wings of the normal spectrum drop off more rapidly than the Gaussian curve. The saturation narrowed spectrum is intermediate between the Gaussian and the Lorentzian curves, but is at least more Lorentzian than Gaussian.

---

\* In Fig 1 the modulation frequency  $\nu_m$  is 80 Hz of p-p amplitude  $2H_m = 0.72$  G. The rf level  $H_1$  is given in mG. The rf frequency  $\nu_0$  is 60 MHz. The calibration line indicates 10 G.

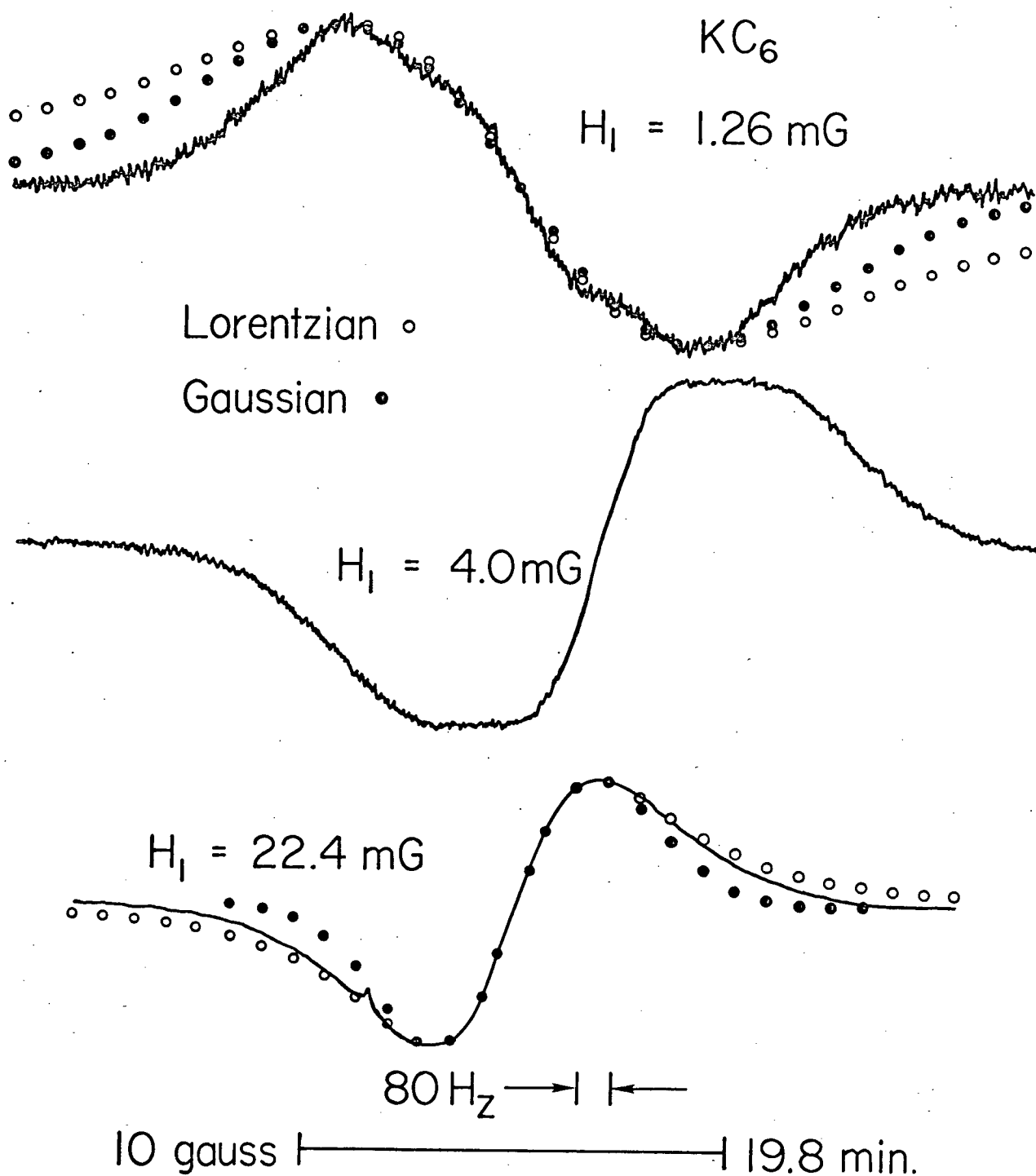


Fig 1 - Absorption spectra of potassium caproate at three rf field intensities.

The second moment of the  $H_1 = 1.26$  mG spectrum in Fig 1 is  $9.9 \text{ gauss}^2$ . The average of this result and three others (obtained from two  $H_1 = 0.40$  mG and one  $H_1 = 0.71$  spectra) is  $10.4 \text{ gauss}^2$ ,\* the maximum deviation being  $\pm 0.5 \text{ gauss}^2$ . The average saturation narrowed line width  $\Delta H_{as}$  obtained from four spectra at high rf levels (two at  $H_1 = 22.4$  mG one of which is shown in Fig 1, and one each at  $H_1 = 12.6$  mG and  $H_1 = 7.1$  mG) is  $3.85$  gauss with a maximum deviation of  $\pm 0.15$  gauss. The modulation was the same as for Fig 1. There was no significant variation in  $\Delta H_{as}$  with  $H_1$  over this range - viz,  $H_1 = 22$  to  $7.1$  mG. From the above average values we calculate, using equation (2-9), an apparent Zeeman to dipolar spin-lattice-relaxation-time ratio  $T_1/T_D$  of 3.2.

## 2. Progressive saturation of absorption

In Fig 2# the absorption signal  $v_1(\text{max})$  from a series of spectra is plotted against the rf field  $H_1$ . The solid line follows  $v_1$  measured at the normal line width; the dashed line

---

\* This value is different from the 40 MHz second moment at  $295^\circ\text{K}$  reported for  $\text{KC}_6$  in ref /1/ because the modulation corrections were in error there. Peak-to-peak modulation amplitudes were used by mistake in the correction term  $-H_m^2/4$  instead of just the peak amplitudes. The corrected  $\text{KC}_6$  second moments in ref /1/ should be  $22.5 \pm 0.8 \text{ gauss}^2$  at  $77^\circ\text{K}$  and  $10.1 \text{ gauss}^2$  at  $295^\circ\text{K}$ . The corrected second moment for  $\text{KC}_8$  at  $77^\circ\text{K}$  is  $23.0 \text{ gauss}^2$  (the error here was only  $0.1 \text{ gauss}^2$ ). The error for  $\text{KC}_{10}$  was negligible.

# In Fig 2  $\nu_m = 40$  Hz,  $2H_m = 0.76$ ,  $\nu_0 = 60$  MHz. Complete spectra were run.

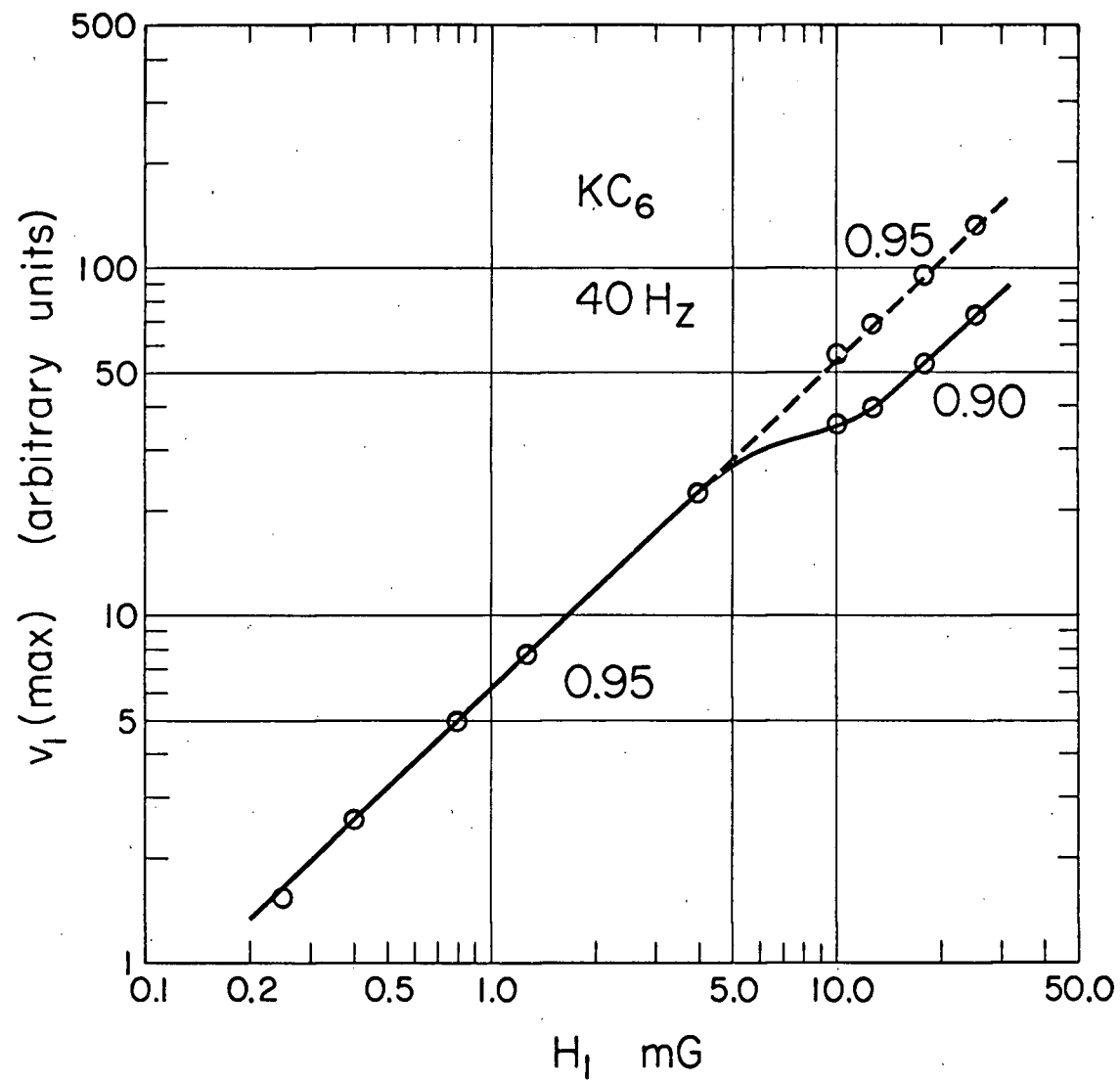


Fig 2 - Maximum absorption signal in potassium caproate as a function of rf field intensity.

$v_1(\text{max})$  of the saturation narrowed curve. Note that this is a log-log plot. The  $v_1(\text{max})$  behaviour here is quite different from that for  $\text{CaF}_2$  in Fig 2-4. In Fig 2-4 the  $v_1(\text{max})$  line has already turned over by the time the narrow component appears, but here in Fig 3-2 the line is still linear and it is remarkable that it extends on through  $v_1(\text{max})$  of the saturation narrowed curves.

This graph was actually obtained quite early in the course of this thesis work and was done to see whether or not two-quantum transitions were responsible for the observed narrowing. Two-quantum transitions are ones in which the energy is supplied by two quanta and they had been observed in the electron spin resonance spectrum of atomic oxygen by Hughes and Geiger /3/. The two-quantum lines appeared  $\frac{1}{2}$  way between, and were  $\frac{1}{2}$  the width of, the normal lines. Their intensity, after they appeared, grew faster with increasing  $H_1$  than that of the normal lines. These features were explained by second-order-time-dependent perturbation theory and it was postulated that multiple-quantum transitions could also occur in NMR. They were observed in liquids by Anderson /4/ and Kaplan and Meiboom /5/. The theory for multiple-quantum transitions in NMR was developed by Yatsiv /6/ using Bloch-Wangsness /7/ NMR theory. It was found, in part, that for a transition of multiplicity  $n$ ; the line width is roughly  $n$  times as narrow as the corresponding line width for  $n = 1$ , and the observed signal grows as  $H_1^{2n-1}$  before saturation begins. The slope, then, of a log-log plot of the signal strength versus the rf field  $H_1$  yields the multiplicity directly. Although Bloch theory was really only formulated for

spin systems like those found in liquids and gases, it was felt that it had some validity in solids. In Fig 2 we see that in the low rf region the slope of the line is nearly 1 (actually 0.95, error may be in  $H_1$  calibration) and this is what we expected. But the same line goes through the saturation narrowed signal points, whereas, the slope for a double-quantum transition would be 3. Consequently we had to look for some other explanation.

Another thing we have learned is that the usual test for saturation — viz, increasing  $H_1$  and seeing whether or not the signal increases proportionately — is not reliable. One might be unfortunate and choose to run an absorption spectrum of  $KC_6$  at  $H_1 = 10$  mG; Fig 2 shows that one could increase  $H_1$  up to a factor of 2.5 and find the signal linear in  $H_1$  all the way; yet we know that this is in the saturation narrowed region.

### 3. Progressive saturation of dispersion

The dispersion signal  $u_1(0)$  in  $KC_6$  was measured for a number of rf levels and a fixed modulation. The result  $u_1(0)/H_1$  is plotted against  $H_1$  in Fig 3.\* The first point is at  $H_1 = 0.29$  mG yet there still appears to be some saturation — the slope would be zero if the saturation were negligible. We therefore are unable to get  $H_1^*$  from this type of plot as we

---

\* In Fig 3  $\nu_m = 200$  Hz,  $2H_m = 1.02$  G,  $\nu_0 = 56.4$  MHz. The signal  $u_1(0)$  was measured in the manner described in chap 2. The sample was at room temperature.

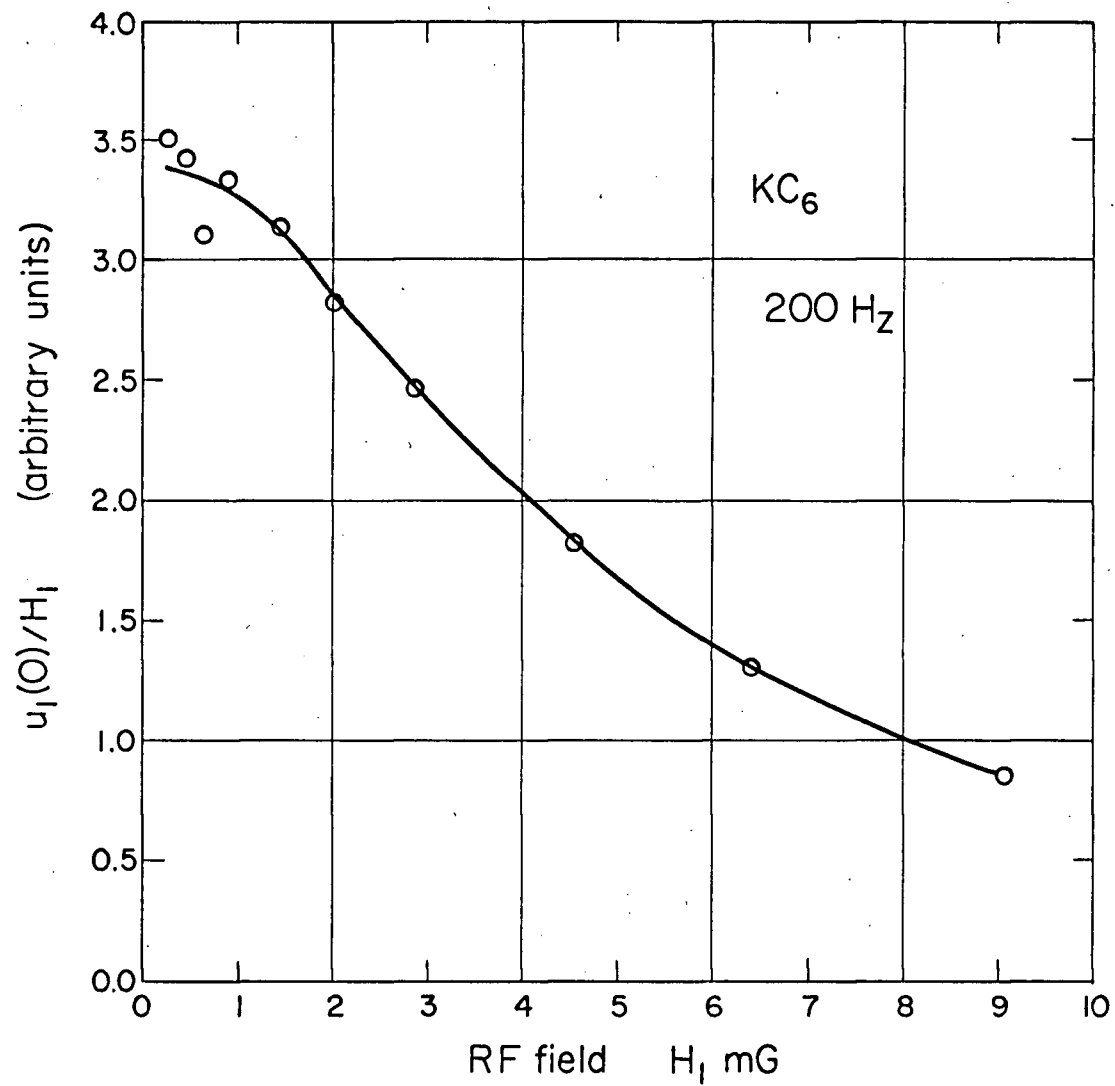


Fig 3 - Normalized dispersion signal,  $u_1(0)/H_1$ , in potassium caproate as a function of rf field intensity.

could for  $\text{CaF}_2$ ; but we can get it from the  $H_1/u_1(0)$  versus  $H_1^2$  plot shown in Fig 4. The intercept  $H_1^2 = 25 \times 10^{-6} \text{ gauss}^2$ . Also, since this plot is a straight line, we have another verification of equation (1-48).

Three absorption spectra were integrated for  $G(0)$ . The average value is  $0.73 \text{ gauss}^{-1}$  with a maximum deviation of  $0.03 \text{ gauss}^{-1}$ . These results yield a spin lattice relaxation time  $T_1 = 4.1_1 \text{ sec}$ .

Let us see if we have conformed to the experimental restrictions imposed by Goldman.  $T_1/T_D$  was found to be 3.2 so  $1/T_D$  is  $0.78 \text{ sec}^{-1}$ . The angular modulation frequency  $\Omega$  is  $1256 \text{ sec}^{-1}$  and the experimental local field in rad/sec is  $5.0 \times 10^4 \text{ sec}^{-1}$ . The point at  $H_1^2 = 82 \times 10^{-6} \text{ G}^2$  ( $H_1 = 9.06 \text{ mG}$ ) in Fig 4 is not far off the straight line and at this point  $2W(0) = 0.80 \text{ sec}^{-1}$ . These values satisfy the conditions in equation (2-12).

Now what about the line width to modulation width restriction? The modulation  $2 H_m$  for the run reported in Fig 3 and 4 is 1.02 gauss. Taking line widths from Fig 1 we find line width to modulation with ratios  $\Delta H_a/2H_m$  of 8.3 at  $H_1 = 1.26 \text{ mG}$  and only 3.8 at  $H_1 = 22.4 \text{ mG}$  when the curve is saturation narrowed. The saturation narrow component is about the same intensity as the normal component for  $H_1 = 4.0 \text{ mG}$ . Looking at Fig 4 we see that  $H_1/u_1(0)$  is still on the line at  $H_1 = 6.4 \text{ mG}$  ( $H_1^2 = 40 \times 10^{-6} \text{ G}^2$ ) but is off, as we have mentioned above, by the time  $H_1 = 9.06 \text{ mG}$ . At this point  $S(0) = 3.3$  and we have reached the practical saturation limit for this case. This point

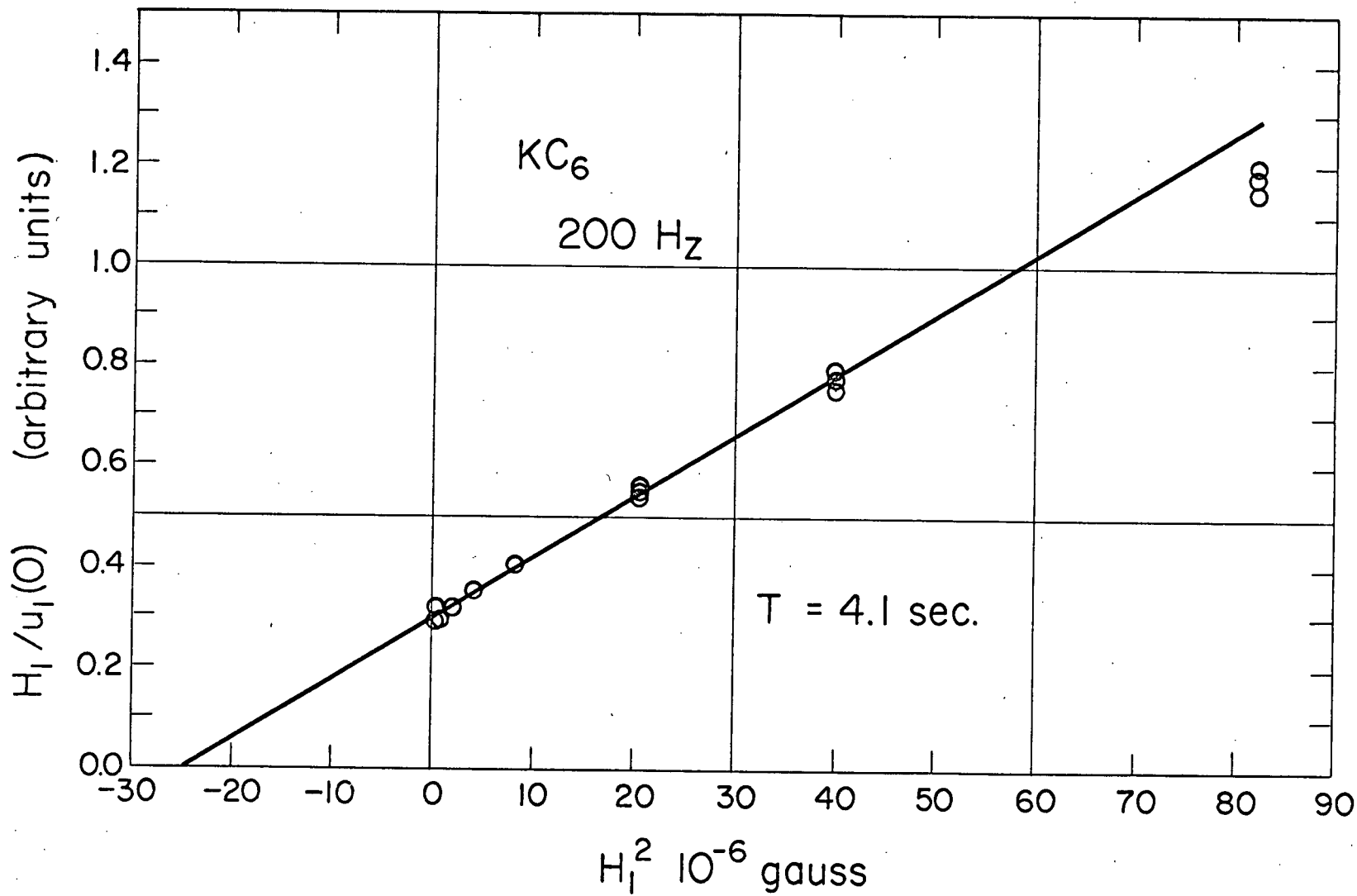


Fig 4 -  $H_1/u_1(0)$  in potassium caproate as a function of  $H_1^2$ .

has been discussed in more detail in chapter 2.

## B. Lithium Stearate

### 1. Absorption saturation

Three lock-in absorption-mode proton magnetic resonance spectra of lithium stearate are reproduced in Fig 5.\* A normal spectrum at  $H_1 = 0.45$  mG, one at  $H_1 = 4.5$  mG in which the normal and narrow components are about the same intensity, and a saturation narrowed one at  $H_1 = 14.3$  mG. The line widths are 14.1 gauss and 8.3 gauss at  $H_1 = 0.45$  and 14.3 mG respectively. Gaussian and Lorentzian curves have been fitted to these two. The normal spectrum again cuts off more rapidly than the Gaussian curve. The saturation narrowed curve is almost pure Gaussian and, although is not what Provotorov theory predicts, the change in shape on saturation is at least in the right direction - viz, the wings do not go to base line at as fast a rate as the normal spectrum. Modulation saturation may again be perturbing the spectrum.

The second moment of the  $H_1 = 0.45$  mG spectrum in Fig 5 is 22.1 gauss<sup>2</sup>. The average second moment from this one and three others at the same rf level is  $21.6 \pm 0.4$  gauss<sup>2</sup>, where

---

\* In Fig 5  $\nu_m = 40$  Hz,  $2 H_m = 1.78$  G,  $\nu_0 = 56.4$  MHz.  $H_1$  is given in mG. The sample is at room temperature.

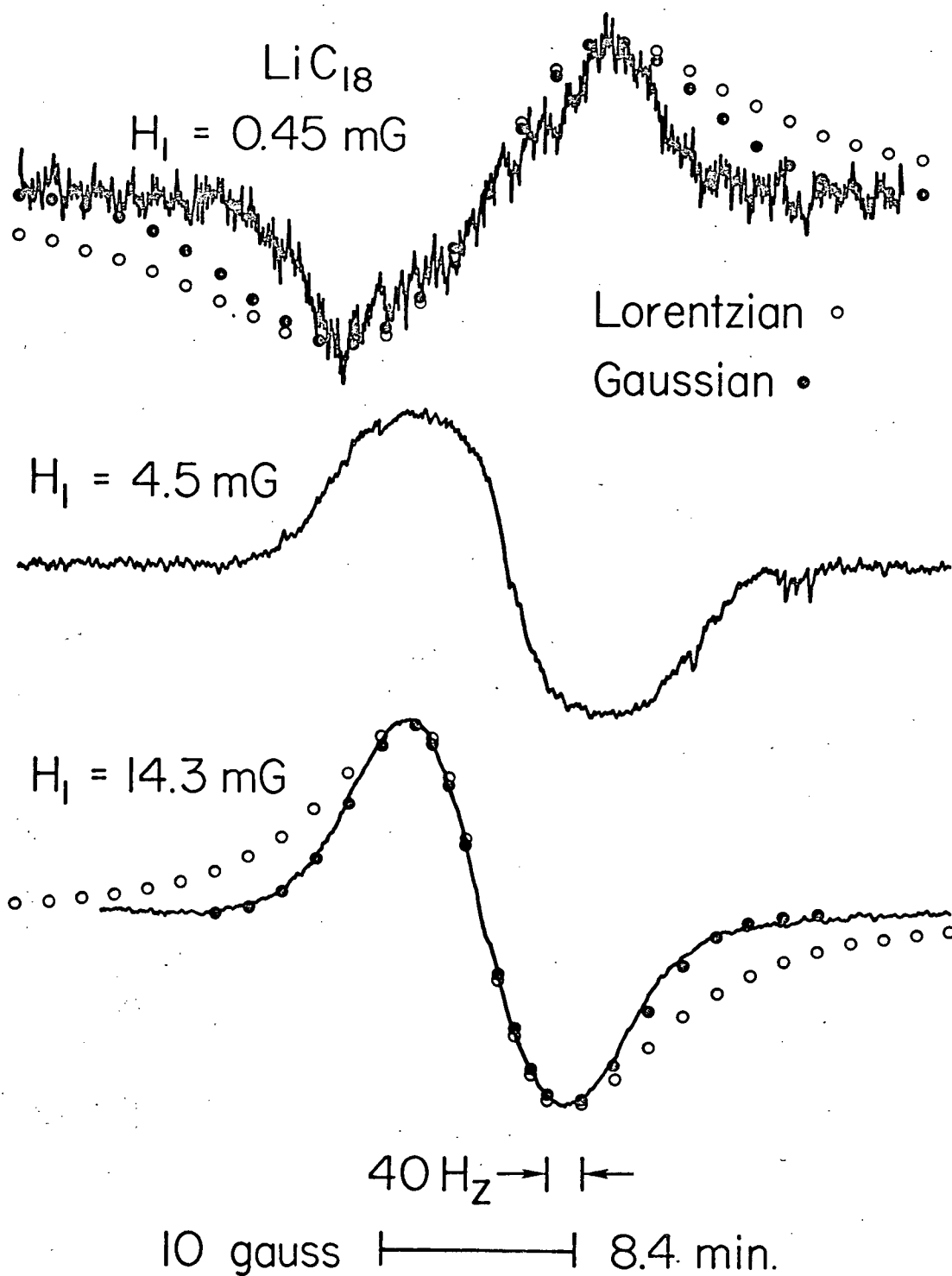


Fig 5 - Absorption spectra of lithium stearate at three rf field intensities.

0.4 gauss<sup>2</sup> is the maximum deviation. The average saturation narrowed line width obtained from six spectra for  $H_1 = 14.3$  mG (the spectrum in Fig 5 included) is  $3.85 \pm 0.15$  gauss<sup>2</sup>, 0.15 being the maximum deviation. The modulation was the same as for Fig 5. These values yield an apparent Zeeman to dipolar relaxation time ratio  $T_1/T_D$  of 7.3 in LiC<sub>8</sub> at room temperature.

## 2. Progressive saturation of dispersion

The dispersion signal  $u_1(0)$  at a fixed modulation was measured in LiC<sub>18</sub> for a series of rf levels. The result  $u_1(0)/H_1$  is plotted against  $H_1$  in Fig 6\* and  $H_1/u_1(0)$  versus  $H_1^2$  in Fig 7. The latter is a straight line and again confirms the theory. Its intercept  $H_1^{*2} = 8.8 \times 10^{-6}$  gauss<sup>2</sup>. The average value of  $G(0)$  calculated from three normal absorption spectra is  $0.487$  gauss<sup>-1</sup>, the maximum deviation being  $0.008$  gauss<sup>-1</sup>. The relaxation time  $T_1$  then is 17.4 sec.

Are the Goldman restrictions obeyed?  $T_1/T_D$  in LiC<sub>18</sub> was found to be 7.3 and so  $1/T_D$  is  $0.42$  sec<sup>-1</sup>.  $\Omega = 1256$  sec<sup>-1</sup> and  $D$  experimental is  $7.3 \times 10^4$  sec<sup>-1</sup>. In an extended version of Fig 7 we find  $H_1/u_1(0)$  deviates from the straight line at  $H_1^2 = 40.8 \times 10^{-6}$  G<sup>2</sup> ( $H_1 = 6.4$  mG). At this point  $2W(0) = 0.266$  sec<sup>-1</sup> and  $S(0) = 4.6$ . The conditions in equation (2-12) are

---

\* In Fig 6  $\nu_m = 200$  Hz,  $2H_m = 2.12$  G,  $\nu_0 = 56.4$  MHz. The signal  $u_1(0)$  was measured as in chap 2. The sample was at room temperature.

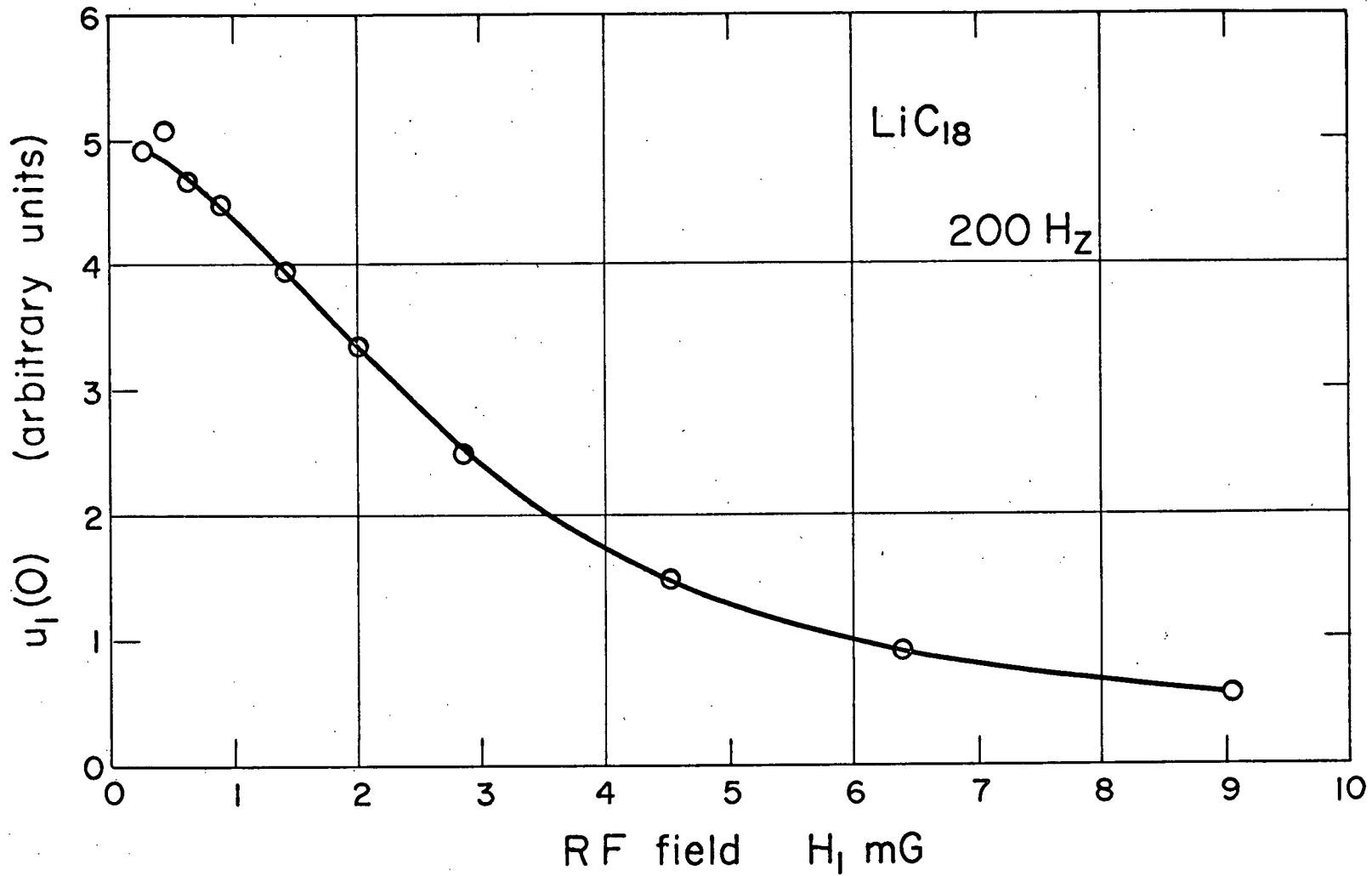


Fig 6 - Normalized dispersion signal,  $u_1(0)/H_1$ , in lithium stearate as a function of rf field intensity.

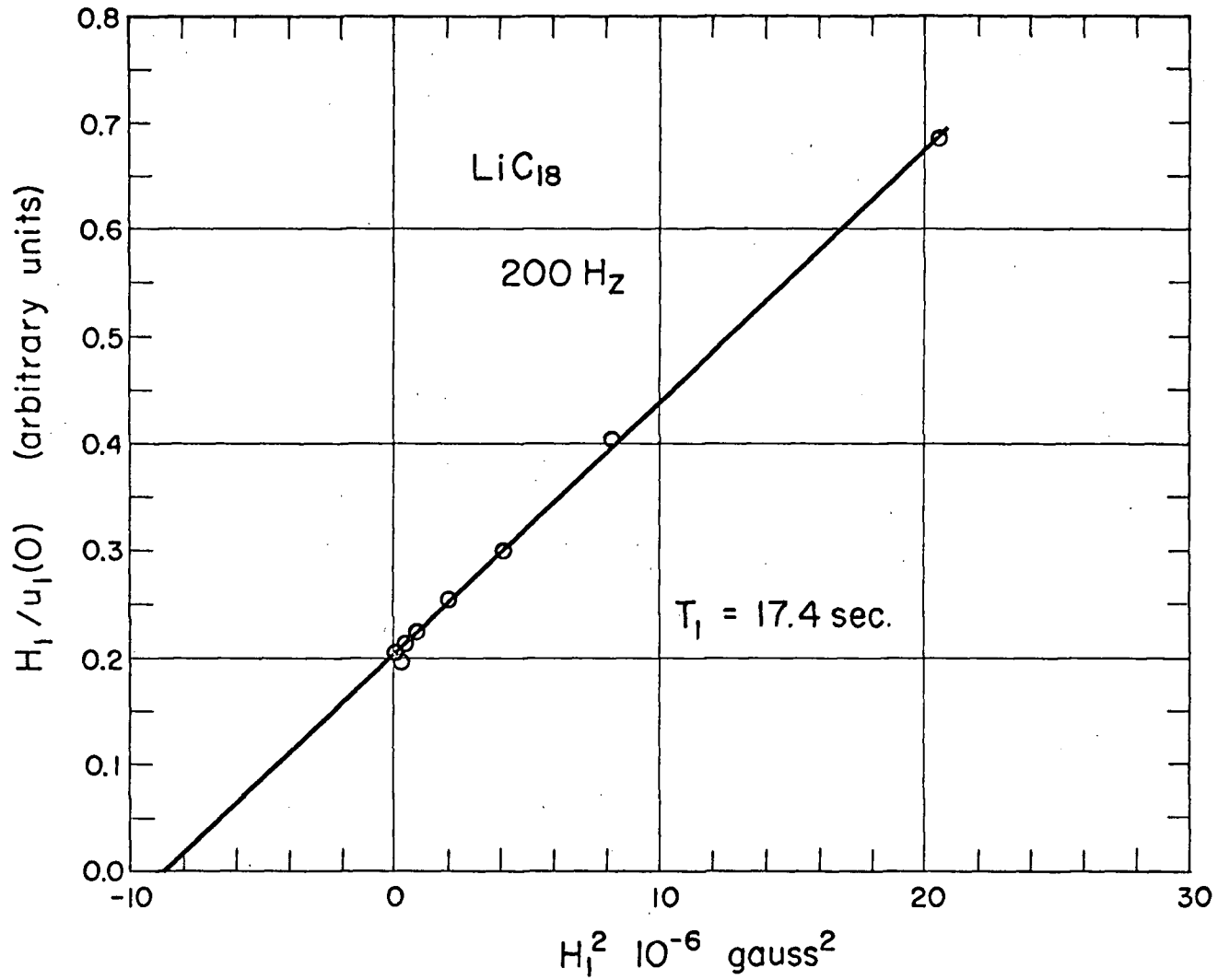


Fig 7 -  $H_1/u_1(0)$  in lithium stearate as a function of  $H_1^2$ .

satisfied. Now let us consider the modulation width restriction. The modulation  $2 H_m$  for the run in Fig 6 and 7 is 2.12 gauss. Taking the line widths from Fig 5 we find  $\Delta H_a/2H_m$  ratios of 6.7 at  $H_1 = 0.45$  mG and 3.9 at  $H_1 = 14.3$  mG when the curve is saturation narrowed. The narrow and normal components are of apparently the same intensity for  $H_1 = 4.5$  mG. At  $H_1 = 6.4$  mG,  $S(0) = 4.6$ ,  $H_1/u_1(0)$  versus  $H_1^2$  is no longer a straight line and we have reached the saturation limit for practical modulation widths. The  $S(0)$  value at this limit is a little higher in  $\text{LiC}_{18}$  than that for  $\text{KC}_6$ . The difference is probably due to line shape and  $T_1/T_D$  ratio differences. This point is discussed in more detail in chapter 2.

### III. CONCLUSIONS

The saturation of the lock-in dispersion signal  $u_1(0)$  in potassium caproate and lithium stearate is described by equation (1-48). This is further evidence for the validity of Provotorov-Goldman saturation theory.

One must take great care to avoid saturation to be certain that the observed lock-in absorption curve is the true absorption derivative spectrum. To do this the spectrum may have to be obtained for a wide range of rf levels. This is not usually possible with the marginal oscillator NMR spectrometers used in many laboratories. In fact it can happen that for samples with long spin lattice relaxation times, only a saturation narrowed

curve can be obtained with this type of spectrometer and the experimenter can be unaware of this fact at the time, Grant /8/.

Even in the normal spectra shown in Fig 1 and 5 there is some saturation and now that the  $T_1$  values are known we can calculate how much. For the  $KC_6$  normal spectrum at  $H_1 = 1.26$  mG the saturation parameter  $S(0) = 0.059$  and so the saturation factor  $Z(0) = 1/1.059$ . For the  $LiC_{18}$  normal spectrum at  $H_1 = 0.45$  mG we find  $S(0) = 0.023$  and  $Z(0) = 1/1.023$ . At these low saturation levels we are probably observing the true line=shape. The signal to noise ratio in the  $LiC_{18}$  spectrum is already lower than we would like and this is with the sample in the 5 mm insert. It appears that some saturation cannot be avoided. The situation would become even worse if the sample were in the variable temperature apparatus. It is probable that much of the work reported in the literature was done under partial saturation conditions, particularly that done with marginal oscillator spectrometers. We have found, however, that phase transitions in  $LiC_{18}$  can be found using saturation narrowed spectra.\* Sudden drops in the line width versus temperature curve correspond in temperature to similar ones in the same plot for normal width spectra. This is not unexpected because the saturation narrowed line width  $\Delta H_{as}$  is related to the second moment of the unsaturated spectrum, equation (1-45). One must be sure, however, that one is not operating close to the saturation narrowing region, otherwise a change in  $T_1$  with temperature could cause the other component of the line to appear and cause one to think that a phase transition is occurring.

---

\*

Details to be presented in a later chapter.

## REFERENCES

- (1) (a) W.R. Janzen and B.A. Dunell, Trans. Faraday Soc. 59, 1260 (1963); (b) W.R. Janzen, M.Sc. Thesis in Chemistry, University of British Columbia, Vancouver, B.C. (1963)
- (2) T.J.R. Cyr, W.R. Janzen, and B.A. Dunell in "Ordered Fluids and Liquid Crystals", Advances in Chemistry Series, No. 63, American Chemical Society, Washington, D.C. (1967) pp 13-25
- (3) V.W. Hughes and J.S. Geiger, Phys. Rev. 99, 1842 (1955)
- (4) W. Anderson, Phys. Rev. 104, 850 (1956)
- (5) J.I. Kaplan and S. Meiboom, Phys. Rev. 106, 499 (1957)
- (6) Shaul Yatsiv, Phys. Rev. 113, 1522 (1959)
- (7) R.K. Wangsness and F. Bloch, Phys. Rev. 89, 728 (1953); F. Bloch, Phys. Rev. 102, 104 (1956); 105, 1206 (1957)
- (8) R.F. Grant, Private Communication.

## chapter 4.

## SATURATION IV.

SIGNAL DECAY EXPERIMENTS IN  
POTASSIUM CAPROATE AND LITHIUM STEARATE

## I. INTRODUCTION

In this chapter we report on experiments using a direct method of measuring  $T_1$  called the signal decay technique. The steady state solution of equation (1-1) is:

$$n(st)/n(0) = [1 + \gamma^2 H_1^2 T_1 f(\Delta)/2]^{-1} \equiv Z \quad (1)$$

where  $n(st)$  is the steady state value of the population difference  $n(t)$  and  $Z$  is the saturation factor - also defined in equation (2-13). We are interested in the rate of approach of the spin system to the above steady state, and this is given by the following solution to the differential equation (1-1):  
Andrew /1, p 21/

$$n(st) - n(t) = [n(st) - n(0)] \exp (-t/T_1 Z). \quad (2)$$

Thus the approach to the steady state in the presence of an rf field has a characteristic time  $T_1 Z$ . When the amount of saturation is negligible, the characteristic time becomes just  $T_1$ .

The signal decay technique to measure  $T_1$  in solids appears to have originated with Linder /2/ in 1957. It has been revived again by Smith /3/ in 1962. In this method the spin system was allowed to equilibrate in the fixed magnetic field corresponding to one of the extrema of the absorption derivative spectrum. A partially saturating rf field was applied and the lock-in absorption signal  $v_1(\max)$  observed as a function of time. The signal decayed from its initial amplitude  $a_0$  to its partially saturated equilibrium value  $a_s$ . If BPP theory is assumed, equation (2) says that the signal decays exponentially with time constant  $T_1 Z$ , where  $Z = a_s/a_0$ . This particular signal decay method, however, suffers from the same deficiencies as progressive saturation of the lock-in absorption signal — namely, saturation narrowing and modulation saturation.

We now know that we can avoid these complications by observing the lock-in dispersion signal  $u_1(0)$ , and that is how the signal decay experiments reported here were done.

## II. EXPERIMENTAL

### A. Samples

The potassium caproate ( $KC_6$ ) and Lithium stearate ( $LiC_{18}$ ) samples were the ones described in chapter 3.

### B. Spectrometer

The spectrometer was the Varian DP60 described in chapter 3

and was operated at a radio frequency of 56.4 MHz. The rf field was turned on for a signal decay measurement with a SPST coaxial switch made from an Amphenol type 83-1T "T" adapter. The switch was built by the chemistry department shop according to a design by Bernard W. Joseph of General Motors Research Laboratories, Warren, Mich.

The 5 mm dia NMR probe insert was used for measurements at room temperature, the 15 mm one at 77 °K. For this temperature the sample tube was in the finger of a Dewar containing liquid nitrogen, the finger fitted into the 15 mm insert.

The signal decay curves taken at room temperature were recorded on a Sanborn model 151 thermal strip chart recorder in conjunction with a Sanborn model 67-300 preamplifier. The decay curves for  $\text{LiC}_{18}$  at liquid nitrogen temperature (where  $T_1$  is quite long) were recorded on a Varian model G-10 strip-chart recorder running at 20 in/min. The response time for this recorder to reach the signal voltage just after switching on the rf field was reduced by the following technique: the servo was switched off and the pen moved to the top of the scale, then after the spin system had reached equilibrium, the rf field and the recorder servo were switched on simultaneously. This way the pen had only a short distance to move before it began recording the signal.

### C. Method

The method used was the same as the Linder signal decay technique /2/ described above, except that the lock-in dispersion

signal  $u_1(0)$  was observed instead of the absorption signal  $v_1(\max)$ . In this case we know that the equation for the decay (assuming the necessary conditions are obeyed) is:

$$a - a_s = (a_0 - a_s) \exp(-t/T_1 Z(0)) \quad (3)$$

where we recall that  $a$  is the observed signal,  $a_0$  is its initial value,  $a_s$  is its partially saturated equilibrium value, and  $Z(0) = a_s/a_0$ .

Typical dispersion signal decay (DSD) curves,  $KC_6$  trace # 119 and  $LiC_{18}$  trace # 406, taken at room temperature are shown in Fig 1. (The small circles mark  $a_0$  obtained from the semilog plots). The recorder was run for some time before and after the signal decay at a slow speed in order to establish a good average base line, it was also switched to the slower speed to get a noise averaged value for  $a_s$  in each case.

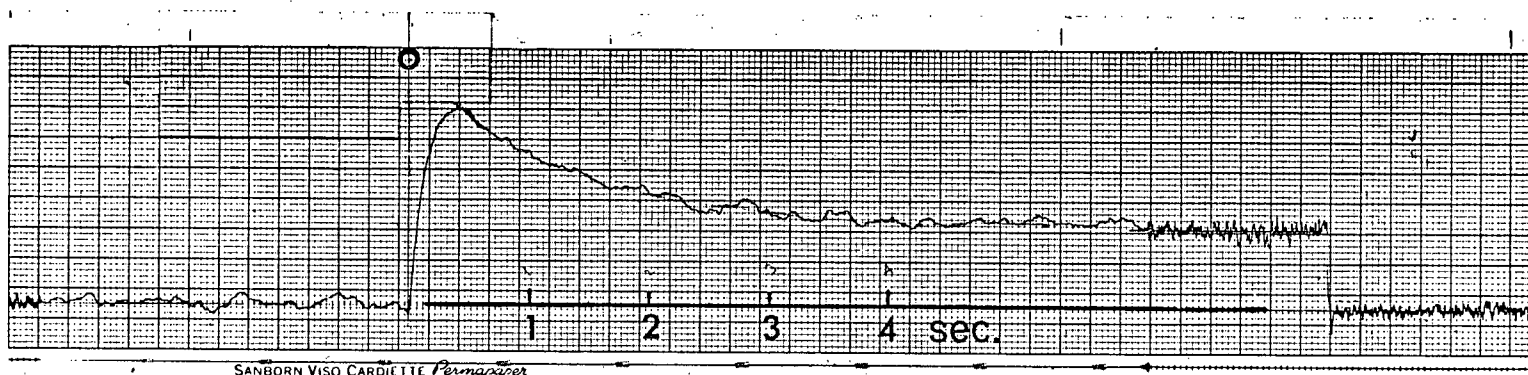
A semilog plot of  $a - a_s$  versus time yields, according to equation (3),  $T_1 Z(0)$  from the slope and  $a_0$  from the intercept. Then  $Z(0)$  is calculated and  $T_1$  obtained. The semilog plots from the decay curves in Fig 1 are shown in Fig 2 and 3 for  $KC_6$  and  $LiC_{18}$  respectively.

### III. RESULTS AND DISCUSSION

#### A. Potassium Caproate

The results from the measured  $KC_6$  decay curves are listed in Table I. They were all taken at room temperature.

KC<sub>6</sub> trace 119 H<sub>1</sub> = 7.2 mG



LiC<sub>18</sub> trace 406 H<sub>1</sub> = 6.4 mG

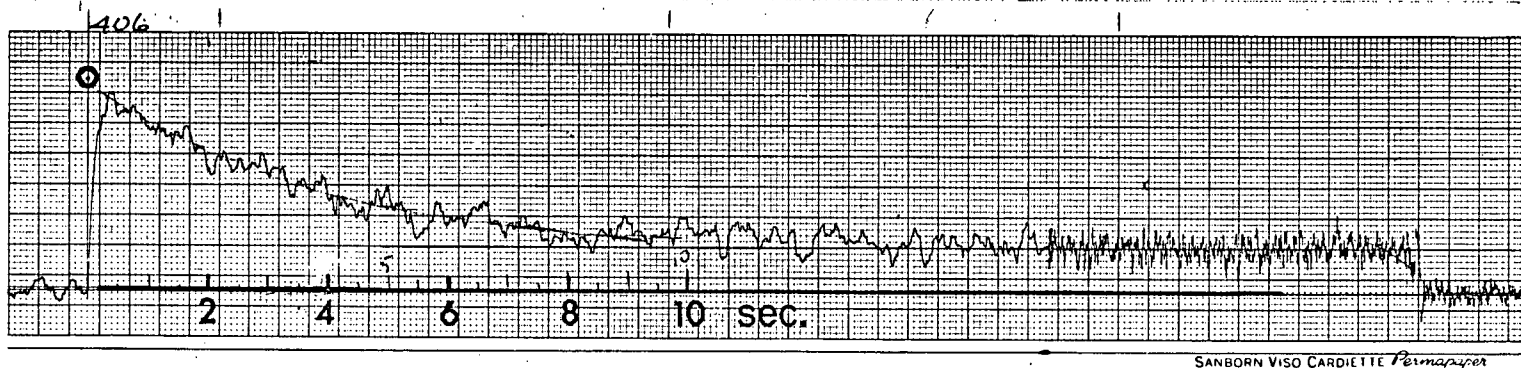


Fig 1 - Typical dispersion signal decay curves for potassium caproate and lithium stearate.

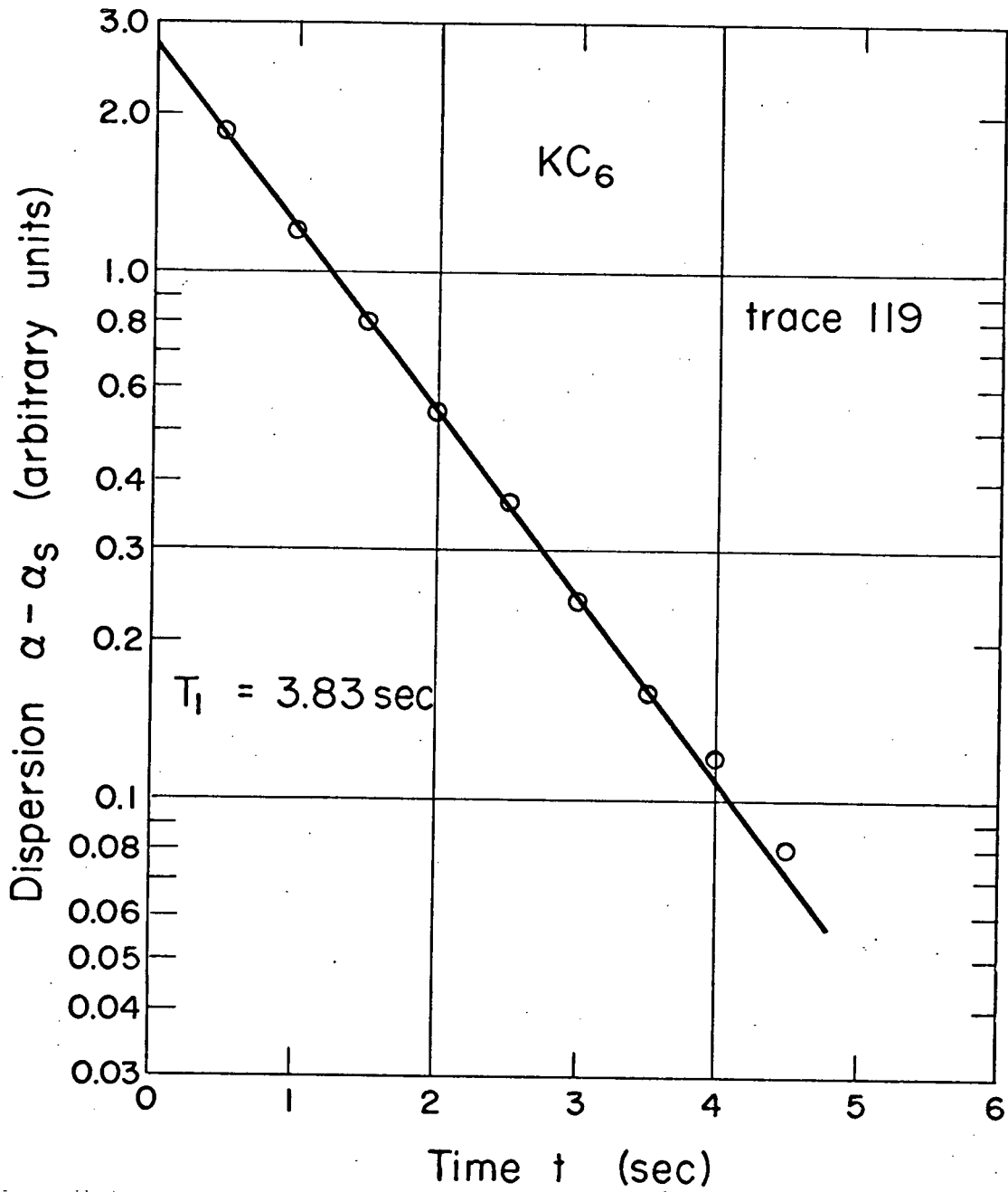


Fig 2 - Semilog plot of  $\alpha - \alpha_s$  versus time for a potassium caproate dispersion signal decay curve.

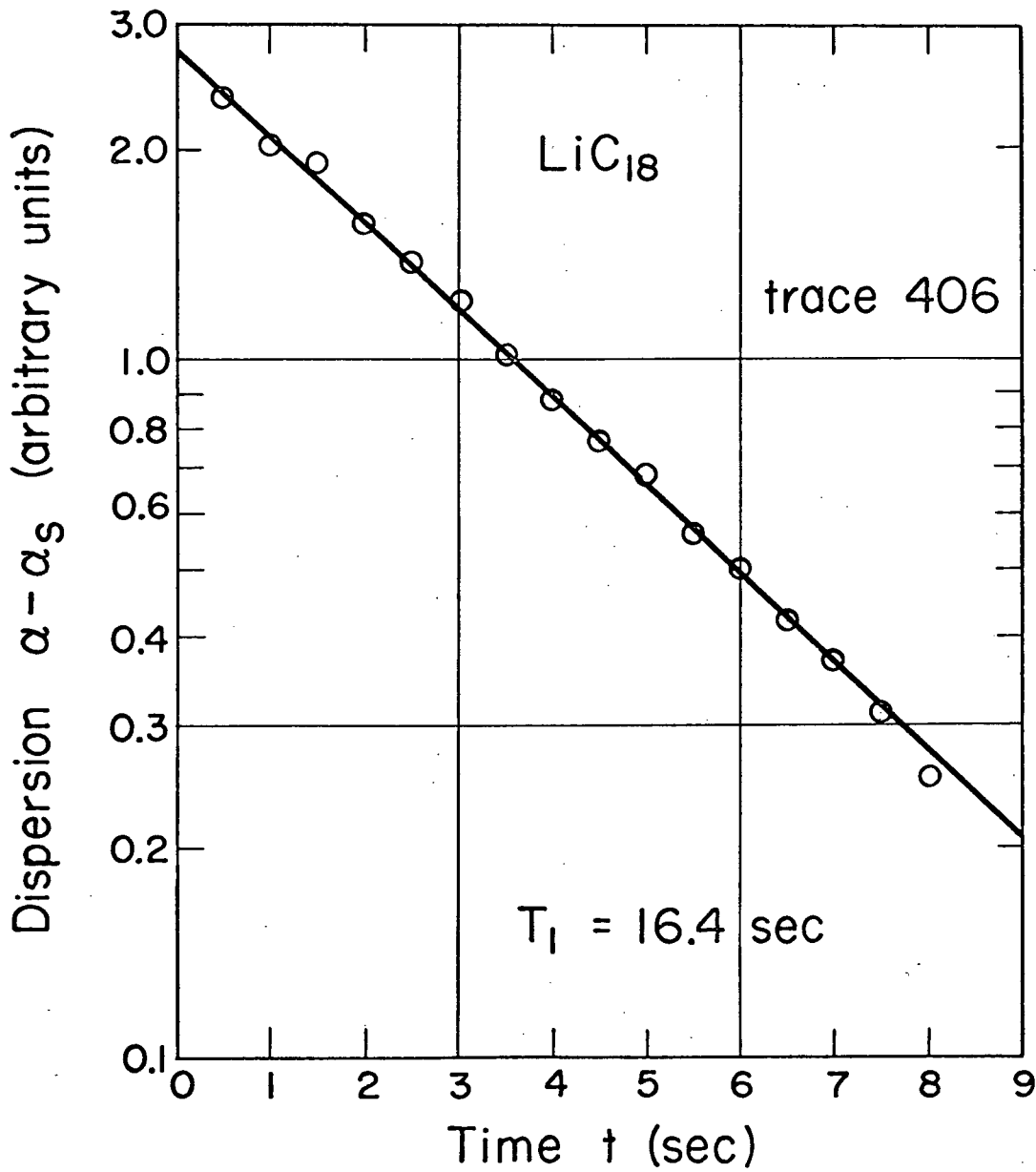


Fig 3 - Semilog plot of  $\alpha - \alpha_s$  versus time for a lithium stearate dispersion signal decay curve.

Table I -  $KC_6$  dispersion signal decay results

Trace number	$H_1$ milligauss	$2H_m^*$ gauss	$Z(0)$	$T_1$ sec
104	9.1	1.02	0.232	4.08
110	7.2	1.02	0.315	3.99
113	9.1	2.12	0.214	3.96
114	9.1	2.12	0.198	4.19
119	7.2	2.12	0.308	3.83
			average	<u>4.01</u>

\*200 Hz modulation frequency.

We have chosen to analyse decay curves for  $Z(0)$  lying roughly in the range 0.2 to 0.3 as this allows  $a_g$  to be measured with reasonable precision and still leave a reasonable amount of signal decay to plot. The average value of  $T_1$  obtained this way is 4.01 sec, the maximum deviation being 0.18 sec. This agrees very well with our progressive saturation of dispersion (PSD) result of 4.1<sub>1</sub> sec reported in chapter 3. We expect the DSD value to be the more accurate one as it does not involve any calibrations.

### B. Lithium Stearate

The results from the measured  $LiC_{18}$  decay curves taken at room temperature are listed in Table II.

Table II -  $\text{LiC}_{18}$  signal decay results

Trace number	Signal# mode	$H_1$ milligauss	$2H_m^*$ gauss	Z	$T_1$ sec
406	D	6.4	2.12	0.210	16.4
408	D	6.4	2.12	0.205	15.4
410	D	6.4	4.23	0.202	16.4
412	D	6.4	4.23	0.194	16.9
				average	16.3
414	A	6.4	2.12	0.498	23.0
417	A	14.3	2.12	0.342	18.9

#D - dispersion signal  $u_1(0)$ , A - absorption signal  $v_1(\text{max})$ .

\*200 Hz modulation frequency.

The average of the DSD  $T_1$  results is 16.3 sec, the maximum deviation being 0.9 sec or 5.5%. This compares quite well with our chapter 3 PSD result of 17.4 sec, the PSD value being only 6.7% higher.

The results from two absorption signal decay (ASD) curves are also listed in Table II. Trace 414 was taken at the same  $H_1$  value as the DSD curves, but Z is much larger (the degree of saturation much smaller) and the  $T_1$  obtained is about 41% higher. This is what we expect for Z — the line shape function  $f(\Delta)$  and thus the saturation parameter  $S(\Delta)$  decrease as we move out to the inflection point — but, if there were no complications,  $T_1$  would not change with Z. Trace 417 with  $Z = 0.342$  yields a  $T_1$  of 18.9 sec, a value still 16% higher than the average DSD result.

We were fortunate that the  $T_1$ 's of  $KC_6$  and  $LiC_{18}$  at room temperature were such that they could be measured by both our continuous wave (CW) methods and the results compared. We have also measured the spin lattice relaxation time of  $LiC_{18}$  at 77 °K, where it is too long to measure by PSD, by the DSD technique. The results of the two decay curves #419 and #421 are 95 and 96 sec respectively. ( $H_1 = 4.5$  mG,  $2H_m = 2.12$  G at 200 Hz,  $Z(0) = 0.0806$  and  $0.0817$ ) since the amount of saturation was quite high here, the time constant of the output unit was increased in addition to going to a slower recorder speed while the base line and  $a_s$  were being recorded in order to improve the accuracy of the  $a_s$  measurements.

#### IV. CONCLUSIONS

The signal decay technique yields correct spin lattice relaxation times in solids provided that the lock-in dispersion signal  $u_1(0)$  is observed rather than the absorption signal  $v_1(\max)$ . The complications of saturation narrowing and modulation saturation are then avoided.

The signal decay technique is particularly suitable for long relaxation times and this is fortunate because the signal to noise is much too poor to do an accurate progressive saturation experiment in this situation.

We have two complimentary CW techniques for measuring spin lattice relaxation times in solids: DSD, dispersion signal decay

for long  $T_1$ 's, and PSD, progressive saturation of dispersion for short  $T_1$ 's.

#### REFERENCES

- (1) E.R. Andrew, "Nuclear Magnetic Resonance", Cambridge University Press, London (1955)
- (2) Solomon Linder, J. Chem. Phys. 26, 900 (1957)
- (3) G.W. Smith, J. Chem. Phys. 36, 3081 (1962);  
Dr. Smith kindly sent us the coaxial switch design of B.W. Joseph.

## chapter 5.

## ADIABATIC RAPID PASSAGE I.

## THEORY AND REVIEW

The nuclear magnetic resonance (NMR) adiabatic rapid-passage (ARP) experiments were originally begun just to measure spin lattice relaxation times  $T_1$  by a direct method that was not dependent on a theory for saturation, in order to check our saturation results. The ARP technique appeared to be the next best thing to a pulse spectrometer and would not require much building of equipment. These ARP experiments soon became a major research problem, however, when it was found that it was not generally known what all the requirements were for valid ARP results in solids, nor how to explain every detail of ARP experiments already in the literature /1, p 550/.

We think we have determined, with the help of experiments, what the proper conditions for ARP in solids are. We have then gone on to use this technique to measure the spin-lattice relaxation time and local field  $H_L$  in a few solid samples — viz,  $\text{CaF}_2$  single crystal and powder, and lithium stearate powder. We think that this is the first time that  $H_L$  has been measured

by ARP, and we think that this technique has great promise since  $H_L$  yields the second moment of the unsaturated absorption line by a simple calculation:  $\langle \Delta H^2 \rangle = 3(H_L)^2$ .

ARP signals can be obtained from solids even when  $T_1$  is so long that it is impossible to get a slow passage lock-in absorption spectrum. The method has the speed of the pulse technique, and the data reduction for second moment determination is much simpler. With our apparatus we were able to measure  $T_1$  values from about 1/2 second to over an hour. Shorter times could be measured with more sophisticated equipment. The method is particularly suitable for long  $T_1$ 's since exact resonance conditions do not have to be maintained as is the case in the pulse technique.

## I. INTRODUCTION

Since the initial NMR experiments on ARP were done by Bloch, Hansen, and Packard /2/, the technique has been developed as a method for measuring  $T_1$ 's in liquids by a number of workers. Drain /3/, Conger and Selwood /4/ and Chiarotti et al /5/ are some of the early ones. In addition to being easier to perform than NMR pulse experiments, ARP can be used to measure  $T_1$ 's for chemically shifted sets of nuclei, Nederbragt and Reilly /6/, Powles /7/.

The requirements for an ARP in a liquid are /1, p 65/

(1) the Bloch adiabatic condition for a complete inversion of the nuclear magnetization

$$\frac{dH_0}{dt} \ll \gamma H_1^2, \quad (1)$$

(2) the rapid passage condition - viz, the effects of relaxation must be negligible during the time of passage  $t_p$  through resonance

$$t_p \approx H_1 / \frac{dH_0}{dt} \ll T_1, T_2. \quad (2)$$

These requirements are not difficult to satisfy for experiments on liquids, however, in solids it is very difficult to meet condition (2) in view of the very short  $T_2$  encountered there. Redfield's analysis /8/ shows that the passage time  $t_p$  does not have to be short compared to  $T_2$  but only to  $T_1$ . Even so, only a few workers have used the ARP technique in solids. Redfield /9/ has measured  $T_1$  in copper and aluminum. He states the ARP conditions in solids to be:

$$T_1 \gg t_p \gg \text{the smaller of } (\gamma H_1)^{-1} \text{ or } T_2. \quad (3)$$

Also,  $H_1$  must be several times the value required to saturate the resonance under steady-state conditions. (4)

Abraham and Proctor /10/ have studied spin temperature using a LiF crystal, Slichter and Holton /11/ have studied adiabatic demagnetization in a rotating reference system using a NaCl crystal.

Perhaps the reason that ARP has not been used more in solids

is that it was not clear how Redfield arrived at the conditions (3, 4), (at least not to us) or perhaps the fact that  $H_1$  might have to be greater than  $H_L$  /1, p 550-4/ may have discouraged others from attempting the technique.

## II. ADIABATIC RAPID PASSAGE SIGNAL

### A. Adiabatic Variation of the Magnetization

Redfield's hypothesis of a spin temperature in the rotating reference frame leads to an adequate description of the ARP signal. From equations (14a) and (14c) in chap 1 we obtain the following expression for the magnetization in the rotating reference frame:

$$\underline{M}_r \equiv \langle \underline{M} \rangle = \frac{-\langle \mathcal{H}_{er} \rangle}{H_{er}^2 + H_L^2} H_{er} = N \frac{I(I+1) \gamma^2 \hbar^2}{3kT_s} H_{er} \quad (5)$$

and we recall that the local field  $H_L$  was given by

$$H_L^2 = \frac{\text{tr} (\mathcal{K}_D')^2}{\text{tr} (\gamma^2 \hbar^2 \sum_1 I_{1z}^2)} = \frac{1}{3} \langle \Delta H^2 \rangle . \quad (6)$$

Equations (1-14a,b,c) were obtained neglecting the lattice (no relaxation) and so equation (5) conforms to the rapid passage condition (2).

We now wish to determine the change in  $\underline{M}_r$  for an adiabatic (in the thermodynamic sense) variation of the effective field

$H_{er}$ . For an isolated system, the variation  $d\langle \mathcal{H}_{er} \rangle$  of the internal energy of the system is equal to the work done by the applied forces /12/

$$d\langle \mathcal{H}_{er} \rangle = - \underline{M}_r \cdot d \underline{H}_{er} , \tag{7}$$

which combined with  $d\langle \mathcal{H}_{er} \rangle$  obtained from equation (5) yields

$$\frac{dM_r}{M_r} = \frac{H_L^2}{H_{er}^2 + H_L^2} \frac{d H_{er}}{H_{er}} . \tag{8}$$

On integrating (8) from the definite limits  $M_0$  and  $H_0$  to  $M_r$  and  $H_{er}$ , and assuming  $H_0 \gg H_L$ , we obtain

$$M_r = \frac{M_0 H_{er}}{[H_{er}^2 + H_L^2]^{\frac{1}{2}}} . \tag{9}$$

We remember that  $\underline{M}_r$  is aligned along  $\underline{H}_{er}$  as shown here in Fig 1.

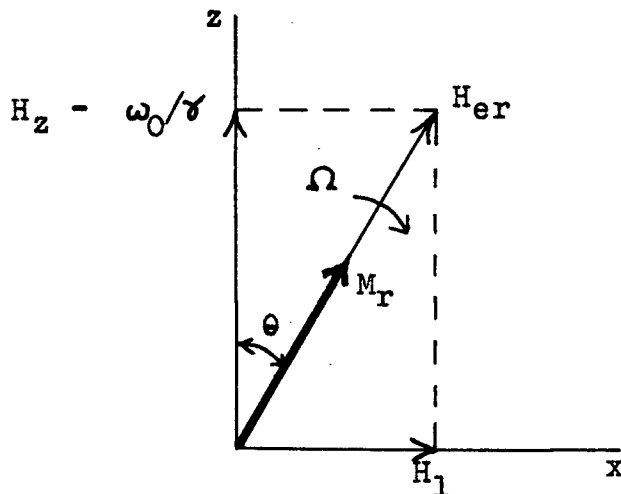


Fig 1 - Magnetization  $\underline{M}_r$  and effective field  $\underline{H}_{er}$  in the rotating reference frame.  $\Omega$  is the angular velocity of  $\underline{H}_{er}$  during a passage.

### B. The Rapid Passage Experiment

Abragam /1, p 547/ nicely describes the rapid passage experiment and gives us a physical understanding of equation (9). The main magnetic field is swept from an initial value,  $H_z'$  say, far above the resonance value  $H_0 = -\omega_0/\gamma$  (so that the angle between  $H_z$  and  $\underline{H}_{er}$  is effectively zero) to another  $H_z''$  far below. The magnitude of the effective field starts with an initial value  $H_{er}' = [(H_z' - H_0)^2 + H_1^2]^{\frac{1}{2}}$ , goes down to a minimum value  $H_1$ , then up again to  $H_{er}'' = [(H_0 - H_z'')^2 + H_1^2]^{\frac{1}{2}}$ . The postulates of a spin temperature and density matrix of the form

$$\rho \propto \exp(-\hat{H}_{er}/kT_s) \quad (10)$$

leads to a spin temperature variation

$$T_s \propto [H_{er}^2 + H_L^2]^{\frac{1}{2}}. \quad (11)$$

The magnetic moment along  $\underline{H}_{er}$  then varies as  $H_{er}/T_s$  and is given by equation (9). Thus  $\underline{M}_r$  starts from an initial value  $M_0$ , which is the thermal equilibrium value if one has waited off-resonance for a time appreciably longer than  $T_1$ , passes through a minimum

$$M_r = \frac{M_0 H_1}{[H_1^2 + H_L^2]^{\frac{1}{2}}} \quad (12)$$

at resonance, and returns to the value  $M_0$  along  $\underline{H}_{er}$  far below resonance. Since  $\underline{H}_{er}$  is then antiparallel to  $\underline{H}_0$ , so also is  $\underline{M}_r$ .

### C. ARP Signal Shape

The axis of our NMR signal pick-up coil is perpendicular to  $H_z$ , the effective field and the magnetic moment move in the z-x plane of the rotating frame, so to observe the ARP signal induced by  $M_T$  we tune our spectrometer to detect the signal voltage in phase with the rf field. That is, along  $H_1$  (the x-direction) in the rotating frame. The observed signal is proportional to the transverse component of the magnetization which is equal to

$$M_{xr} = \pm \frac{H_1}{H_{er}} M_T = \frac{\pm M_0 H_1}{[H_1^2 + h^2 + H_L^2]^{\frac{1}{2}}} \quad (13)$$

where  $h = H_z - H_0$  is the distance from resonance and we have substituted  $H_1^2 + h^2 = H_{er}^2$ . The sign in (13) is + or - depending on whether the rapid passage was started from above resonance or from below.

If we define  $\delta H$  as the width of the ARP signal at half its peak height, equation (13) gives us:

$$\delta H = [12 (H_1^2 + H_L^2)]^{\frac{1}{2}} \quad (14)$$

If  $H_1 \ll H_L$ , the line width is just  $\delta H = \sqrt{12} H_L$ . The second moment corresponding to the unsaturated absorption line can then be calculated using equation (6).

It is interesting to note that ARP signals in solids have the same shape as the curves obtained by Slichter and Holton /11/ in their rotating reference frame adiabatic demagnetization

experiments. But this is not surprising since an ARP indeed involves an adiabatic demagnetization and magnetization in the rotating frame /1, p 547/.

### III. ADIABATIC INVERSION CONDITIONS

#### A. Bloch Adiabatic Condition

Slichter /13/ proves the following theorem: the magnetic moment  $\underline{M}_r$  in Fig 1 will follow  $\underline{H}_{er}$  if

$$\gamma H_{er} \gg \Omega . \quad (15)$$

Assuming  $\underline{\Omega}$  to be a constant in the y-direction, Slichter transforms to a new frame rotating with this angular frequency. The effective field in this frame is:

$$\underline{H}_{eff} = \underline{H}_{er} + \underline{\Omega}/\gamma \quad (16)$$

and makes an angle  $\phi$  with  $\underline{H}_{er}$  such that

$$\tan \phi = \Omega / \gamma H_{er} . \quad (17)$$

$\underline{M}_r$  will precess about  $\underline{H}_{eff}$ , but  $\underline{M}_r$  and  $\underline{H}_{er}$  can be kept effectively parallel if  $\Omega / \gamma H_{er} \ll 1$ .

At resonance  $\Omega$  will be at its maximum value  $\frac{dH_0}{dt} / H_1$ , also  $H_{er}$  will be at its minimum value  $H_1$  and so expression (15) yields the Bloch adiabatic condition

$$dH_0/dt \ll \gamma H_1^2 . \quad (1)$$

### B. Possible Weaker Adiabatic Condition

Powles /14/ says that an ARP is a non-resonant perturbation experiment in the rotating frame and that the adiabatic condition is then

$$1/\tau \ll \gamma H_1, \quad (18)$$

where  $\tau$  is the time of application of the perturbation. In the case of a liquid  $\tau$  is obviously  $H_1 (dH_0/dt)^{-1}$  and we get condition (1) again. If in the case of a solid the perturbation time is supposed to be  $H_L (dH_0/dt)^{-1}$ , expression (18) becomes:

$$dH_0/dt \ll \gamma H_1 H_L. \quad (19)$$

If this condition were valid for solids it would represent an appreciably weaker condition than (1) and one which is more accessible with a normal CW commercial spectrometer. The experimental results in the next chapter will show that it is not, and that condition (1) is the one that must be satisfied.

### C. Comments on the $H_1$ to $H_L$ Ratio, Spin Temperature, and $T_2$

The features of ARP in solids become very simple if  $H_1 \gg H_L$ . "The fact that the magnetization along the effective field remains constant until affected by the spin lattice coupling can be expressed simply by saying that in the rotating frame the spins are quantized along that field and that the spin-spin coupling is unable to provide the large quanta  $\gamma \hbar H_{er}$  required for the reversal of a spin quantized along  $\underline{H}_{er}$ , /1, p 550/."

The concept of a spin temperature in the rotating frame, however, correctly describes ARP results even when  $H_1$  is less than  $H_L$ . Slichter and Holton /11/ demonstrate that the magnetisation  $M_0$  ( $\text{Na}^{23}$  in NaCl) can be inverted by an ARP with  $H_1$  much less than  $H_L$ .\* We have measured  $H_L$  in several solid samples using ARP signals obtained with  $H_1$  less than  $H_L$ . These results agreed very well with calculated and other experimental values. They are presented in the next chapter. What remains then is to state the criteria for application of spin temperature. Goldburg /15/ shows that the rotating frame spin temperature assumption is valid if

$$\gamma^2 H_1^2 T_1 \pi g(0) \gg 1 \quad (20)$$

and if  $H_0$  and  $H_1$  are large enough so that the time-dependent terms in the dipole Hamiltonian  $\hat{H}_D^r$  produce negligible effects. This is the case when /9, 11/

$$H_0 \gg H_L \quad \text{and} \quad H_1 > H_L^2 / H_0 \quad (21)$$

In order to explain the final details of the ARP experiment we need to review the superposition of subsystems concept used in the Provotorov /16/ section in chapter 1. A spin system in a solid placed in a large magnetic field can be described as a superposition of a "Zeeman" subsystem and a "dipole-dipole" subsystem. The couplings inside each subsystem is strong whereas

---

\* Their results should be analysed a little further than they have done, however, in order to be certain of this fact. This is done in appendix A.

the couplings between subsystems are weak. Consequently one can ascribe an energy, and entropy..., to each of them /17/.

Thus the order of the spin system that exists along  $H_{er}$  (the Zeeman subsystem) before the ARP (or the demagnetization and magnetization) is not lost when  $H_{er}$  goes below  $H_L$  but is transferred to the dipole-dipole subsystem. This can happen because the coupling between them becomes strong when  $H_{er}$  becomes less than a few times the local field  $H_L$  /18/. The time constant for this strong coupling is probably of the same order as the spin-spin (or dipole-dipole) interaction time  $T_2$ . So, for the process of energy and order transfer between subsystems to be reversible, one requires the restriction

$$t_p \gg T_2 \quad (22)$$

on the passage time through resonance. In solids  $T_2$  is approximately  $\gamma H_L$  and has been defined as  $\pi g(0)/1$ , p 543/. Note that condition (22) for solids is just the opposite of the condition required for liquids; viz, expression (2).

#### IV. MEASUREMENT OF THE RELAXATION TIME $T_1$

##### A. ARP Two Pass Method

By the Two Pass Method we mean the following experiment which is similar to the  $\pi - \pi/2$  pulse sequence commonly used in NMR

pulse spectroscopy. The spin system is allowed to reach thermal equilibrium at a magnetic field  $H_0+h$  some distance above resonance, (far enough so that  $H_{er}$  is effectively along  $H_0$  but we shall assume for simplicity that  $h \ll H_0$ ) then two consecutive adiabatic rapid passages separated by a time  $t$  are performed, the field being swept down to  $H_0-h$  and back up again to  $H_0+h$ . The experiment can be repeated for various values of  $t$ , and  $T_1$  obtained graphically. We shall consider two cases.

### 1. Complete inversion of the magnetisation

The Bloch /18/ equation for the rate of change of the magnetization  $M_z$  to its equilibrium value  $M_0$  for a system of spins placed in a magnetic field  $H_0$  (in the  $z$ -direction) is:

$$\frac{dM_z}{dt} = -\frac{(M_z - M_0)}{T_1} \quad (23)$$

On integration we obtain:

$$M_z - M_0 = C \exp(-t/T_1) \quad (24)$$

If the first pass completely inverts the magnetization, then we can set our initial condition (just after the pass) as

$$M_z(0+) = -M_0 \quad \text{so} \quad C = -2M_0 \quad \text{and}$$

$$M_0 - M_z = 2M_0 \exp(-t/T_1) \quad (25)$$

The relationship of the ARP signals one observes to the magnetization is the following: the sign of the signal on the

first pass (the down pass) is the same as  $M_z$  and of opposite sign on the return pass. Thus the signal obtained on the first pass equals

$$S_0 = k M_0 , \quad (26)$$

where  $k$  is the constant of proportionality and we mean  $S$  to be the peak signal amplitude. The signal obtained on the return pass some time  $t$  after becomes:

$$S_t = -k M_z , \quad (27)$$

the long time asymptote signal will be:

$$S_\infty = -k M_0 , \quad (28)$$

and a plot of  $(S_\infty - S_t)$  vs  $t$  will obey equation (25) in the form:

$$S_\infty - S_t = 2S_\infty \exp(-t/T_1) . \quad (29)$$

So if we plot  $\ln(S_\infty - S_t)$  vs  $t$  we expect a straight line of slope  $-1/T_1$  and intercept  $\ln 2S_\infty$ . Equation (29) also gives us a quick method for measuring  $T_1$  since the time at which  $S_t$  passes through a null is

$$t_{\text{null}} = T_1 \ln 2 . \quad (30)$$

Some scope pictures of ARP signals from doped water that nicely demonstrate the behaviour predicted by the above equations can be found in Abragam /1/ Fig III-5.

## 2. Incomplete inversion of the magnetism

We now consider the case when the Bloch condition is not well satisfied and the inversion of the magnetism is not complete. Let us suppose that the two rapid passages each invert a fraction  $x$  of the magnetization. Our initial condition then just after the first pass will be:

$$M_z(0+) = -xM_0 + M_0(1-x) = M_0(1-2x) , \quad (31)$$

the integration constant becomes:

$$C = M_0(1-2x) - M_0 = -2xM_0 , \quad (32)$$

and the formula for the magnetization is:

$$M_z = M_0 - 2xM_0 \exp(-t/T_1) . \quad (33)$$

The signal on the return pass in this case will be proportional to  $-xM_z$  so equation (33) becomes:

$$-S_t = kxM_0 - k2x^2 M_0 \exp(-t/T_1) , \quad (34)$$

and on substituting for the long-time signal

$$S_\infty = -kxM_0 \quad \text{we get}$$

$$S_\infty - S_t = 2xS_\infty \exp(-t/T_1) . \quad (35)$$

We see that a plot of  $\ln(S_\infty - S_t)$  vs  $t$  will again be a straight line and the slope gives us  $T_1$  even though the rapid passages are not performing a complete inversion. The inversion factor  $x$  can be obtained from the intercept  $\ln 2xS_\infty$ . We cannot, however, just use the null method for measuring  $T_1$

since in this case

$$t_{\text{null}} = T_1 \ln 2x \quad . \quad (36)$$

### B. ARP Symmetric Sweep Method

In this method we perform a periodic symmetric sweep through resonance and observe the amplitudes of the ARP signals after their steady state values are reached. We shall again consider two cases. The first being that we have complete inversion of the magnetization on each passage, that is, that we have proper ARP conditions; and the second being the case when the inversion is incomplete.

#### 1. Complete inversion of the magnetization

Suppose that just before a rapid passage  $M_z = M_1$  and just after it  $M_z = -M_1$ . Then if we call the time of this passage "time zero", the integration constant in equation (24) becomes  $C = -M_1 - M_0$  and the magnetization

$$M_z = M_0 \left[ 1 - e^{-t/T_1} \right] - M_1 e^{-t/T_1} \quad . \quad (37)$$

Now suppose at some later time  $t_1$  that  $M_z(t_1) = M_1$ , then on substituting this value in equation (37) we get an equation for the steady state value of  $M_z$  developed by periodic symmetric sweeps separated by a time  $t_1$

$$M_1 = M_0 \frac{[1 - e^{-t_1/T_1}]}{[1 + e^{-t_1/T_1}]} \quad . \quad (38)$$

If a different interval between sweeps  $t_2$  is chosen, we will obtain a different steady state value of magnetization, say  $M_2$ , and get the result of Chiarotti et al /5/

$$\frac{M_1}{M_2} = \frac{[1 - e^{-t_1/T_1}][1 + e^{-t_2/T_1}]}{[1 + e^{-t_1/T_1}][1 - e^{-t_2/T_1}]} \quad (39)$$

If  $t_2 = \infty$ ,  $M_2 = M_\infty$  (and  $M_0$  for  $h \ll H_0$ ) and we obtain the relation:

$$\frac{M_t}{M_\infty} = \frac{[1 - e^{-t/T_1}]}{[1 + e^{-t/T_1}]} \quad (40)$$

where  $t$  is now the interval between sweeps.

The signals observed for a particular periodic sweep interval  $t$  will be proportional to  $M_t$ , but of alternating sign, and will obey the relations (39) and (40). Pictures of signals of this type can be found in Abragam /1/ Fig III-6.

If the  $M_t/M_\infty$  ratio in equation (40) is called  $r$ , we have the following convenient relation\*:

$$(1 - r)/(1 + r) = \exp(-t/T_1) \quad (41)$$

We can then obtain  $T_1$  from the linear plot of  $\ln(1-r)/(1+r)$  vs  $t$  and take advantage of the data smoothing and averaging possible with a plot such as this.

---

\*

We are indebted to Dr. L.G. Harrison for pointing this out to us.

## 2. Incomplete inversion of the magnetism

Let  $x$ , the fraction inverted, be the same for both sweep directions. Then suppose again that just before a rapid passage  $M_z = M_1$ . But in this case just after it  $M_z = M_1(1 - 2x)$  and this initial condition results in the following equation:

$$M_z(t) = M_0 [1 - e^{-t/T_1}] + M_1(1 - 2x)e^{-t/T_1} \quad (42)$$

This time our choice of  $t_1$  such that  $M_z(t_1) = M_1$  gives us:

$$M_1 = M_0 \frac{[1 - e^{-t_1/T_1}]}{[1 - (1 - 2x)e^{-t_1/T_1}]} \quad (43)$$

The fact that the signals here are proportional to  $xM_1$  presents no problem as we only measure signal ratios in the symmetric sweep experiment, however, the plot of  $\ln(1-r)/(1+r)$  vs  $t$  is no longer linear and the determination of  $T_1$  becomes complicated. Graphical or successive approximation methods have to be used and we cannot get  $T_1$  without finding  $x$  some other way.

The analogous equation to (39) in this case is

$$\frac{M_1}{M_2} = \frac{[1 - e^{-t_1/T_1}][1 - (1 - 2x)e^{-t_2/T_1}]}{[1 - (1 - 2x)e^{-t_1/T_1}][1 - e^{-t_2/T_1}]} \quad (44)$$

We see that for the same  $T_1$  and the same pair of sweep intervals (assuming  $t_1 < t_2$ ) equation (44) yields a larger  $M_1/M_2$  ratio than equation (39). Consequently if we have symmetric sweep signals obtained under incomplete inversion conditions and just use equation (39) the  $T_1$  result will be too small.

## REFERENCES

- (1) A. Abragam, "The Principles of Nuclear Magnetism", Oxford University Press, Oxford (1961)
- (2) F. Bloch, W.W. Hansen, and M. Packard, Phys. Rev. 70 474, (1946)
- (3) L.E. Drain, Proc. Phys. Soc. (London) A62, 301 (1949)
- (4) R.L. Conger and P.W. Selwood, J. Chem. Phys. 20, 383 (1952)
- (5) G. Chiarotti, G. Cristiani, L. Giulotto, and G. Lanzi, Nuovo Cimento 12, 519 (1954)
- (6) G.W. Niderbragt and C.A. Reilly, J. Chem. Phys. 24, 1110, (1956)
- (7) J.G. Powles, Berichte der Bunsengesellschaft 67, 328 (1963)
- (8) A.G. Redfield, Phys. Rev. 98, 1787 (1955)
- (9) A.G. Redfield, Phys. Rev. 101, 67 (1956)
- (10) A. Abragam and W.G. Proctor, Phys. Rev. 109, 1441 (1958)
- (11) C.P. Slichter and W.C. Holton, Phys. Rev. 122, 1701 (1961)
- (12) I. Solomon and J. Ezzatty, Phys. Rev. 127, 78 (1962)
- (13) C.P. Slichter, "Principles of Magnetic Resonance", Harper and Row, New York (1963)
- (14) J.G. Powles, Proc. Phys. Soc. (London) 71, 497 (1958)
- (15) W.I. Goldberg, Phys. Rev. 122, 831 (1961); 128, 1554 (1962)
- (16) B.N. Provotorov, Zh. Eksperim. i Teor. Fiz. 41, 1582 (1961) English Transl.: Soviet Phys. - JETP 14, 1126 (1962)
- (17) J. Jeener, H. Eisendrath and R. Van Steenwinkel, Phys. Rev. 133, A478 (1964)
- (18) F. Bloch, Phys. Rev. 70, 460 (1946)

## chapter 6.

## ADIABATIC RAPID-PASSAGE II.

## RAPID PASSAGE EXPERIMENTS

We first exhibit the experiments that have helped us determine the proper conditions for adiabatic rapid passage in solids. Then we present our local field measurements (which also gives us the second moment) in powder and single crystal samples of  $\text{CaF}_2$  and in lithium stearate. Finally our  $T_1$  values for the above samples and a very pure single crystal of maleic anhydride are given.

## I. EXPERIMENTAL

A. Spectrometer

The experiments reported here were done on the NMR spectrometer system described in chap 2 but with some modifications and additional equipment. The in-phase component of the NMR

signal was selected with the appropriate probe leakage (dispersion paddle).

An attempt was made to get higher  $H_1$  values at 16 MHz than the Varian rf unit could produce. An Eico 90 watt amateur transmitter was modified for use with a Varian V-4360C power supply (300 V B+ and 12.6 V dc filament supply) and was connected to the NMR probe. An  $H_1$  value of about 1.5 gauss was obtained and ARP signals were observed, but a coil in the probe burnt up and so this project was abandoned.

### 1. Magnetic field sweep

The rapid passage was accomplished by applying the square-wave output from a Hewlett-Packard 202A low-frequency function generator to the sweep input of the V-2200B magnet power supply. The magnetic field sweep rates obtained this way varied from 154 to 340 gauss/sec depending on the square-wave voltage and magnetic field intensity; the sweep ranged from  $\pm 64$  to  $\pm 135$  gauss about  $H_0$ . For sweep intervals longer than could be obtained with the 202A generator, the sweep input was derived from a 1.5 volt battery which was controlled by a hand-operated reversing switch.

The negative sync pulse from the 202A generator was used to trigger the oscilloscope for presentation of the ARP signals.

### 2. Signal display

Since we wanted to observe the true rapid-passage signal shapes, the signal was taken out of the receiver in the V-4210 rf

unit just after the diode detector. In this way the distortion caused by the a-c coupled output amplifier was avoided. Initially a DuMont model 304H oscilloscope with a long persistence screen (P7 phosphor) was used. An external capacitor bank was built to get the slow sweeps necessary for  $T_1$  measurements. Measurements made by visual inspection of traces on this scope indicated that  $T_1$  and  $H_1$  values could be obtained by the ARP technique. Also the dependence of the ARP signal shape on  $H_1$  was observed for a fixed magnetic field sweep rate.

More precise measurements were desired, however, and this was accomplished as a result of the kindness of the UBC Electrical Engineering Department who made available the following: Tektronix model 561A scope with a P7 phosphor CRT, model 2A63 and 2B67 plug-ins (differential amplifier and time base units), and a Tektronix model C12 scope camera with Polaroid roll film back. The camera lens magnification was X0.9.

### 3. ARP spectrometer system

A block diagram of our ARP spectrometer system is shown in Fig 1. The probe leakages used, result in a constant voltage output from the diode detector of about 1 to 2 volts. The rapid passage signal voltages were much less than this, so in order to use d-c coupling in the scope, a buck-out voltage was applied to the -ve input of the scope differential amplifier. Buck-out voltages were obtained with a 25 k $\Omega$  potentiometer across a 1.5 or 3.0 volt battery.

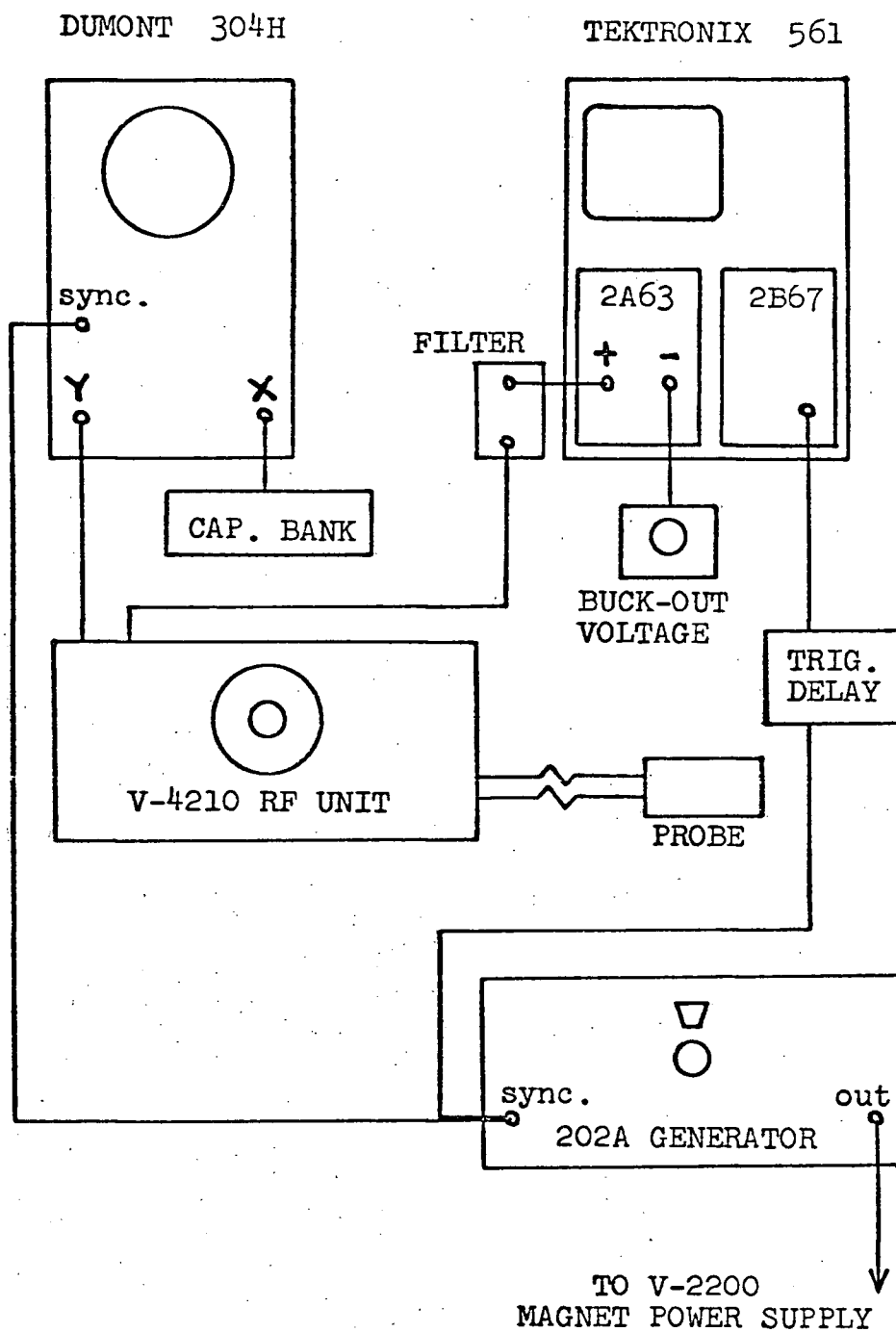


Fig 1 - Diagram of Adiabatic Rapid Passage Spectrometer Magnet System Not Shown.

In order to observe the shape of the ARP signal, a fast scope sweep is needed which can be delayed with respect to the start of the magnetic field sweep (point at which the 202A generator puts out the scope trigger pulse). Often this effect could be accomplished by using the 5X sweep expansion of the Tektronix scope. However, not enough effective delay could be obtained this way for narrow ARP signals from liquids. Therefore a Trigger Pulse Delay Unit was built. It is a battery powered solid-state unit and the circuit diagram is given in appendix B.

A simple RC low-pass filter was built to attenuate the high frequency noise in the ARP signals. With the filter connected to the Tektronix scope, the roll-over frequencies (-6 db points) were calculated to be 7.6, 13, 27, 54 and 160 kHz.

The Dumont scope was connected to the usual audio signal output jack of the V-4210 rf unit and used to tune-up the spectrometer and monitor the rapid passage signals.

#### 4. Calibrations

The  $H_1$  calibrations described in chap 2 were used for rapid passage experiments done at the 16 MHz frequency.  $H_1$  at 8 MHz was calibrated using the Anderson method (for a reading of  $50 \times 10 \mu\text{a}$  on the rf level meter). Since the X10 meter range was linear in  $H_1$  at 16 MHz, it was assumed that one calibration point on this range at 8 MHz was enough.  $H_1$  at  $13 \times 100 \mu\text{a}$  was found by comparing the ARP signal widths in liquid trifluoroacetic acid and  $\text{CaF}_2$  powder.

The magnetic field sweep rates at resonance  $dH_0/dt$  were obtained by measuring the width-at-half-height ( $\delta H$ ) passage time  $t_p$  for liquid sample ARP signals. For liquids  $\delta H = \sqrt{12} H_1$ .

## B. Samples

The  $\text{CaF}_2$  powder sample was the one described in chap 2.

The  $\text{CaF}_2$  crystal sample was a colourless naturally occurring single crystal kindly supplied by the Geology Department. It was cleaved along the (111) planes and some of the edges chipped away until it fitted inside the 16 mm dia probe receiver coil with the  $[\bar{0}11]$  crystal direction perpendicular to the coil plane.

The lithium stearate ( $\text{LiC}_{18}$ ) powder sample was in a 15 mm dia test tube and was from the same batch of not-fused soap used for the  $\text{LiC}_{18}$  sample described in chap 3.

The maleic anhydride single crystal was in a sealed-off 15 mm dia glass tube. The sample came to us from the National Research Council of Canada, Pure Chemistry Division. Dr. W.G. Schneider of N.R.C. requested of Prof. L.W. Reeves of this department, a measurement of  $T_1$  in this very pure crystal. Dr. Reeves' pulse spectrometer was not suitable for solids and so we agreed to attempt the measurement by ARP.

The samples were at room temperature for all the experiments in this chapter.

## C. Method

### 1. CaF<sub>2</sub> crystal mounting

The CaF<sub>2</sub> single crystal was attached to the bottom of a 15 mm dia test tube with the  $[0\bar{1}1]$  crystal direction along the tube axis. This put  $[0\bar{1}1]$  perpendicular to the field  $H_0$  when the tube was held in the NMR probe with the Varian sample holder. The crystal could then be rotated about the  $[0\bar{1}1]$  axis to place  $H_0$  along the  $[111]$ ,  $[011]$  or  $[100]$  crystal directions. The  $(111)$  cleavage planes gave us the  $[111]$  directions and a paper scale marked in  $5^\circ$  intervals taped to the probe was used to position the holder for the others. It was estimated that the errors in the crystal orientations obtained this way were not greater than  $\pm 3^\circ$ . Although this alignment is not as precise as that obtained by other workers /1, 2, 3/, we did not use the NMR experiment to get it as they did.

### 2. Signal shape and $H_L$ measurements

The spectrometer system shown in Fig 1 was used to make  $H_L$  measurements and to study the dependence of the rapid passage signals on  $H_L$  and  $dH_0/dt$ . Although sweeping back and forth by means of the 202A generator was not necessary for these experiments, this method provided a convenient means for scope triggering, optimizing amplifier settings, and scope camera operation.

### 3. $T_1$ measurements

The set-up in Fig 1 and the symmetric sweep method was used to measure the  $T_1$  values in the  $\text{CaF}_2$  and  $\text{LiC}_{18}$  samples. The following procedure was developed: The steady-state signal amplitudes for a series of sweep intervals, each differing by a factor of 2, are measured. The signal ratios  $S(4t)/S(t)$  are tabulated (where  $t$  is the interval between sweeps). Then  $t/T_1$  and hence  $T_1$  are found graphically from the universal plot  $R(4t/T_1)$  vs  $t/T_1$ , where:

$$R(4t/T_1) = \frac{[1 - e^{-4t/T_1}][1 + e^{-t/T_1}]}{[1 + e^{-4t/T_1}][1 - e^{-t/T_1}]} \quad (1)$$

Expression (1) is just equation (5-39) for a particular case. See Fig 1\*, ref /4/ for a series of  $R(nt/T_1)$  vs  $t/T_1$  curves. The best results are obtained when we have a  $S(4t)/S(t)$  ratio in which  $t \approx T_1$ . If  $t = T_1$ , an error of 6.3% in the  $S(4t)/S(t)$  measurement results in a 10% error in the  $T_1$  value. We can also use the  $S(2t)/S(t)$  ratios and the appropriate plot to get  $T_1$ , but an error of only 3.1% in the ratio now yields a 10% error in  $T_1$ .

---

\* The curves in this figure were calculated by T.J.R. Cyr on the U.B.C. IBM 7040 computer. The author established the technique of doubling ARP symmetric sweep intervals and hand calculated values for the initial  $R(4t/T_1)$  vs  $t/T_1$  curve. See appendix C for further comments on ref<sup>1</sup>/4/.

The relation (5-41) was discovered after the experiments described here were completed and the author had left the university. Thus the signal values proportional to  $M_{\infty}$  were not measured and we cannot use the  $\ln(1-r)/(1+r)$  vs  $t$  plot described in chap 5 to obtain  $T_1$  values from our symmetric sweep measurements.

The long  $T_1$  value in the maleic anhydride crystal was measured by the two pass ( $\pi - \pi/2$ ) method. The magnet sweep was controlled with the hand operated switch. Several equilibration times had to be tried. The final experiment was performed after the sample had been in the magnetic field 14 hr.

## II. RESULTS AND DISCUSSION

### A. Signal Shape and the Adiabatic Condition

In order to simplify notation let us rewrite the Bloch adiabatic condition (5-1) as

$$A \equiv \gamma H_1^2 / (dH_0/dt) \gg 1 \quad (2)$$

Expression (2) also defines the parameter  $A$  and its value will tell us to what degree we have satisfied the above condition. Similarly the weaker condition (5-19), obtained from the Powles adiabatic condition (5-18), becomes:

$$B \equiv \gamma H_1 H_L / (dH_0/dt) \gg 1 . \quad (3)$$

Since we shall be examining rapid passage signals obtained under various conditions, let us write down now for comparison the signal expected when the rapid passage is adiabatic. The transverse component of the magnetization  $M_{xr}$  during an ARP is given by eqn (5-13) and since the ARP signal is that induced by  $M_{xr}$ , the form of the signal is:

$$S(h) = \frac{\pm k M_0 H_1}{[H_1^2 + h^2 + H_L^2]^{\frac{1}{2}}} , \quad (4)$$

where  $k$  is a proportionality constant and we recall that  $h$  is the distance from the centre of the line in gauss.

Fig 2 shows the variation of the rapid passage signal shape ( $H^1$  resonance) in  $LiG_3$  with  $H_1$  for a fixed magnetic field sweep rate. The rf frequency is 16 MHz and  $dH_0/dt = 226$  gauss/sec. The  $H_1$  values and adiabatic condition parameters  $A$  and  $B$  are listed in Table I.

Table I - Conditions for  $LiC_{18}$  signals in Fig 2

Trace* number	$H_1$ gauss	A	B#
27a	0.207	5.1	62
b	0.155	2.85	47
c	0.104	1.30	31
28a	0.078	0.71	23.2
b	0.052	0.32	15.6
c	0.037	0.16	11.0

\*Labeled a,b,c, from top to bottom for each scope picture.  
# $H_L = 2.53$  gauss by ARP.

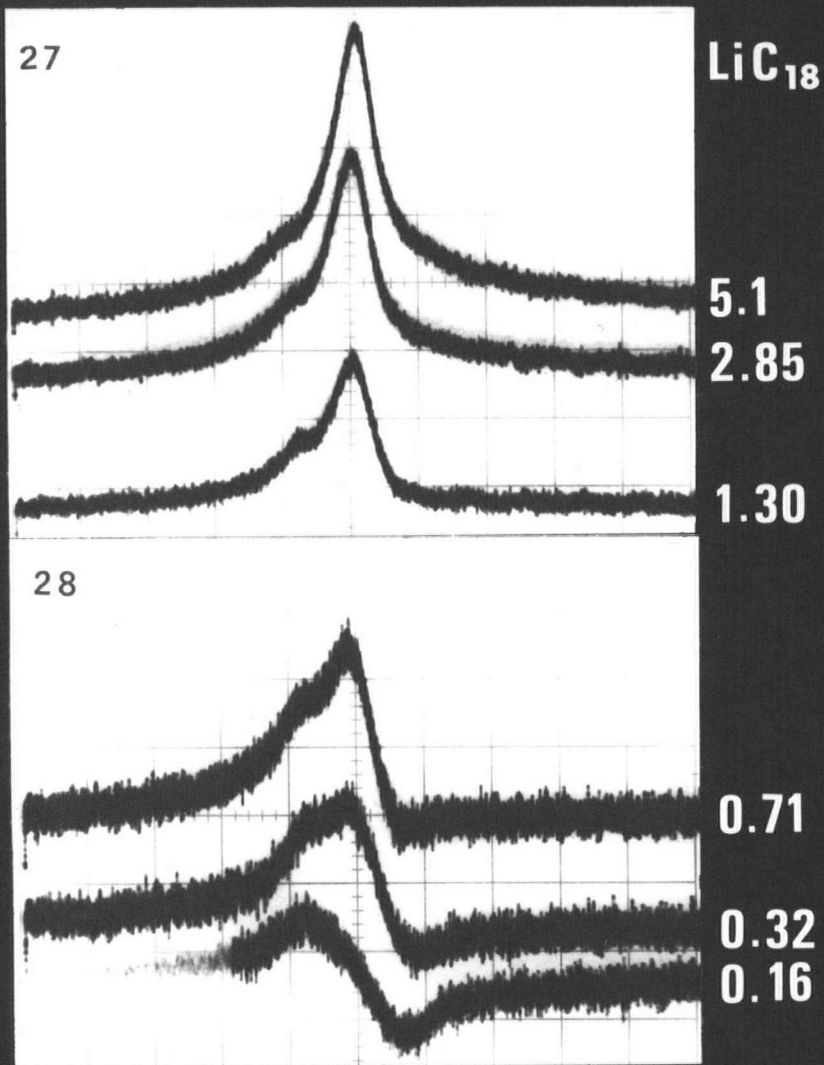


Fig 2 - Rapid passage signal shape in lithium stearate as a function of the adiabatic parameter A.

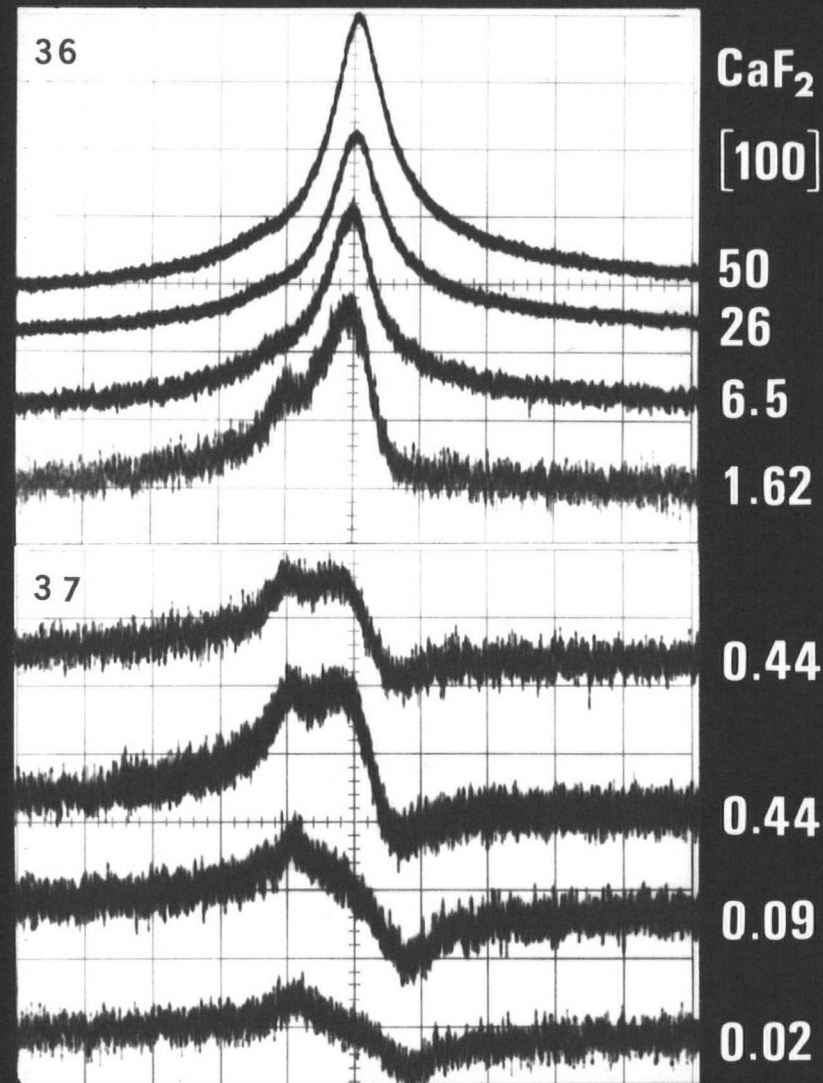


Fig 3 - Rapid passage signal shape in CaF<sub>2</sub>, H<sub>0</sub> along [100], as a function of the adiabatic parameter A.

We see that for low  $H_1$  (0.037 G) the signal is the steady-state dispersion curve and that the shape transforms as  $H_1$  is increased until at  $H_1 = 0.207$  we have a trace of the shape expected for an ARP signal. We propose that the signal shape can be used as a criterion of whether or not the adiabatic condition is fulfilled. For Trace 28c ( $H_1 = 0.037$  G) the Powles adiabatic parameter B equals 11.0 and this is  $\gg 1$ . Yet we see that the signal shape is that of a dispersion curve. This suggests that the weaker condition (3) is not a satisfactory criterion for adiabatic passage. The shape of Trace 27a ( $H_1 = 0.207$  G) appears to be reasonably close to that expected for an ARP signal (equation 4) and one might expect that the correct adiabatic condition to be largely satisfied. Here  $A = 5.1$  which is reasonably large compared to unity in conformity with the Bloch condition (2).

Similar results at 16 MHz ( $F^{19}$  resonance) were obtained with the  $CaF_2$  powder sample. Also an experiment was done in which  $H_1$  was constant and  $dH_0/dt$  varied. The same dependence of signal shape on A was observed.

In order to use higher values of  $H_1$  and thus obtain a larger range of A and B values, the following experiments were done at 8 MHz. The rapid passage signals obtained from the  $CaF_2$  crystal ([100] along  $H_0$ ) for various  $H_1$  values are reproduced in Fig 3. We again see the transformation of the signal from a dispersion curve at the bottom to an ARP signal shape at the top. The data for Fig 3 are given in Table II.

Table II - Conditions for  $\text{CaF}_2$  signals in Fig 3\*.

Trace number	$H_1$ gauss	A	B <sup>#</sup>
36a	0.800	50	131
b	0.574	26	94
c	0.287	6.5	47
d	0.144	1.62	23.5
37a	0.075	0.44	12.2
b	0.075	0.44	12.2
c	0.034	0.09	5.6
d	0.017	0.02	2.8

\*  $dH_0/dt = 319$  gauss/sec.

#  $H_L = 2.07$  gauss from theoretical second moment /5/.

We see in Fig 3 that traces 37a and 37b still have a large degree of dispersion curve character yet  $B = 12.2$ . A, on the other hand, is 0.44 at this point. The shape of trace 36c appears to be satisfactory and here  $A = 6.5$ .

Fig 4 shows that  $\text{CaF}_2$  crystal rapid passage signals obtained at various  $H_1$  values when  $[111]$  is along  $H_0$ . For this crystal direction  $H_L$  is only 0.86 gauss (from theoretical second moment in ref /5/). Thus  $H_1$  has to be larger to achieve a given B value, but there is still a significant amount of dispersion character in the trace for which  $B = 11.2$  (51.b).  $A = 1.9$  for this trace. The adiabatic condition is probably satisfied for trace 49b. The signal has the shape expected for a true ARP except for a little bump on the left side which we shall discuss later. The Bloch adiabatic parameter A for this trace equals 7.7, a value large with respect to 1. The data for Fig 4 are listed in Table III.

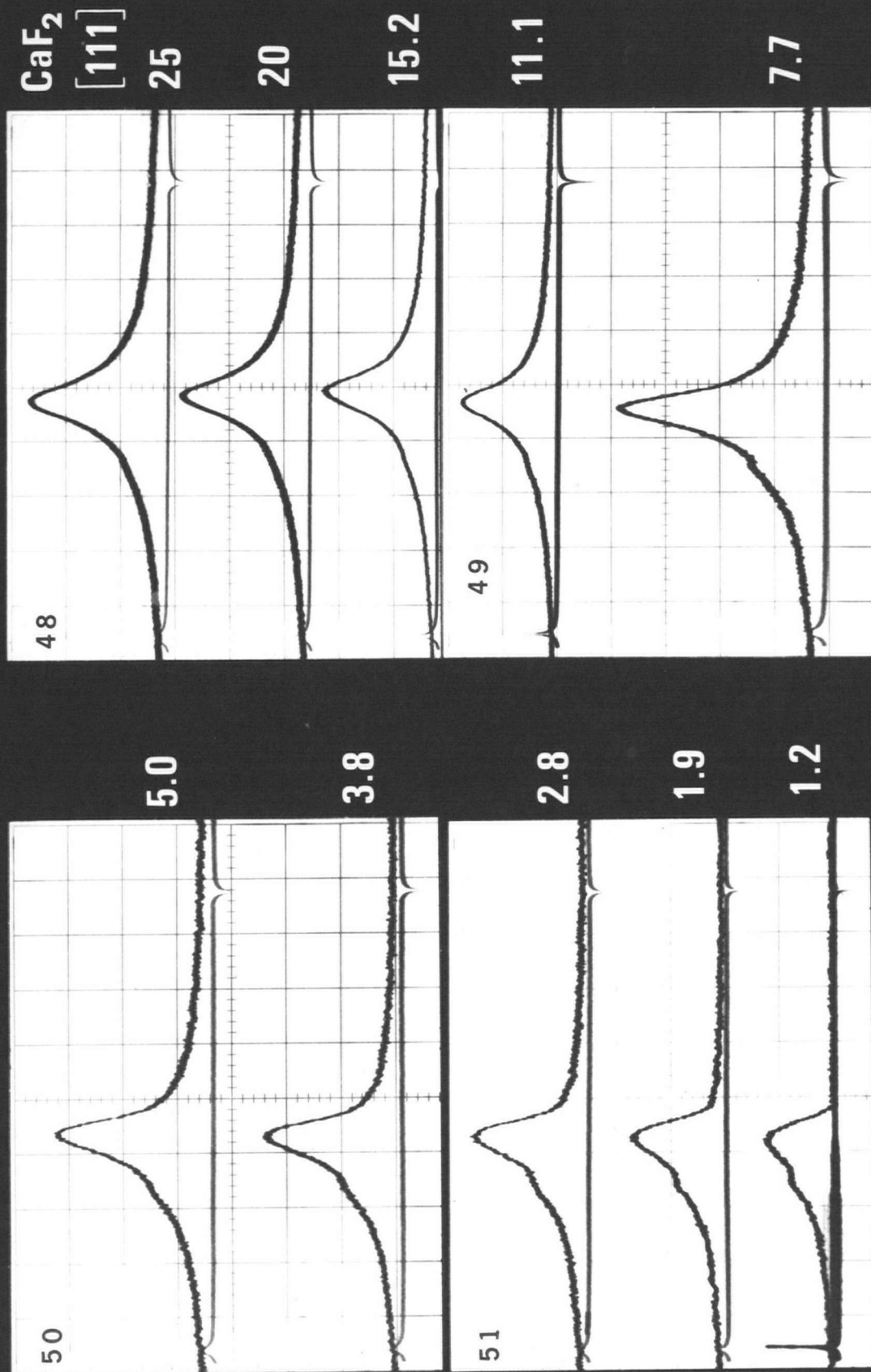


Fig 4 - Rapid passage signal shape in  $\text{CaF}_2$ ,  $H_0$  along  $[111]$ , as a function of the adiabatic parameter  $A$ .

Table III - Conditions for  $\text{CaF}_2$  signals in Fig 4\*.

Trace	$H_1$ gauss	A	B	Trace	$H_1$ gauss	A	B
50a	0.238	5.0	17.9	48a	0.534	25	40
b	0.208	3.8	15.6	b	0.475	20	36
51a	0.178	2.8	13.4	c	0.416	15.2	31
b	0.148	1.9	11.2	49a	0.356	11.1	27
c	0.119	1.2	8.9	b	0.297	7.7	22

\*  $dH_0/dt = 288$  gauss/sec.

The above results strongly suggest that condition (2) determines the rapid passage signal shape. The following observation makes us more certain of this. Trace 51c in Fig 4 has a characteristic shape that makes for easy comparison.  $A = 1.2$  for this trace and  $B = 8.9$ . Now one should look at the  $\text{LiC}_{18}$  and  $\text{CaF}_2$  signals in Figs 2 and 3, and interpolate to find the A and B values for the points at which the shapes are about the same as 51c. One finds that  $A \sim 1.0$  for both, whereas the B values are about 27 and 18 respectively. Therefore we conclude that the signal shape depends on the adiabatic parameter A and the Bloch adiabatic condition (2) is the condition that must be satisfied.

What remains now is to decide how large A is required to be. As mentioned above, the  $\text{CaF}_2$  trace 49b ( $A = 7.7$ ) in Fig 4 has a little bump on the left side of the signal. It appears to be some vestigial dispersion signal and is gone when  $A = 11.1$ . There might be a similar bump in the  $\text{CaF}_2$  trace 36 c ( $A = 6.5$ ) in Fig 3, but we cannot be sure because of the noise. There is a bump on the  $\text{LiC}_{18}$  trace 27a ( $A = 5.1$ ) in Fig 2. It is much

smaller in a signal obtained with  $A = 7.7$  and is probably completely gone when  $A = 10$ . Therefore in view of the above results we suggest that adiabatic conditions are obtained and the inversion of magnetization is complete during a rapid passage when  $A \geq 10$ .

The above requirement is a little stronger than that calculated by Benoit /6/. Benoit solved the Bloch /7/ equations with an electronic analog computer for the rapid passage experiment. He found and tabulated the inversion factor  $F = M_f/M_i$ , where  $M_i$  and  $M_f$  are the magnetic moments in the z-direction before and after the passage, for various  $A$  values. For example:  $F = -0.92$  for  $A = 2$ ,  $-0.99$  for  $A = 3.13$ , and  $-0.99995$  for  $A = 10$ . These results have been verified experimentally for rapid passages in liquids /6, 8/. Zhernovoi /9/ has recently solved the Bloch equations for this case analytically and obtains the equation

$$F = 2 \cdot \exp(-\pi A/2) - 1 \quad . \quad (5)$$

He says that it agrees very well with Benoit's values.

## B. Local Field Measurements

### 1. Measurements at 16 MHz

Fig 5 reproduces a pair of ARP signals ( $F^{19}$  resonance) obtained at 16 MHz for which the rf level and field sweep rates are identical. See Table IV. Number 17 is of the  $\text{CaF}_2$  powder

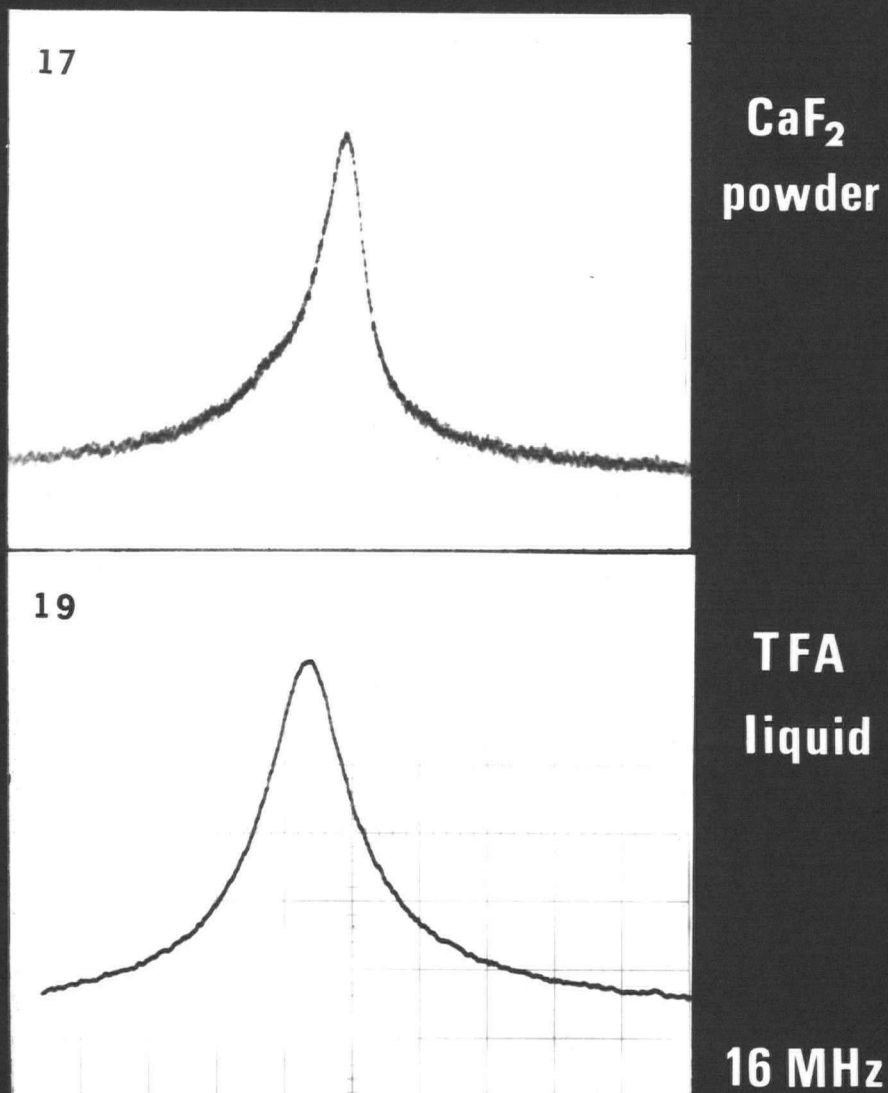


Fig 5 - ARP signals in polycrystalline CaF<sub>2</sub> and liquid tri-fluoroacetic acid at 16 MHz. A = 6.7.

sample and 19 of liquid trifluoroacetic acid (TFA) in a 10 mm dia tube. We recall that the ARP signal width at half height is  $\delta H = [12 (H_1^2 + H_L^2)]^{\frac{1}{2}}$  (equation 5-14). The measured ratio of the  $t_p$ 's (CaF<sub>2</sub> to TFA) in Fig 5 is 5.83/1.0 ( $t_p = \delta H / (dH_0/dt)$ , base lines are grid lines 1 cm from bottom of scope screen). This yields a  $H_L$  value of 1.47 gauss for powdered CaF<sub>2</sub>.  $H_L$  calculated from the theoretical rigid lattice second moment for polycrystalline CaF<sub>2</sub> /5, 10/ is also 1.47 gauss. This excellent agreement gave us confidence in the method and so we went on to measure  $H_L$  in other samples.

ARP signals from the CaF<sub>2</sub> single crystal with [111], [011] and [100] successively along  $H_0$  are reproduced in Fig 6. The conditions are the same as above. In fact the magnetic field sweep and rf level settings were not touched. Thus the field sweep rate calibration obtained from trace 19 (liquid signal) can be used here. The data and results for Fig 6 are also listed in Table IV.

There is again very good agreement with theory. The percentage differences between the experimental and theoretical  $H_L$  values are 2.3, 0.4, and 4.0% for the [111], [011] and [100] directions respectively. The line width for the [111] direction is quite orientation-sensitive /1/ and any misalignment results in a significant error in the measured  $H_L$ . After these experiments were done it was found that the narrowest signal was obtained when the crystal was rotated about 2.5° from the orientation we had thought corresponded to [111] along  $H_0$ . The direction in which our results deviate from the theoretical values is compatible

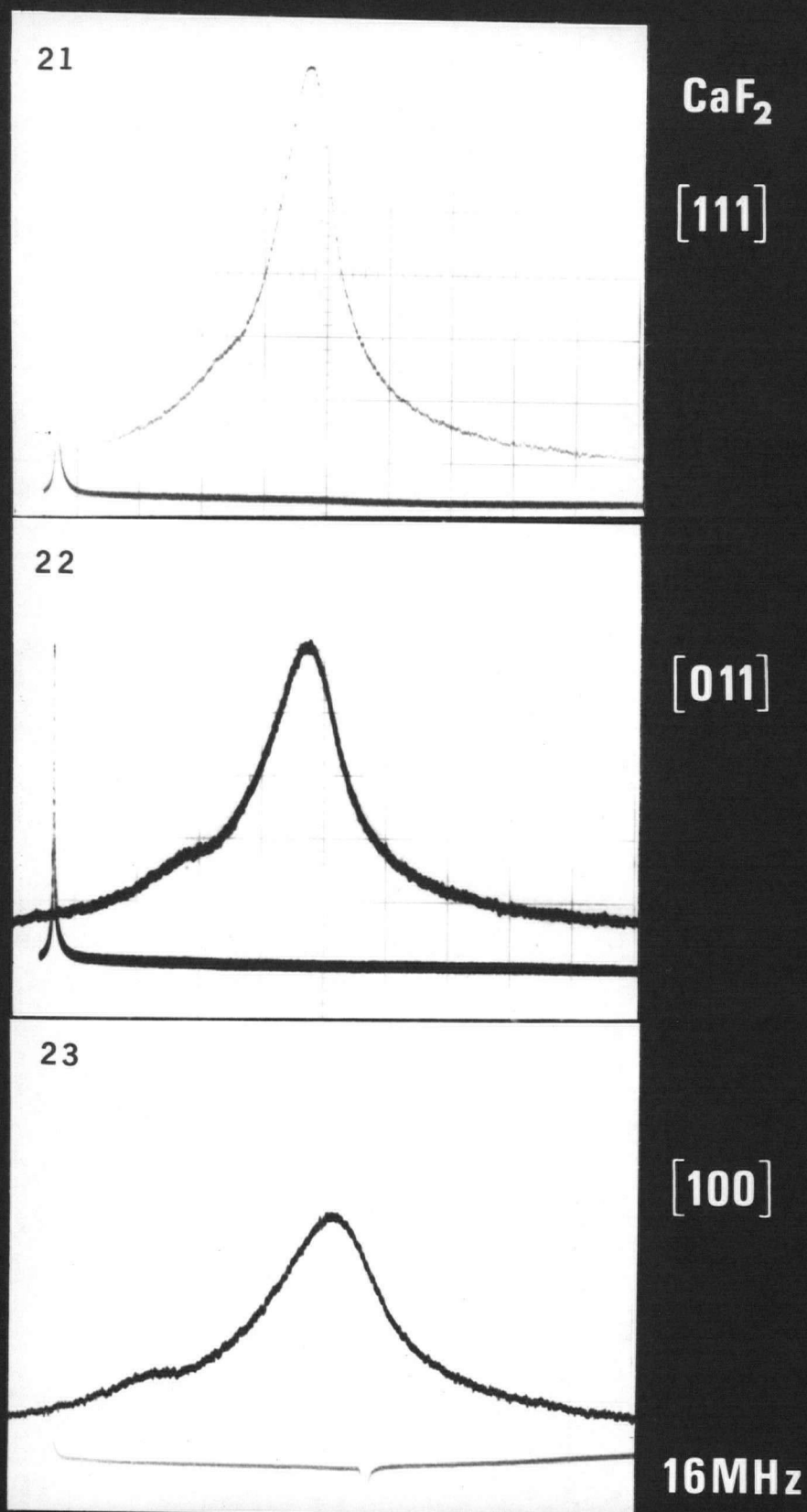


Fig 6 - ARP signals in the  $\text{CaF}_2$  single crystal for  $H_0$  along the [111], [011], and [100] directions.  $A = 6.7$ .

with such a misalignment - viz, [111]  $H_L$  a little too high and [100] too low.

Table IV -  $H_L$  measurements in  $CaF_2$  at 16 MHz \*

Trace	Sample	$H_O$ direc- tion	Scope# sweep ms/cm	$\delta H^\dagger$ pic. cm	$t_p$ msec	$H_L$ expt. gauss	$H_L^{**}$ theo. gauss
17	powder	-	20	0.95	21.1	1.47	1.47
19	TFA	liq.	2	1.63	3.62		
20	Xtal	[111]	10	1.16			
21	"	"	"	1.17	12.9	0.88	0.86
22	"	[011]	"	1.65	18.3	1.27	1.275
23	"	[100]	"	2.55	28.3	1.99	2.07

$\dagger$ Measurement in picture which is scope screen size X0.9.

\* $H_1 = 0.256$  G,  $dH_O/dt = 245$  G/sec,  $A = 6.7$ .

#Fast sweeps. The slow sweeps that can be seen in the Xtal signals were used to help establish base line position.

\*\*Calculated from the theoretical second moments in ref /5/.

The local field ( $H^1$  resonance) was also measured in a  $LiC_{18}$  powder sample at room temperature. The calibration signal was from water in a 6 mm dia tube. ( $H_1 = 0.255$  G at 16 MHz,  $dH_O/dt = 227$  G/sec,  $A = 7.7$ ). The measured  $t_p$  ratio, 9.95/1.0, yielded  $H_L = 2.53$  gauss. This is less than 6% different from 2.68 gauss the  $H_L$  value calculated from the experimental average second moment value given in chap 3.

The above results were very good in spite of the fact that the values of the adiabatic parameter  $A$  were less than we would have liked them to be. Some asymmetry which we have ascribed to residual dispersion can be seen in all the solid sample ARP

signals in Figs 5 and 6. The small amount of dispersion appears to add a little to one side of the line and subtract a little from the other with the net result that the error in the width-at-half-height measurement is quite small.

## 2. Measurements at 8 MHz

The following measurements were done at 8 MHz to make use of the higher  $H_1$  levels available at this frequency. ARP signals could then be obtained for high values of the Bloch adiabatic parameter  $A$ . Examples of the ARP signals obtained from the  $\text{CaF}_2$  powder and TFA liquid samples are shown in Fig 7 ( $H_1 = 0.594$  G,  $dH_0/dt = 329$  G/sec,  $A = 27$ , #40 is  $\text{CaF}_2$ , #39 is TFA). We see that trace #40 is quite symmetric and shows no residual dispersion. Two  $\text{CaF}_2$  powder ARP signals for  $H_1 = 0.594$  G were measured. A pair of TFA liquid sweep calibration signals were obtained for each. The data and results are listed in Table V.

Table V -  $H_L$  measurements in powder  $\text{CaF}_2$  at 8 MHz\*

Trace	Sample	Scope sweep ms/cm	$\delta H$ pic. cm	$t_p$ msec	$H_L$ gauss
33	TFA	10	0.56	6.22	
34	"	4	1.40	6.22	
35	$\text{CaF}_2$	10	1.54	17.10	1.52
38	TFA	4#	1.38		
39	"	4#	1.43	6.25	
40	$\text{CaF}_2$	10#	1.50	16.67	1.47

\* $H_1 = 0.594$  G,  $A = 27$

#Fast sweeps. The slow sweeps seen in Fig 7 are 0.5 sec/cm

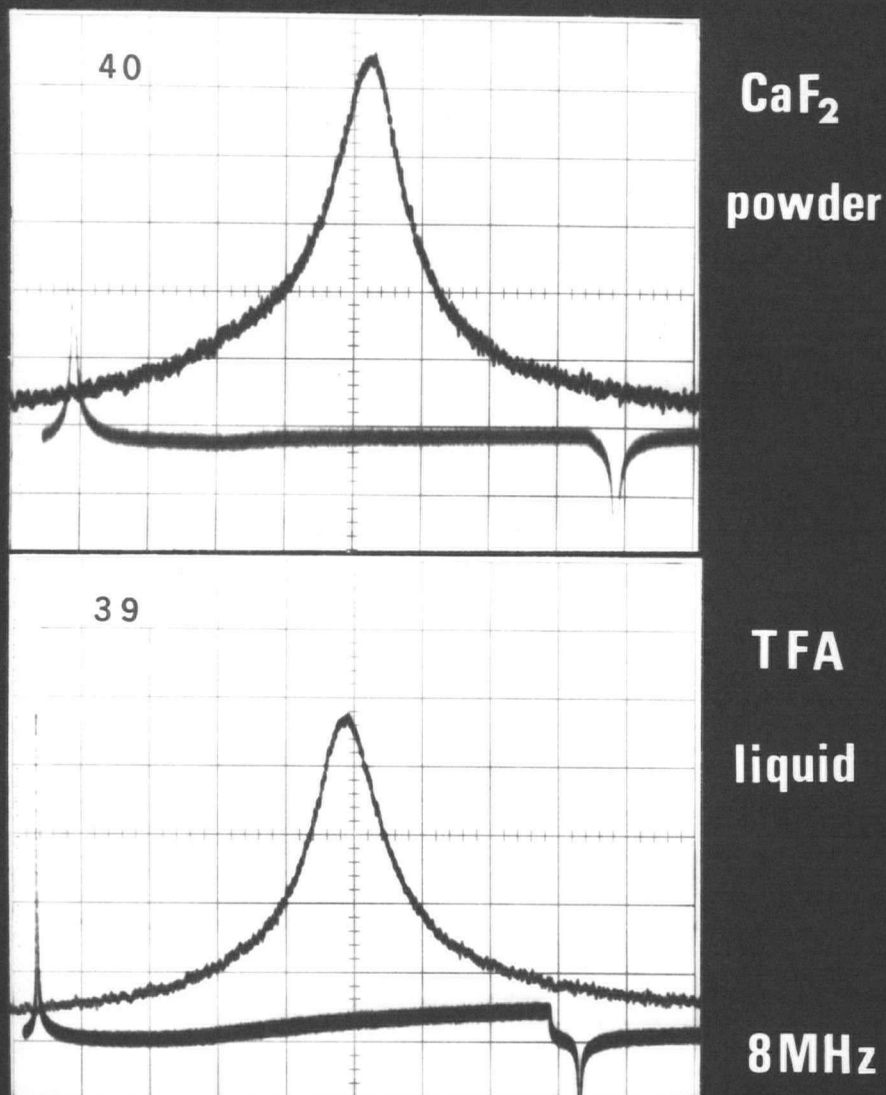


Fig 7 - ARP signals in polycrystalline  $\text{CaF}_2$  and liquid tri-fluoroacetic acid at 8 MHz.  $A = 27.$

These  $H_L$  results (1.52 and 1.47 G) are in excellent agreement with the theoretical value of 1.47 gauss (the 1.52 G result differs by only 3.4%).

ARP signals in the  $\text{CaF}_2$  single crystal for the usual three crystal directions were also observed and photographed at 8 MHz. The data are listed in Table VI. Unfortunately  $H_L$  values could not be obtained here because we did not record a calibration signal from a liquid sample for the particular field sweep settings used here\*. The square wave amplitude setting on the 202A generator was the same as that used for the measurements listed in Table V ( $\text{CaF}_2$  powder) but the frequency was different.

Table VI -  $\delta H$  measurements in the  $\text{CaF}_2$  crystal at 8 MHz

Trace	$H_0$ direc- tion	$\delta H$ pic. cm	$\delta H$ ratios		Diff.
			obs.	calc.*	
45	[111]	1.41	0.83	0.775	6.6%
44	[011]	1.70	1.00	1.00	
43	[100]	2.42	1.42	1.48	4.1%

\*For  $H_L = 0.77$  G and theoretical  $H_L$  values from second moments in ref /5/.

The longer  $T_1$  in the  $\text{CaF}_2$  single crystal dictated a longer period between sweeps. (The field sweep rate calculated from trace 43 is 285 G/sec and so  $A = 52$ .) We therefore have listed in Table VI the observed  $\delta H$  ratios, with respect to  $\delta H$  for [011] along  $H_0$ , for comparison with calculated ratios.

\*

Unfortunately this was realised after the author had left the university.

The agreement is quite good considering the fact that  $H_1$  here is approaching  $H_L$  and so an error in its calibration is reflected more strongly in  $\delta H$  than in the 16 MHz measurements.

### 3. Second moments

The root mean square second moment  $\langle \Delta H^2 \rangle^{\frac{1}{2}}$  is equal to  $\sqrt{3} H_L$ . The root second moments obtained from our average result for  $H_L$  in polycrystalline  $\text{CaF}_2$  (av. of 2 at 8 MHz and 1 at 16 MHz) and from our  $H_L$  results for  $H_0$  along [111], [011] and [100] in the  $\text{CaF}_2$  single crystal (at 16 MHz) are presented in Table VII.

Table VII -  $\langle \Delta H^2 \rangle^{\frac{1}{2}}$  in gauss, for  $\text{F}^{19}$  in  $\text{CaF}_2$

Sample	$H_0$ direction	ARP this work	Pulse Lowe	CW Bruce	Theory O'Reilly
powder	-	2.58	2.51	2.49*	2.55
Xtal	[111]	1.52	1.47	1.55	1.49
"	[011]	2.20	2.18	2.2	2.21
"	[100]	3.45	3.54	3.49	3.59

\* This work. Other results: 2.53 (Lowe), 2.65 (O'Reilly).  
 Lowe: From free induction decay signal /3/.  
 Bruce: Averages of moments from CW spectra /1/.  
 O'Reilly: Theoretical moments for a rigid lattice /5/.

The moments determined by Barnaal and Lowe /3/ from free-induction-decay curves, the averages of the moments reported by Bruce /1/, and the theoretical moments calculated for rigid lattice parameters by O'Reilly and Tsang /5/ are also given in Table VII.

Our results compare very well with those obtained by Barnaal and Lowe using an NMR pulse spectrometer. In fact our result

for  $\text{CaF}_2$  powder (where there is no error due to misalignment) is slightly better. Their results represent nine years of refinement of the free-induction-decay-shape measurement technique /2, 3/. See also references in /3/. The photographed fid-curves have to be measured, corrected for finite pulse widths and receiver bandwidth, and a power series or other function fitted to them /3/. Our ARP method only involves a pair of line width measurements and an  $H_1$  calibration. Also the apparatus is simpler than that for pulse spectroscopy.

Like the pulse experiment, the ARP experiment is performed in less than a second. Therefore second moment versus temperature studies can be done by ARP in much less time than by the usual CW technique. In addition the ARP method is potentially more accurate. There seems to be less chance of error in the ARP signal line width measurement than in the result of the numerical double integration of the CW derivative spectrum. Also a second moment measurement can be made by ARP even if the spin lattice relaxation time is very long and the normal CW signal is saturated.

## C. $T_1$ Measurements

### 1. $\text{CaF}_2$ single crystal

Some typical ARP symmetric sweep signals are shown in Fig. 8. They were obtained from the  $\text{CaF}_2$  single crystal sample at 8 MHz.  $H_0$  is along [111],  $H_1 = 0.76$  gauss and  $A$  is about 62. The scope

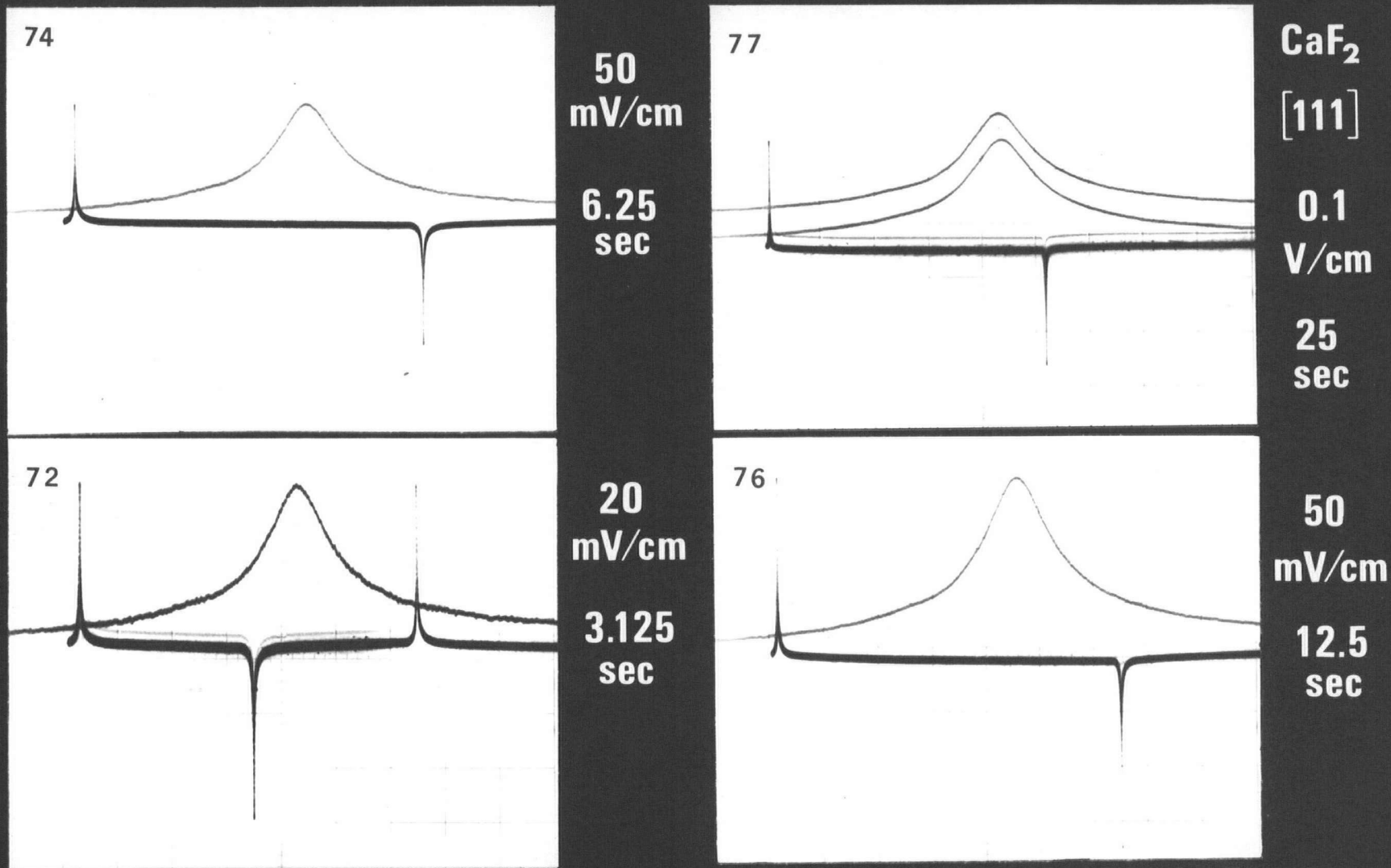


Fig 8 -  $T_1$  measurement in  $\text{CaF}_2$  crystal by ARP symmetric sweep method. Intervals between sweeps and scope ranges are given in figure.

slow sweep rate (lower trace) was 1.0 sec/cm for plates 72 and 74, 2.0 sec/cm for 76, and 5.0 sec/cm for 77. The fast rate was 10 msec/cm for all four. Other data and the results for this run are listed in Table VIII. This table also shows how the scope photographs are measured and  $T_1$  calculated. A summary of the  $\text{CaF}_2$  single crystal  $T_1$  results obtained by ARP symmetric

Table VIII -  $\text{CaF}_2$  ARP sym. sweep data for Fig 8 run,  $H_0$  along [111]

Plate #	t sec	Scope mv/cm	Signal* cm	mv	$\frac{S(4t)}{S(t)}$	$\frac{t\#}{T_1}$	$T_1$
77	25	100	3.62	362			
76	12.5	50	5.95	} 297			
75	12.5	"	5.93				
74	6.25	"	3.87	194	1.87	1.16	5.4
73	3.13	20	5.30	} 107			
72	3.13	"	5.35				

\*Peak-to-peak signals.  $F^{19}$  resonance at 8 MHz.  
 #From graph like that in Fig 1, ref /4/.

sweep is presented in Table IX. The run at  $H_1 = 0.208$  gauss (an rf field that can also be easily achieved at 16 MHz) was done in order to see if  $T_1$ 's obtained at a low value of  $A$  were valid. We would then know whether or not correct  $T_1$ 's could be obtained at 16 MHz. Unfortunately  $A$  for this run turned out to be a little higher than we expected from preliminary calibrations. The average  $T_1$  value for  $H_1 = 0.208$  gauss ( $A = 7.1$ ) was  $5.0 \pm 0.3$  sec. This is a little less than  $5.2 \pm 0.2$  sec, the average value of the  $T_1$ 's obtained at high  $H_1$ , but the difference could be due to errors caused by the poorer signal-to-noise-ratio at the lower  $H_1$  level. If the difference were real, it would mean that the inversion of the

of the magnetization is not quite complete during the rapid passage when  $A = 7.1$ .

Table IX -  $T_1$  in  $\text{CaF}_2$  by ARP,  $F^{19}$  at 8 MHz,  $H_0$  along [111]

Plates	$H_1$ gauss	$dH_0/dt$ G/sec	A	$T_1$ sec	$T_1$ sec
54-63	0.208	154	7.1	5.3	4.7
64-71	0.77	154	97	5.5	5.0
72-77	0.76	241	62	5.4	5.0

$T_1$  in  $\text{CaF}_2$ , with  $H_0$  along [111], was also measured by ARP symmetric sweep at 16 MHz. The conditions were:  $H_1 = 0.253$  G, and  $A = 5.4$ . The results of a single run were 7.2 and 8.7 sec, the average being  $7.9 \pm 0.8$  sec.  $S(2t)/S(t)$  ratios were used to avoid comparing signals on different scope voltage ranges. A  $T_1$  value of 7.6 sec was found by recovering from saturation (3 curves). The observing rf level was quite low ( $H_1 = 0.4$  mG), thus the signal-to-noise-ratio was rather poor, and consequently the accuracy is not expected to be better than 20%. The average value of  $T_1$  obtained from a larger number of recovery from saturation curves from the same sample is reported in ref /4/. The result therein is  $T_1 = 9.3 \pm 1.8$  sec ( $\pm 1.8$  sec is the standard deviation calculated from the 27 runs made). An ARP two-pass ( $\pi - \pi/2$  type) measurement,  $T_1 = 9.5 \pm 1$  sec, is also reported in ref /4/. Our ARP sym. sweep result of  $7.9 \pm 0.8$  sec is less than both of the above results (although it is within the standard deviation of the recovery from saturation value) and this suggests that the inversion of the magnetization is not complete when  $A$  is only 5.4. The ARP sym. sweep  $T_1$  value

given in ref /4/ for this sample is only  $6.5 \pm 1.0$  sec. This\* must correspond to a somewhat lower value of the adiabatic condition parameter  $A$  than we report here. More work needs to be done to clear up these points.

The difference in the  $T_1$ 's obtained at 8 and 15 MHz is not unreasonable for a sample of this purity. See Bloembergen /11/.

### 2. $\text{CaF}_2$ powder sample

The ARP sym. sweep signals obtained from the  $\text{CaF}_2$  powder sample at 8 MHz are shown in Fig 9 ( $H_1 = 0.76$  G,  $A$  is about 62). Fig 9 yields  $T_1$  values of 0.45 and 0.47 sec.

The  $T_1$  value found at 16 MHz is  $0.45 \pm 0.05$  sec. Conditions were:  $H_1 = 0.253$  G,  $A = 5.3$ . The independence of  $T_1$  on  $H_0$  in this sample agrees with the results and theory of Bloembergen /11/. Apparently the adiabatic condition is reasonably well satisfied in this case.

### 3. $\text{LiC}_{18}$ powder sample

A  $T_1$  value of 12.1 sec ( $H^1$  resonance at 16 MHz) was found in the not-fused  $\text{LiC}_{18}$  sample at room temperature by ARP sym. sweep. Conditions were:  $H_1 = 0.253$  G,  $A = 5.6$ . This sample is from the same batch as the sample used in chapters 3 and 4.

---

\* Unfortunately the magnetic field sweep rates for the ARP  $T_1$  measurements in ref /4/ were not measured.

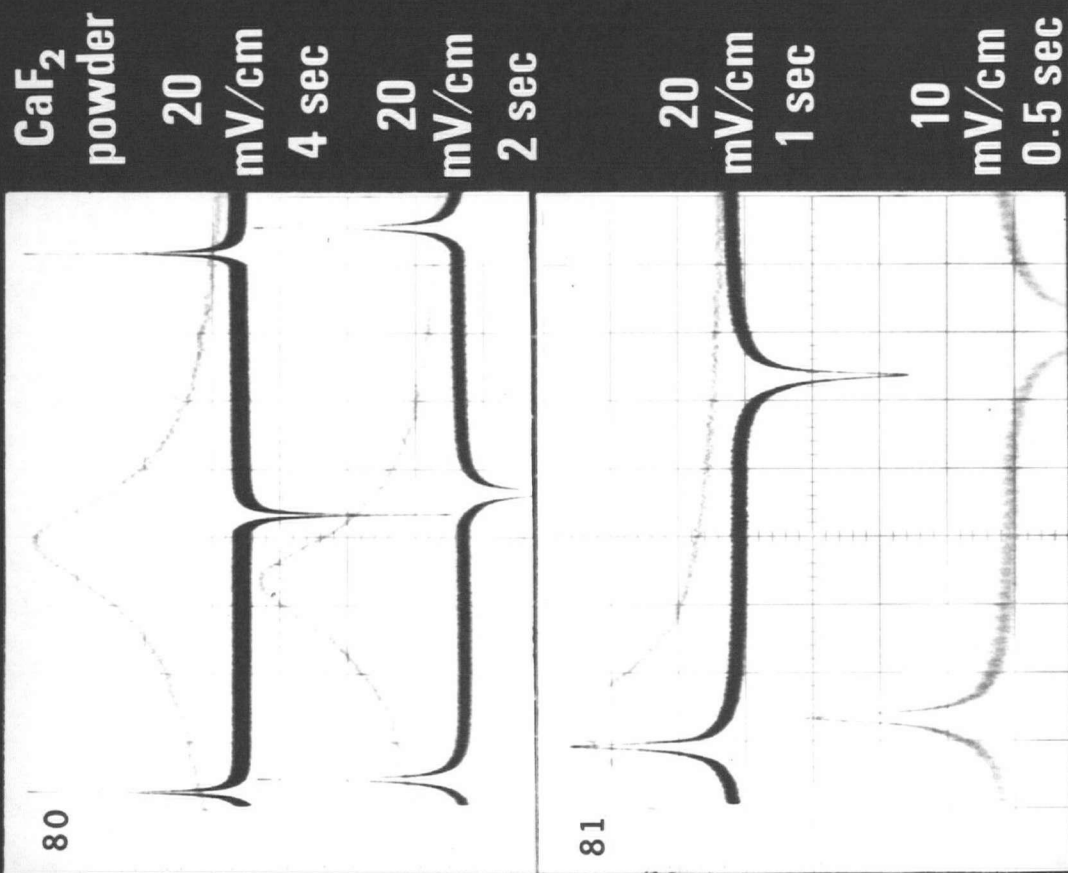


Fig 9 -  $T_1$  measurement in CaF<sub>2</sub> powder by ARP symmetric sweep method.

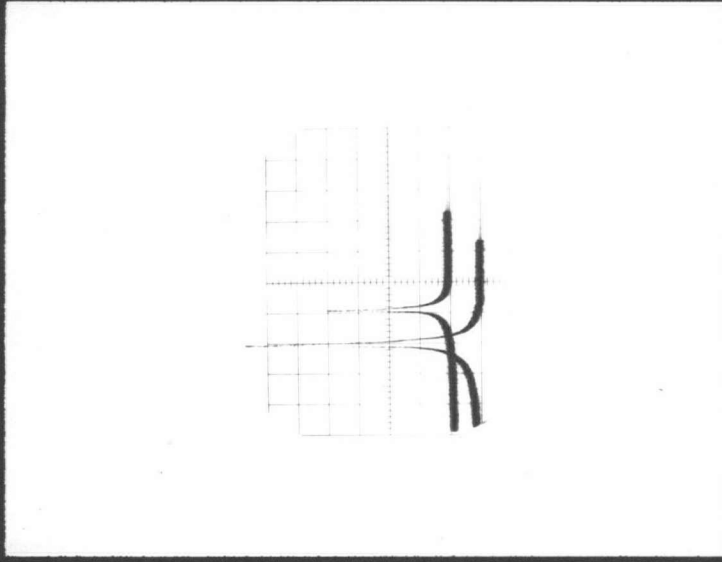


Fig 10 -  $T_1$  measurement in maleic anhydride single crystal by ARP two-pass method. The period between the sweeps was 20 min. 35 sec.

$T_1$  in the latter sample at room temperature and 56.4 MHz was found to be 17.4 sec by progressive saturation of dispersion (PSD), and 16.3 sec by dispersion signal decay (DSD). The lower value observed by ARP at 16 MHz is not unreasonable /11/. At 77°K and 56.4 MHz a  $T_1$  value of 95 sec was found by DSD. The results reported in ref /4/ are for a different batch of  $\text{LiC}_{18}$  (different stearic acid purification and preparation procedures). The amount of paramagnetic impurity (which is believed to be primarily responsible for spin-lattice relaxation /11/) may be different by reason of the vicissitudes of the preparation.

#### 4. Maleic anhydride sample

The signals from an ARP two pass ( $\pi - \pi/2$ ) experiment on a single crystal of maleic anhydride are shown in Fig 10. The sample was allowed to equilibrate in the magnetic field (just above resonance) 14 hr before the first pass was made. The return pass was made 20 min 35 sec later. We see that the signals are both of the same sign and so  $T_1$  is longer than the interval between the sweeps. The result is  $T_1 = 76$  min. The equilibration time then was 11 times greater than  $T_1$  and should be sufficient.

This is a particularly good example of an application of the ARP technique. A signal could not even be seen by conventional CW NMR spectroscopy /12/. The  $T_1$  measurement could be made by the usual pulse technique, but it is difficult to maintain the exact resonance conditions required by this technique for long periods of time. In the ARP method we wait off resonance between sweeps. Therefore high field stability is not required and very long  $T_1$  values can be measured.

## REFERENCES

- (1) C.R. Bruce, Phys. Rev. 107, 43 (1957)
- (2) I.J. Lowe and R.E. Norberg, Phys. Rev. 107, 46 (1957)
- (3) D.E. Barnaal and I.J. Lowe, Phys. Rev. 148, 328 (1966)
- (4) W.R. Janzen, T.J.R. Cyr, and B.A. Dunell, J. Chem. Phys, 48, 1246 (1968)
- (5) D.E. O'Reilly and Tung Tsang, Phys. Rev. 128, 2639 (1962); 131, 2522 (1963)
- (6) H. Benoit, Ann. Phys. (Paris), 4, 1439 (1959)
- (7) F. Bloch, Phys. Rev. 70, 460 (1946)
- (8) C. Fric, Ann. Phys. (Paris), 5, 1501 (1960)
- (9) A.I. Zhernovoi, Fizika Tverdogo Tela, 9, 673 (1967)  
English transl: Soviet Physics - Solid State 9, 523 (1967)
- (10) H.S. Gutowsky, R.E. McClure, and C.J. Hoffman, Phys. Rev. 81, 635 (1951)
- (11) N. Bloembergen, Physica, 15, 386 (1949)
- (12) J.P. Messa, NRC of Canada. Private communication.

## chapter 7.

VARIATION OF THE NORMAL AND SATURATION NARROWED  
LINES IN LITHIUM STEARATE WITH TEMPERATURE

## I. EXPERIMENTAL

The same Varian DP 60 spectrometer described in chap 3 was used except that a special Varian "proton-free" insert and probe were used. The insert was 15 mm in diameter and accepted the temperature apparatus described in ref /1/. We obtained this insert and probe after observing that the back-ground signal at high  $H_1$  levels from the usual system was nearly as large as our  $\text{LiC}_{18}$  signal.

The purification of the stearic acid used to make the  $\text{LiC}_{18}$  has been described in ref /1/ and /2/. The stearic acid had a freezing point of  $69.6^\circ\text{C}$  (it is incorrectly given as  $69.5^\circ\text{C}$  in ref /2/). The preparation of the two  $\text{LiC}_{18}$  samples, both dried but only one of them fused, is described in reference /2/. The sample not fused is the same one used in chapters 3 and 4.

## II. RESULTS AND DISCUSSION

Normal absorption line widths  $\Delta H_a$  for the  $\text{LiC}_{18}$  fused on preparation and for the  $\text{LiC}_{18}$  not fused on preparation are shown in Fig 1 as a function of temperature. Evidence of two phase transitions can be seen. In the sample not fused, the first of these transitions occurs between  $110^\circ$  and  $119^\circ\text{C}$ , and is thought to be a change from one crystalline form to another. The second occurs between  $184^\circ$  and  $191^\circ\text{C}$  and has the character of a change from a crystal phase to a waxy phase. We see that in the sample fused on preparation the crystal phase transition is not as sharp and that both transitions occur at lower temperatures. The behaviour of the fused sample over the temperature range  $-196^\circ$  to  $230^\circ\text{C}$  has been discussed before /2, 3/. Data and spectra for the not-fused sample in the region  $136^\circ$  to  $193^\circ\text{C}$  are also presented and discussed in these papers. We have now extended the study of the not-fused sample down to room temperature and have included the crystal phase transition.

Saturation narrowed absorption line widths  $\Delta H_{as}$  for the not-fused  $\text{LiC}_{18}$  are shown in Fig 2 as a function of temperature. The normal line widths from Fig 1 are reproduced here for comparison. We see that there are sudden drops in the  $\Delta H_{as}$  vs temperature plot similar to those in the usual  $\Delta H_a$  vs temperature curve and they occur at about the same temperatures. This is not unexpected because the saturation narrowed line width is related to the second moment of the unsaturated absorption line, thus

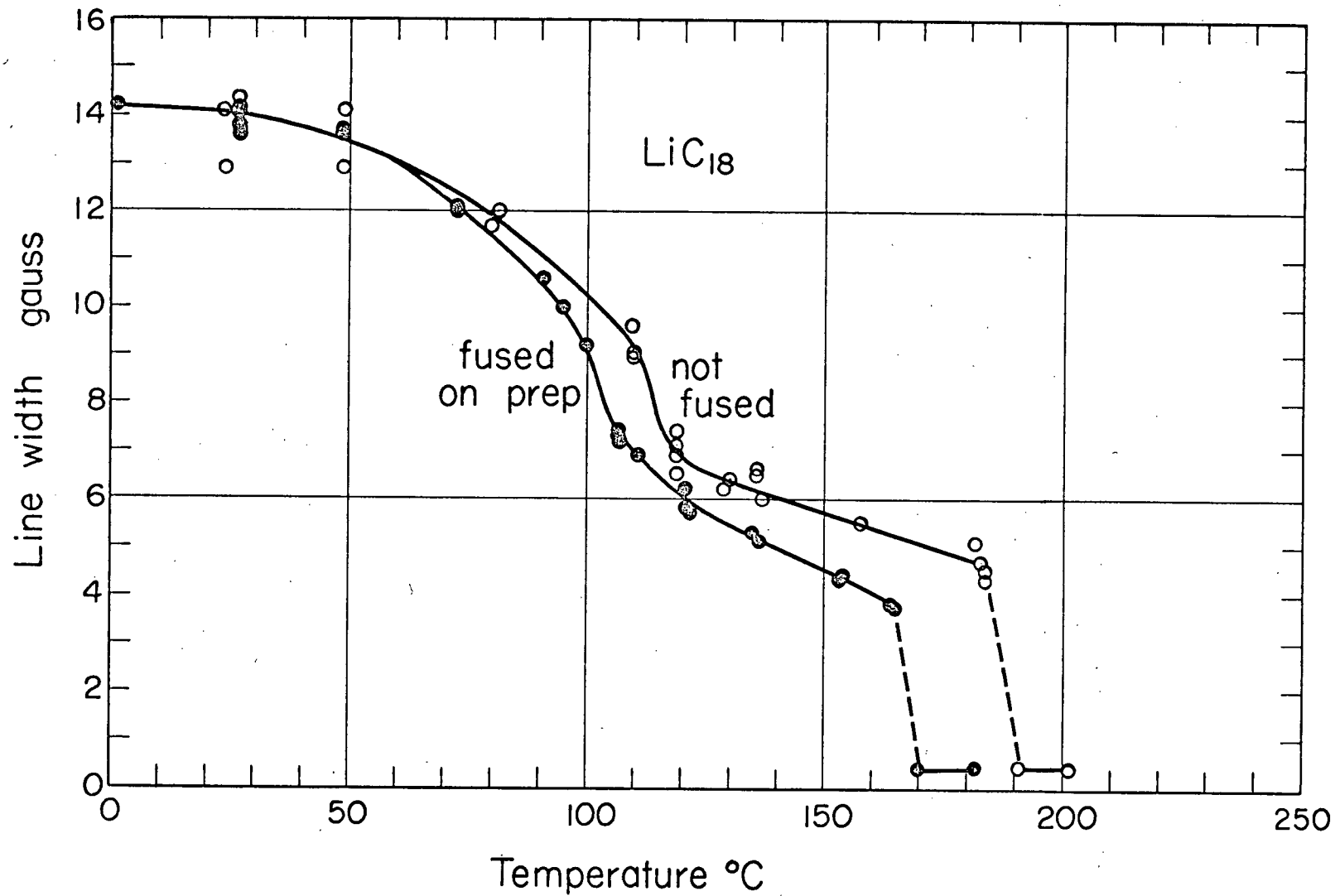


Fig 1 - Line width in fused and not-fused lithium stearate as a function of temperature.

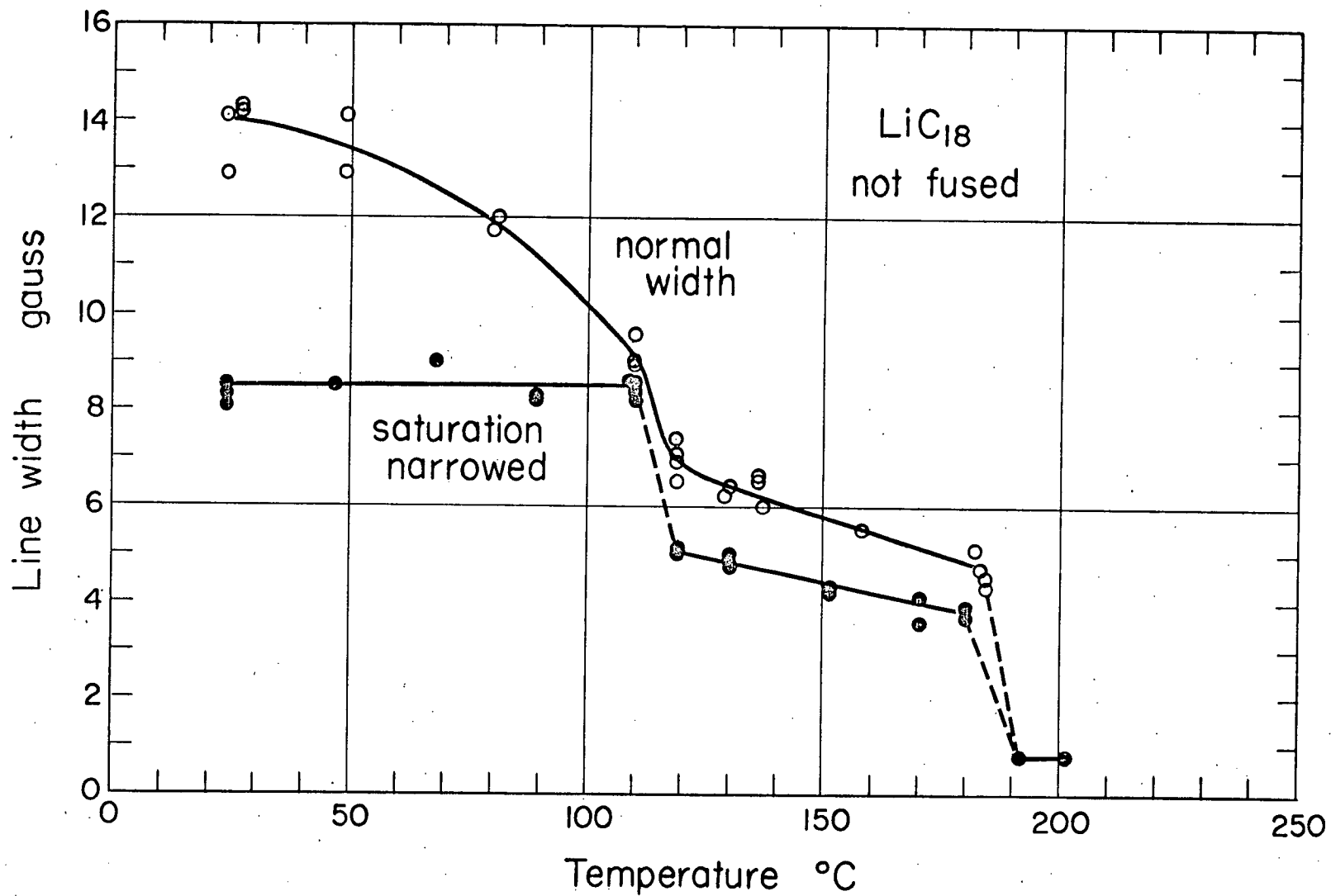


Fig 2 - Saturation narrowed and normal line widths in not-fused lithium stearate as a function of temperature.

$$\Delta H_{as} = \frac{2}{3} \sqrt{\frac{T_1}{T_D}} \langle \Delta H^2 \rangle^{\frac{1}{2}} . \quad (1-45)$$

Second moments of the unsaturated absorption line as a function of temperature in  $\text{LiC}_{18}$ , fused and not-fused, are given in Fig 3. The more abrupt drops in these curves correspond to those in the normal absorption line width vs temperature plots in Fig 1 and so the saturation narrowed line widths are expected to do so too. We have seen in Fig 2 that for the not fused sample this does occur.

It therefore appears that one might be able to study phase transitions by using saturation narrowed spectra. In samples with very long spin lattice times this may be the only type of spectrum that can be observed. Even in other cases when the normal absorption spectra can be observed, the saturation narrowed spectra have a more favorable signal to noise ratio and hence would be useful in observing transitions in samples when the packing factor in the probe is poor.

More work needs to be done, however, to see whether or not the above procedure can be used. If we look at Fig 2 and Fig 3 again, it is apparent that the  $T_1/T_D$  ratio can also change with temperature. The saturation narrowed width does not change between  $25^\circ$  and  $110^\circ\text{C}$ , yet the second moment decreases by about 32% over this range. We do not know how much this phenomenon will complicate the use of saturation narrowed spectra in detecting phase transitions in solids. It would seem to be worth investigating further. Ideally one would like to measure  $\Delta H_a$ ,  $\langle \Delta H^2 \rangle$ ,  $\Delta H_{as}$ ,  $T_1$ , and  $T_D$  for a variety of samples as a

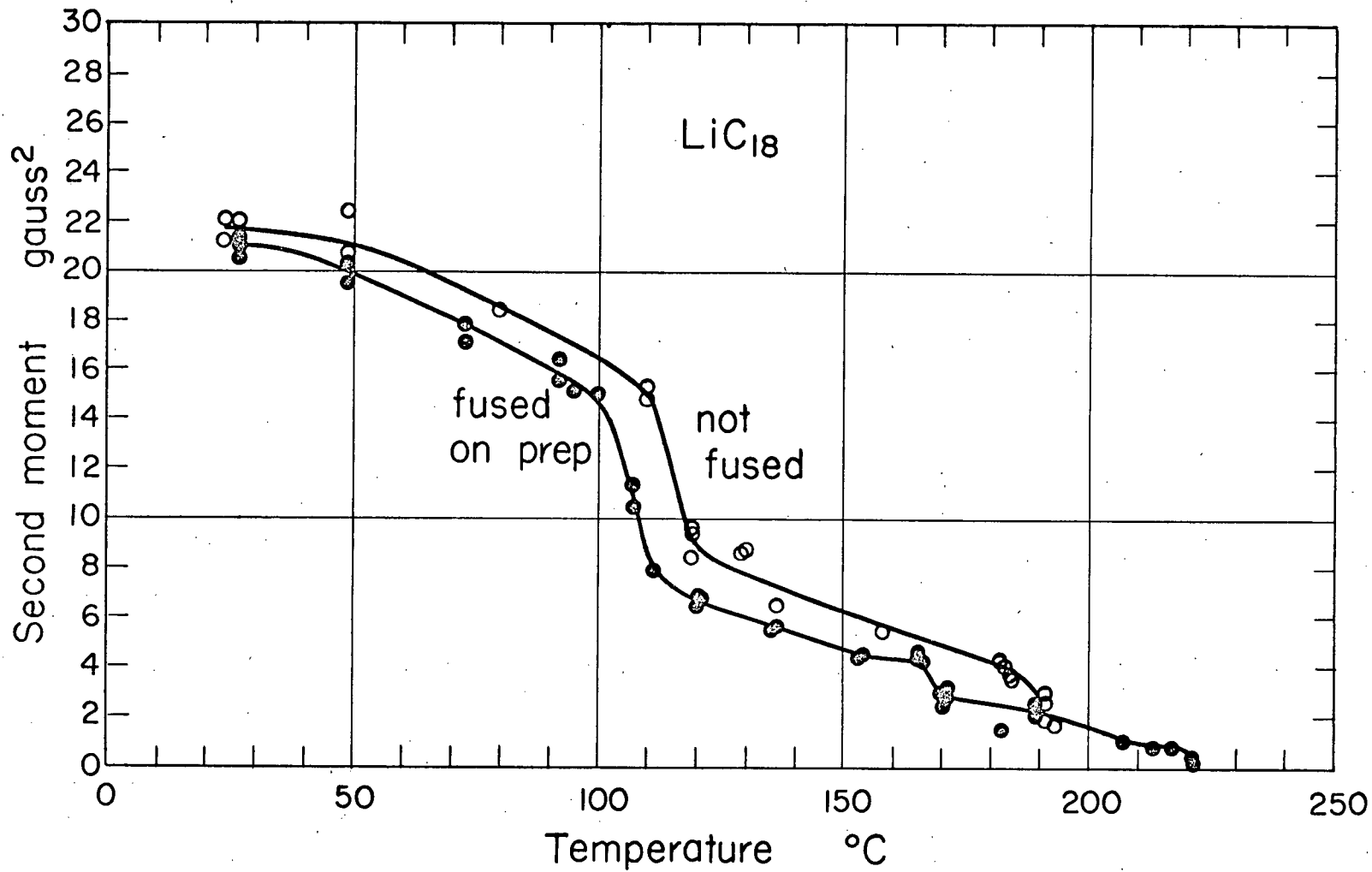


Fig 3 - Second moment in fused and not-fused lithium stearate as a function of temperature.

function of temperature. This could be done if both a CW and a suitable pulse spectrometer were available.

#### REFERENCES

- (1) W.R. Janzen, M.Sc. Thesis in Chemistry, University of British Columbia, B.C. (1963)
- (2) T.J.R. Cyr, W.R. Janzen, and B.A. Dunell "Ordered Fluids and Liquid Crystals", Advances in Chemistry Series, No.63, American Chemical Society, Washington, D.C. (1967) pp 13-25
- (3) B.A. Dunell and W.R. Janzen, Wiss. Z. Friedrich-Schiller Univ., Jena, 14, 191 (1965)

## APPENDIX A

Two Pass ARP with Low then High  $H_1$ 

Slichter and Holton /1/ in "Adiabatic Demagnetization in a Rotating Reference System" as well as studying the title subject did some two pass ARP experiments of the  $\pi - \pi/2$  type. The experiments were performed on the  $\text{Na}^{23}$  resonance in a single crystal of NaCl. The static magnetic field was along the [100] direction. According to Goldberg /2/,  $H_L$  in this direction is 0.61 G, theoretical and experimental. Goldberg suggests that Slichter and Holton's  $H_1$  calibration was probably in error because they found experimental values of 0.88 to 0.95 G although their calculated value was 0.57 G.

Two passes were made through resonance, the first pass with low  $H_1$  ( $H_1 \approx H_L/4$ ), the return pass with high  $H_1$  ( $H_1 \approx 2.5 H_L$ ). The Bloch adiabatic condition seems to have been satisfied for each case. The return pass will invert the magnetization completely and the question is, "will the first?". Fig 7 was exhibited as proof that the first pass inverted the magnetization and it was stated that the results therein behave just as one would expect if the first pass inverted  $M_0$ , and if spin-lattice relaxation took place before the return pass. We have analysed the experiment a little further and find that one can get the signal behaviour shown in Fig 7 even if the first pass only partially inverts  $M_0$ .

The equations we need have already been derived in chap 5.

If the first pass only inverts a fraction  $x$  of the magnetization  $M_0$ , the formula for the magnetization is equation (5-33)

$$M_z = M_0 - 2xM_0 \exp(-t/T_1). \quad (A1)$$

Now since the return pass is made with high  $H_1$  the signal  $S_t$  equals  $-kM_z$  ( $k$  being the proportionality constant), rather than  $-kxM_z$  as in case 2 in chap 5, we get the following equation

$$-S_t = kM_0 - k2xM_0 \exp(-t/T_1). \quad (A2)$$

Then on substituting for the long-time signal  $S_\infty = -kM_0$  we get

$$S_\infty - S_t = 2xS_\infty \exp(-t/T_1), \quad (A3)$$

which is identical to equation (35). We see that a plot of  $\ln(S_\infty - S_t)$  vs time will still be a line of slope  $-1/T_1$ . Therefore obtaining a correct  $T_1$  this way is not proof that the first pass completely inverted the magnetization. However we can tell whether or not  $x = 1.0$  if we examine the intercept of this plot which is  $\ln 2xS_\infty$ .

Slichter and Holton's "long-time asymptote" signal  $S_\infty$  is 2.0 divisions and so  $2S_\infty = 4.0$ . This is close to the intercept value 3.7 from their semilog plot. If the difference is real, we can find  $x$  by setting  $2x2.0 = 3.7$ . The result is  $x = 0.92$  and this suggests that the first pass may not be performing complete inversion. However, the inversion is probably complete;  $x = 1.0$  requires an experimental error of only 8% in their  $S_\infty$  value.

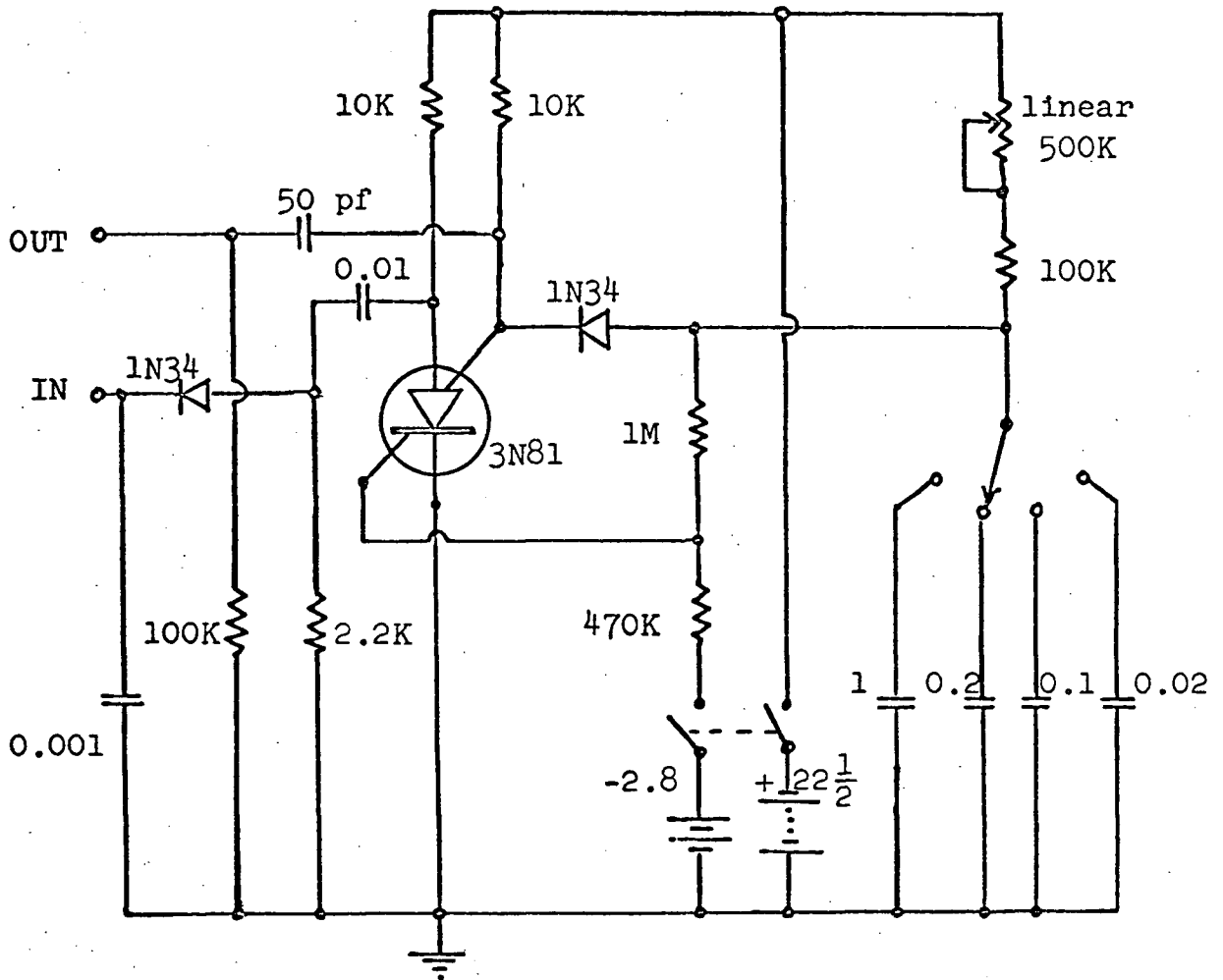
Another difference from the case of complete inversion on both passes is that now  $S_t$  passes through a null when  $t_{\text{null}} = T_1 \ln 2x$  instead of  $T_1 \ln 2$ . If just the latter formula is used we get  $T_1 = 11$  sec from their results. This compares well with  $T_1 = 12$  sec found by Wikner et al /3/.

- (1) C.P. Slichter and W.C. Holton, Phys. Rev. 122, 1701 (1961)
- (2) W.I. Goldberg, Phys. Rev. 128, 1554 (1962)
- (3) E.G. Wikner, W.E. Blumberg, and E.L. Hahn, Phys. Rev. 118, 631 (1960).

## APPENDIX B

WRJ Trigger Pulse Delay Unit

Delay range is 1.5 to 450 milliseconds.



3N81 is a General Electric silicon controlled switch.

Capacitance is in microfarads unless marked otherwise.

INPUT: - will trigger on a -18 volt 1.3 microsec pulse.

OUTPUT: - a +10 volt pulse then a delayed -11 volt pulse.

The output pulses have half-widths of about 5 microsecs.

## APPENDIX C

Comments on "Adiabatic Rapid-Passage Experiments in Some Solids" by Janzen, Cyr, and Dunell /1/

The reader may be wondering why we are presenting now in section 1 of chapter 6,  $T_1$  measurements which are still somewhat crude, whereas supposedly more refined results have already been published in ref /1/. The reason for this is that the present author, having completed his experiments in June 1967, left the University to take up employment in early July 1967. The work was carried on by another student. The author regrets that communications were not very good and that magnetic field sweep rates were not measured for the ARP  $T_1$  measurements and for Fig 5 in the above paper.

- (1) W.R. Janzen, T.J.R. Cyr, and B.A. Dunell, J. Chem. Phys. 48, 1246 (1968).